

AD-A076 069

ILLINOIS UNIV AT CHICAGO CIRCLE DEPT OF PHYSICS
LASER EXCITATION OF INNER-SHELL ATOMIC STATES BY MULTIQUANTUM P--ETC
OCT 79 C K RHODES, R T HAWKINS

F/G 7/4
N00014-78-C-0625
NL

UNCLASSIFIED

1 of 2

AD
A0 78069





MICROCOPY RESOLUTION TEST CHART
NATIONAL BUREAU OF STANDARDS-1963-A

LEVEL

(Handwritten marks: circled '12' and other scribbles)

AD A 076069

Report N00014-78-C-0625 - 1

LASER EXCITATION OF INNER-SHELL ATOMIC STATES BY MULTIQUANTUM PROCESSES

Charles K. Rhodes
R. Thomas Hawkins

Department of Physics
University of Illinois at Chicago Circle
P. O. Box 4348
Chicago, Illinois 60680

**DDC
REPRODUCED
NOV 2 1979
UNIVERSITY OF ILLINOIS**

31 October 1979

Annual Summary Report for Period 1 August 1978 - 31 July 1979

Approved for public release; distribution unlimited.
Reproduction in whole or in part is permitted for
any purpose of the United States Government.

Prepared for:

ONR OFFICE OF NAVAL RESEARCH
800 North Quincy
Arlington, Virginia 22217

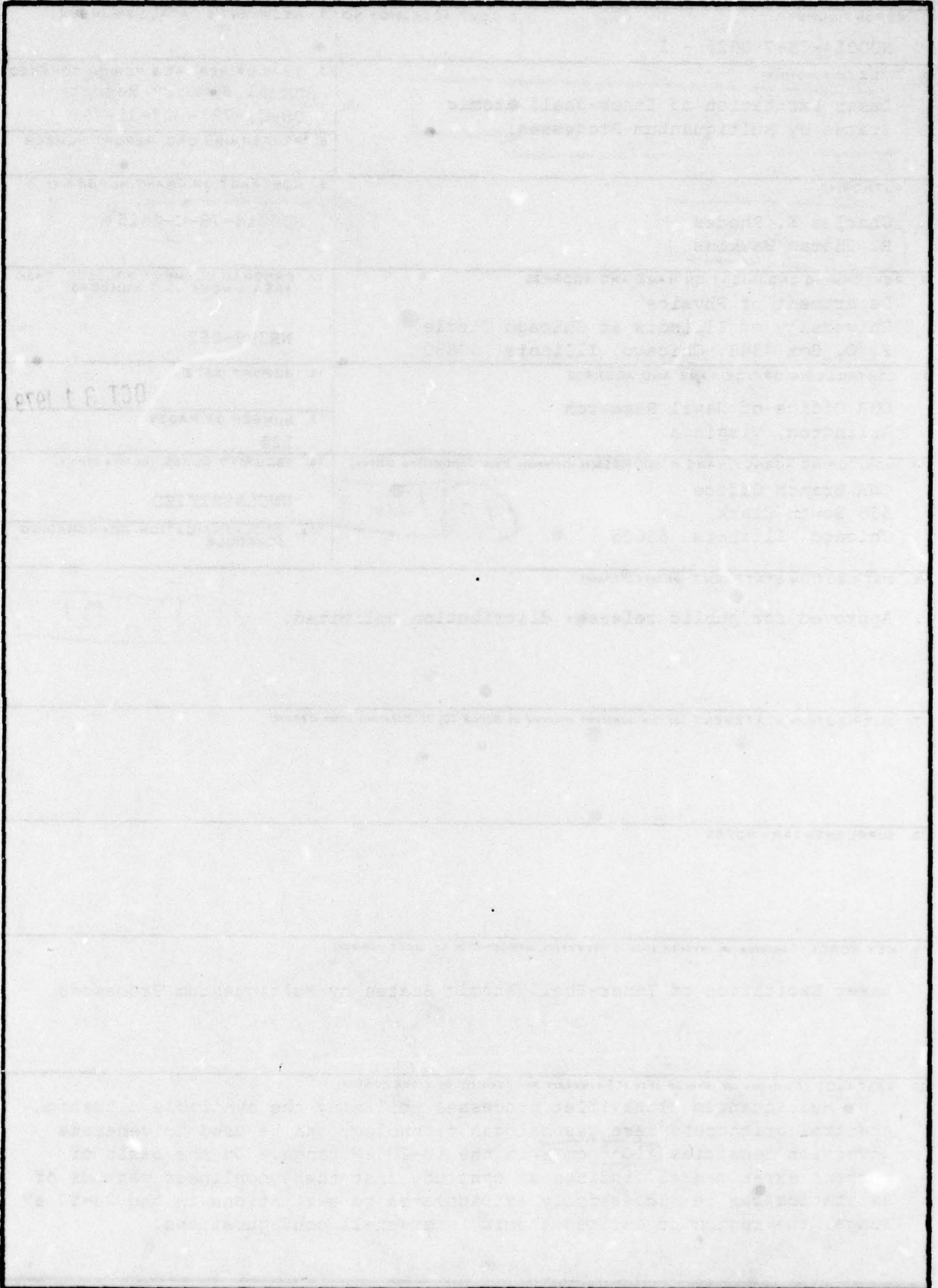
ONR BRANCH OFFICE
536 South Clark Street
Chicago, Illinois 60605

DDC FILE COPY

79 11 02 011

SECURITY CLASSIFICATION OF THIS PAGE (When Data Entered)

REPORT DOCUMENTATION PAGE		READ INSTRUCTIONS BEFORE COMPLETING FORM
1. REPORT NUMBER N00014-78-C-0625 - 1	2. GOVT ACCESSION NO.	3. RECIPIENT'S CATALOG NUMBER
4. TITLE (and Subtitle) Laser Excitation of Inner-Shell Atomic States by Multiquantum Processes.	5. TYPE OF REPORT & PERIOD COVERED Annual Summary Report 08-01-78 - 07-31-79	
7. AUTHOR(s) Charles K. Rhodes R. Thomas Hawkins		6. CONTRACT OR GRANT NUMBER(s) N00014-78-C-0625
9. PERFORMING ORGANIZATION NAME AND ADDRESS Department of Physics University of Illinois at Chicago Circle P. O. Box 4348, Chicago, Illinois 60680	10. PROGRAM ELEMENT, PROJECT, TASK AREA & WORK UNIT NUMBERS NR395-052	
11. CONTROLLING OFFICE NAME AND ADDRESS ONR Office of Naval Research Arlington, Virginia	12. REPORT DATE OCT 31 1979	13. NUMBER OF PAGES 124
14. MONITORING AGENCY NAME & ADDRESS (if different from Controlling Office) ONR Branch Office 536 South Clark Chicago, Illinois 60605	15. SECURITY CLASS. (of this report) UNCLASSIFIED	15a. DECLASSIFICATION/DOWNGRADING SCHEDULE
16. DISTRIBUTION STATEMENT (of this Report) Approved for public release; distribution unlimited.		
17. DISTRIBUTION STATEMENT (of the abstract entered in Block 20, if different from Report)		
18. SUPPLEMENTARY NOTES		
19. KEY WORDS (Continue on reverse side if necessary and identify by block number) Laser Excitation of Inner-Shell Atomic States by Multiquantum Processes > 10 to the 15th power/cm cm		
20. ABSTRACT (Continue on reverse side if necessary and identify by block number) Multiquantum ultraviolet processes utilizing the available ultrahigh spectral brightness rare gas halogen technology can be used to generate inversion densities $>10^{15} \text{ cm}^{-3}$ in the 10-20 eV range. On the basis of current experimental findings we conclude that these nonlinear methods of excitation can be successfully extrapolated to excitations in the 20-50 eV range, the region of excited atomic inner-shell configurations.		



OCT 9 1973

CONTENTS

I INTRODUCTION 2

II DISCUSSION OF RESEARCH PROGRESS 4

 A. Ultrahigh Spectral Brightness Ultraviolet Source 4

 B. Excited State Photoionization 4

 C. Multiquantum Excitation Processes 5

III CONCLUSIONS 6

IV REFERENCES 8

V APPENDICES

 A. A Tunable, Ultrahigh Spectral Brightness KrF*
 Excimer Laser Source 10

 B. Multiphoton Ultraviolet Spectroscopy of Some 6p
 Levels in Krypton 23

 C. Collisional and Radiative Properties of the H_2 E, F $^1E_g^+$
 State 50

 D. Isotope Effect in Multiphoton Ultraviolet Photolysis of CO. 93

 E. Estimate of Four Quantum Excitation of Rubidium Core
 Excited States at 248 nm 127

Accession For	
NTIS G.M.I.	<input checked="" type="checkbox"/>
DDC TAB	<input type="checkbox"/>
Unannounced	<input type="checkbox"/>
Justification	
By _____	
Distribution/	
Availability Codes	
Dist	Avail and/or special
A	

I. Introduction

Recent developments in ultraviolet laser technology should open new multiphoton pathways of selective excitation of excited inner-shell atomic configurations which are virtually impossible to excite at an appreciable rate by any other means. Direct excitation of such states, which decay primarily by radiation in the soft X-ray range, is a possible method for frequency conversion into that spectral region. States with depressed Auger rates naturally fall in this class; the subclass of this group consisting of core excited Rydberg states is explicitly considered. An essential element in developing the laser methods for excitation of atomic inner-shell configurations centers on the suppression of unwanted reactions leading to losses into modes of ionization. It is here that dynamical cancellations such as that arising in the formation of the Fano minimum can play a critical role. The consequences of the coincidence of the Fano minimum in Na with the wavelength available from the ArF* laser at 193.5 nm and a similar minimum in Rb at 248 nm is of considerable interest. Rydberg states feature in this discussion in three important ways: (1) their depressed Auger rates, (2) their very weak photoionization, and (3) their large transition matrix elements which enable the existence of greatly enhanced multiphoton amplitudes. It is estimated that in Na for a sixth order process at 193.5 nm at an intensity $\sim 10^{10}$ W/cm² a cross section $\sim 10^{-18}$ cm² will apply for the production of excited core species. In Rb, for a corresponding fourth order process at 248 nm, a cross section of $\sim 10^{-17}$ cm² is obtained at an intensity of $\sim 10^7$ W/cm². Cross sections of this magnitude would allow the production of excited inner-shell species at densities in the range of $\sim 10^{15}$ cm⁻³, a value sufficient for the generation of stimulated emission.

A major factor enabling the study of these processes is the availability of the recently developed rare gas halogen laser technology. At the moment, several wavelengths can be conveniently generated at megawatt power levels, as shown in Table I below. In anticipation of the research value of this technology, we have developed a strong experimental capability in this area.

Table I

<u>Laser System</u>	<u>Wavelength (nm)</u>	<u>Energy (mj)</u>	<u>Power (MW)</u>
XeCl*	308	100	10
KrF*	248	500	50
ArF*	193	250	25
F ₂ *	158	15	1.5

The efficacy of this type of instrumentation for the study of a wide range of atomic and molecular processes in the excitation range of 10-20 eV has been solidly demonstrated.¹ Consequently, we have utilized this laser technology to study several phenomena relevant to the generation of soft X-rays by ultraviolet multiquantum processes. This report discusses the results and progress in these pertinent areas. They are (1) the development of an ultrahigh spectral brightness source at 248 nm, the study of multiquantum excitation rates for a variety of systems [Na, Rb, H₂, HD, N₂, CO, Ar, Kr, and Xe], and (3) photoionization loss mechanisms of excited states. As discussed in previous documents², these matters are of central importance for efficient upconversion to the X-ray region by multiquantum processes.

II. Discussion of research progress

A. Ultrahigh spectral brightness ultraviolet source

For the examination of multi-quantum processes, the spectral brightness of the ultraviolet source is the key experimental parameter. With this thought in mind, we have developed over the past year a source at 248 nm (KrF*) whose properties approach the fundamental limits in terms of both spectral linewidth and divergence. Furthermore, this source, which is discussed thoroughly in Appendix A, combines tunability over the KrF* gain profile with accurate (~ 1 part in 10^7) frequency control. The linewidth of this source has been measured as $\sim 150 \pm 30$ MHz and focussed intensities $> 10^{14}$ W/cm² have been obtained. In terms of the quality of the radiation for multi-quantum studies, the stated properties represent an improvement in the ultraviolet laser technology of $\sim 10^9$.

B. Excited state photoionization

Photoionization of excited states can be an important loss mechanism, particularly in circumstances under which the ambient radiative flux is high. Certain classes of states, however, display significantly reduced photoionization cross sections², namely Rydberg states and states exhibiting a Fano minimum.

In light of the importance of these photoionization rates, we have developed and experimentally implemented a simple technique for their evaluation. This method has been successfully utilized on krypton atoms and molecular hydrogen.³ The measurements involving krypton are described in Appendix B. It should be noted that this technique is simple, selective, and generally applicable.

C. Multiquantum excitation processes

Multiquantum processes have demonstrated their utility for the excitation of states in the 10-20 eV range.¹ The details of our estimates for a wide range of materials have been given elsewhere.^{1,2} It is encouraging to note, however, that in two cases (H_2 and Kr) for which we have been able to measure absolute values of the coupling coefficient, the measured and estimated magnitudes agree to well within a factor of two. The measurements dealing with krypton appear in Appendix B; the corresponding discussion of hydrogen is given in Appendix C.

Molecular systems can exhibit complicated patterns of dissociation as a result of multiquantum excitation. Since certain diatomics such as H_2 , CO, and N_2 have properties that may be suitable for optical conversion to short wavelengths, studies on these systems are in progress and interesting results have been obtained in CO at 193 nm. In this case, isotopically selective two quantum dissociation was observed. In was, in addition, possible to detect the influence of spin-exchange electron collisions on excited atomic carbon atoms. From these results we have concluded that a selective analysis of electron collisions can be made by simple optical means. Electron collisions may, of course, represent a limiting mechanism in media that optically upconvert to the X-ray region. Appendix D contains the detailed discussion of the results on carbon monoxide.

Higher order processes (three and four quantum) have also been considered. Three quantum excitation at 248 nm of argon atoms has been observed.⁴ Four quantum excitation of Rb core excited states⁵ has also been estimated, since the Fano minimum⁶ in that case falls very close to the available KrF* wavelength (248 nm). In the case of rubidium, the

Rydberg scaling law previously estimated² was assumed to derive a cross section of $\sim 10^{-17}$ cm² at an optical intensity of $\sim 4 \times 10^6$ W/cm². The ultraviolet laser bandwidth used in this estimate was 150 MHz, the value observed in our system. Further details of this calculation appear in Appendix E.

Experimental measurements of both photoionization and multi-quantum excitation in Rb at 248 nm will be performed shortly under atomic beam conditions. A beam machine is now operating in which high quality atomic beams of both Na and Rb have been generated at $\sim 10^7$ cm⁻³ density. The beam current to background, as detected by a hot wire, has been measured to be well over one hundred.

III. Conclusions

Multi-quantum processes in the ultraviolet can be used to generate copious inversion densities in the 10-20 eV range. A key factor in this application of the rare gas halogen technology is the development of an ultrahigh spectral brightness source with output parameters approaching the fundamental limits. Such a source has been implemented.

On the basis of the improved technology now available and the experience gained through the examination of two- and three-quantum processes, it is concluded that these nonlinear methods of excitation can be successfully extrapolated to excitations in the 20-50 eV range. Excited inner-shell configurations lie in this spectral region.

As noted in earlier discussions,² an essential element in the development of laser methods for excitation of excited atomic inner-shell configurations centers on the suppression of unwanted reactions leading to losses into modes of ionization. It is here that dynamical cancellations such as that arising

in the formation of the Fano minimum can play a critical role. Several systems exhibit this feature. The consequences of the coincidence of the Fano minimum in Na with the wavelength from the ArF* source at 193 nm show that this process should be suppressed by a factor of $\sim 10^6$, with a cross section $\sigma_{pi} \sim 10^{-23} \text{ cm}^2$. A similar circumstance is present for Rb at 248 nm. Other loss mechanisms, such as two quantum photoionization, appear to be sufficiently weak at currently available intensities.

The use of Rydberg states features in three important ways for the laser production of inner-shell excitations.² First, they have greatly suppressed Auger rates, and considerable evidence supports the conclusion that a substantial number of these states decay primarily through radiative channels; second, the excited levels photoionize very weakly; and third, it appears that a coherent amplitude can be constructed which enables the large transition moments characteristic of Rydberg levels to enormously enhance the multiphoton coupling. We plan to test the features in the near future with experiments on Rb at 248 nm.

IV. References

1. W. K. Bischel, J. Bokor, D. J. Kligler, and C. K. Rhodes, IEEE J. Quantum Electron. QE-15, 380 (1979).
2. C. K. Rhodes, "Laser Excitation of Inner-Shell Atomic States by Multiquantum Processes," Research Proposal to Office of Naval Research, submitted July, 1978; R. T. Hawkins and C. K. Rhodes, "Laser Excitation of Inner-Shell Atomic States by Multiquantum Processes," Research Proposal to Office of Naval Research, submitted May, 1979.
3. D. J. Kligler, J. Bokor, and C. K. Rhodes, "Collisional and Radiative Properties of the H_2 E,F $^1\Sigma_g^+$ State," Phys. Rev. (to be published).
4. J. Bokor, Multiphoton Ultraviolet Excitation of Atoms and Molecules, Thesis, Stanford University, 1979.
5. M. W. Mansfield, Proc. Roy. Soc. (London) A364, 135 (1978); V. Pejčev, D. Rassi, K. J. Ross, and T. W. Ottley, J. Phys. B10, 1653 (1977).
6. J. C. Weisheit, Phys. Rev. A5, 1621 (1972).

V. APPENDICES

APPENDIX A

A tunable, ultrahigh spectral brightness
KrF* excimer laser source

R. T. Hawkins, H. Egger, J. Bokor[†],
and C. K. Rhodes

Department of Physics
University of Illinois at Chicago Circle
P. O. Box 4348, Chicago, Illinois 60680

ABSTRACT

An extremely high spectral brightness KrF* (248 nm) excimer source is described. This instrument combines the property of continuous tunability over the full gain profile with the following output pulse characteristics: pulse energy ~ 60 mJ, pulse duration ~ 10 nsec, spectral width 150 ± 30 MHz, absolute frequency control to within 300 MHz, and beam divergence ~ 50 μ rad. Within the uncertainty of measurement, the spectral width of the output

radiation is Fourier transform limited, and the beam divergence corresponds to the diffraction limit of the radiating aperture.

[†]Also affiliated with the Department of Electrical Engineering, Stanford University, Stanford, California 94305/

Rare gas halide excimer sources have proven to be extremely useful in studies of multiphoton processes.¹ Nevertheless, the utility of these sources in such studies could be considerably enhanced. Heretofore, limitations of available sources have been (1) a broad ($\sim 100 \text{ cm}^{-1}$) emission profile, (2) the absence of a convenient, accurate, and reliable tuning system for control of the output wavelength, and (3) an output beam divergence on the order of one hundred times the diffraction limit. Overall, an enhancement of several orders of magnitude in spectral brightness, the key parameter in multiquantum processes, is achievable if the output parameters of these sources are made to conform to the most stringent limits fundamentally possible.

To specifically illustrate the desirability of these improvements, we may briefly consider the optical excitation of an atomic system. Optical excitation rates have been demonstrated² to be proportional to $\Delta\nu_a / (n\Delta\nu_a^2 + \Delta\nu_l^2)^{1/2}$, where $\Delta\nu_a$ is the atomic linewidth, $\Delta\nu_l$ is the laser bandwidth, and n is the number of photons absorbed in the excitation process. Since Doppler-free excitation allows $\Delta\nu_a$ to be taken as the homogeneous width of the atomic transition, which is often $\sim 10^{-3} \text{ cm}^{-1}$, an enhancement in the coupling strength of approximately a factor of 10^5 can be achieved through the reduction of the laser bandwidth to $\Delta\nu_l = \Delta\nu_a$. We note that the typical discharge-pumped rare gas halide excimer laser has a pulse duration of $\sim 10 \text{ ns}$, which corresponds to a Fourier transform limited spectral bandwidth of $\sim 2 \times 10^{-3} \text{ cm}^{-1}$. An additional enhancement in production of excited states may be obtained through reduction of the spatial divergence of the output beam; typical excimer systems operate with a beam divergence of $\sim 3\text{-}5 \text{ mrad}$, while the diffraction limit corresponds to $\sim 30\text{-}50 \text{ } \mu\text{rad}$.

Previous studies^{3,4} have shown that substantial improvement in source properties can be obtained by using the output of a tunable, intracavity etalon line-narrowed, discharge-excited oscillator to injection lock a high-energy, unstable resonator oscillator. The best linewidth reported was $\sim 10^{-1} \text{ cm}^{-1}$ in a beam with a divergence approximately twice the diffraction limit.⁴

In this Letter, we report the properties of a KrF* excimer source with performance parameters which closely approach the fundamental limits governing spectral width, beam divergence, and absolute wavelength control. The basic laser system is illustrated schematically in Fig. (1). The output of a frequency-stabilized, cw dye laser (Coherent 599-21, $\Delta\nu < 5 \text{ MHz}$, $\sim 30 \text{ mW}$ at 500 nm) is pulse amplified in a 3-4 stage XeF* pumped (30-50 mJ at 351 nm) dye amplifier, producing a 7 ns visible pulse with an energy of $\sim 3 \text{ mJ}$ at a repetition rate up to 1 sec^{-1} (limited by thermal recovery time in the dye cuvettes). The linewidth of this visible radiation was examined with a scanning interferometer (Tropel 240) and was found to be $85 \pm 10 \text{ MHz}$. Frequency doubled radiation corresponding to any wavelength within the KrF* gain profile may readily be generated in a temperature-tuned, 90° phase-matched ADP crystal, producing $\sim 5 \text{ ns}$ second harmonic pulses with energy $> 100 \mu\text{J}$. This spectrally narrow ($120 \pm 20 \text{ MHz FWHM}$, Fourier transform limited) second harmonic radiation is subsequently amplified in a single pass through a discharge-pumped KrF* amplifier (Lambda Physik EMG 500) to produce output pulses of $\sim 10 \text{ ns}$ duration and energies up to 60 mJ.

A study of the spatial properties of the 2 cm x 0.5 cm output beam reveal it to have a diffraction limited divergence of $\sim 50 \mu\text{rad}$. We note

that at the peak measured power, ~ 6 MW, focal intensities at 248 nm in excess of 10^{15} W/cm² can be generated with fl optics. In preliminary studies, we have observed optical breakdown in pure helium at pressures above 1.85 bar with a KrF* laser intensity of $\sim 3 \times 10^{14}$ W/cm².

Furthermore, since the frequency of the cw dye laser can be electronically scanned over 1 cm^{-1} , continuously tunable coverage of the ultraviolet radiation over a 2 cm^{-1} interval is readily accomplished. In addition, the dye laser frequency is known to within 300 MHz by interferometric comparison with a stable HeNe laser source.⁵ In our current experiments, we have observed amplification at wavelengths λ_{KrF} in the range $248.2 \text{ nm} < \lambda_{\text{KrF}} < 250.3 \text{ nm}$. In this range, the output pulse energy was observed to monotonically decrease with increasing wavelength. In contrast to previous reports of a strong absorption centered at $\sim 248.8 \text{ nm}$ in both e-beam pumped KrF* amplifiers⁶ and discharge-pumped tunable KrF* lasers,^{3,7} no reduction in output energy was observed at that wavelength in our apparatus.

In order to establish the linewidth of our source, direct interferometry has been used. A 1 GHz FSR Fabry-Perot interferometer was constructed with two dielectric coated mirrors of 98% reflectivity. Analysis shows that this interferometer will exhibit a finesse of ~ 20 for our typical 10 ns pulse duration. The radiation transmitted through this Fabry-Perot was recorded directly on high contrast (Type 47 Polaroid Land) film at $\sim 10 \text{ m}$ from the interferometer, with the result shown in Fig. (2). The dominant ring pattern has a separation to width ratio of 6.5 ± 1.2 , which corresponds to an amplified ultraviolet linewidth $\Delta\nu_{\text{KrF}} = 150 \pm 30 \text{ MHz}$. The subsidiary ring patterns appearing in Fig. (2) may arise from multiple

reflections in beam steering optics between the interferometer and the film, as well as etalon effects elsewhere in the optical system. We observe that this measured linewidth of 150 ± 30 MHz is equivalent, within our experimental uncertainty, to the Fourier transform limited linewidth $\Delta\nu_{\text{SHG}} = 120 \pm 20$ MHz of the second harmonic output of the ADP crystal.

In order to further verify the narrow linewidth of the laser output, a preliminary study of the xenon ($6p[4]_0 + 1S$) two-photon absorption at 249.63 nm was performed under Doppler-free conditions through detection of the resulting ($6s[3/2]_1 + 6p[4]_0$) fluorescence at 828 nm. Upon scanning the KrF* source frequency across the resonance, a single feature was observed, centered at $80118.73 \pm 0.10 \text{ cm}^{-1}$, with a width of ~ 450 MHz (FWHM, at the KrF* frequency), as shown in Fig. (3). These measurements were made at a xenon pressure of 0.25 torr and an ultraviolet intensity of $\sim 5 \times 10^5 \text{ W/cm}^2$. Although this width is a factor of three less than the Doppler width, the resonance is still a factor of ~ 3 broader than would be expected with a source linewidth of ~ 150 MHz. Since we experimentally determined the pressure broadening coefficient of this xenon two quantum transition to be $25 \pm 15 \text{ MHz/torr}$, which gives a minor contribution to the linewidth at 0.25 torr, we have concluded that unresolved isotope splittings (five xenon isotopes with natural abundances $> 3\%$) lead to the observed width. An estimate⁸ of the isotope shift for such a ($5p^6 \rightarrow 5p^5 6p$) transition yields a relative shift of ~ 50 -100 MHz for two Xe isotopes whose masses differ by 1 amu. This estimate agrees well with both the linewidth of the observed absorption, and the absence of additional resonances within ± 6 GHz of the one observed.

In conclusion, we state that an ultrahigh spectral brightness ultraviolet source, continuously tunable over the KrF* excimer band, has been constructed with the following demonstrated performance characteristics: $P \sim 6$ MW, $\Delta\nu_{\text{KrF}} = 150 \pm 30$ MHz, pulse repetition rate $\sim 1 \text{ sec}^{-1}$, and divergence $\theta_D = 50 \mu\text{rad}$.

This work was supported by the Office of Naval Research, the Department of Energy through agreement ED-78-S-08-1603, and the National Science Foundation through grant NSF78-27610. One of us (Bokor) also acknowledges support by the Fannie and John K. Hertz Foundation.

REFERENCES

1. W. K. Bischel, J. Bokor, D. J. Kligler, and C. K. Rhodes, *IEEE J. Quantum Electron.* QE-15, 380 (1979); C. K. Rhodes and P. W. Hoff in Excimer Lasers, edited by C. K. Rhodes (Springer-Verlag, Berlin, 1979) p. 175.
2. B. R. Marx, J. Simons, and L. Allen, *J. Phys. B* 11, L273 (1978).
3. J. Goldhar and J. R. Murray, *Opt. Lett.* 1, 199 (1977).
4. J. R. Murray, J. Goldhar, and A. Szöke, *Appl. Phys. Lett.* 32, 551 (1978).
5. F. V. Kowalski, R. T. Hawkins, and A. L. Schawlow, *J. Opt. Soc. Am.* 66, 965 (1976).
6. A. M. Hawryluk, J. A. Mangano, and J. H. Jacob, *Appl. Phys. Lett.* 31, 164 (1977).
7. T. R. Loree, K. B. Butterfield, and D. L. Barker, *Appl. Phys. Lett.* 32, 171 (1978).
8. I. I. Sobel'man, Introduction to the Theory of Atomic Spectra (Pergamon Press, New York, 1972).

FIGURE CAPTIONS

1. Ultraviolet laser system illustrating the cw dye laser, the dye amplifier chain, the ADP doubling crystal, and the final KrF* amplifier stage.
2. Transmission of 1 GHz FSR Fabry-Perot at 248 nm, recorded on high contrast film.
3. Observed fluorescence at 828 nm following two-photon absorption in $\text{Xe}(6p[3/2]_0 + 1S)$ at 249.63 nm, at 0.25 torr Xe pressure and $\sim 5 \times 10^5$ W/cm^2 KrF* intensity (unfocussed).

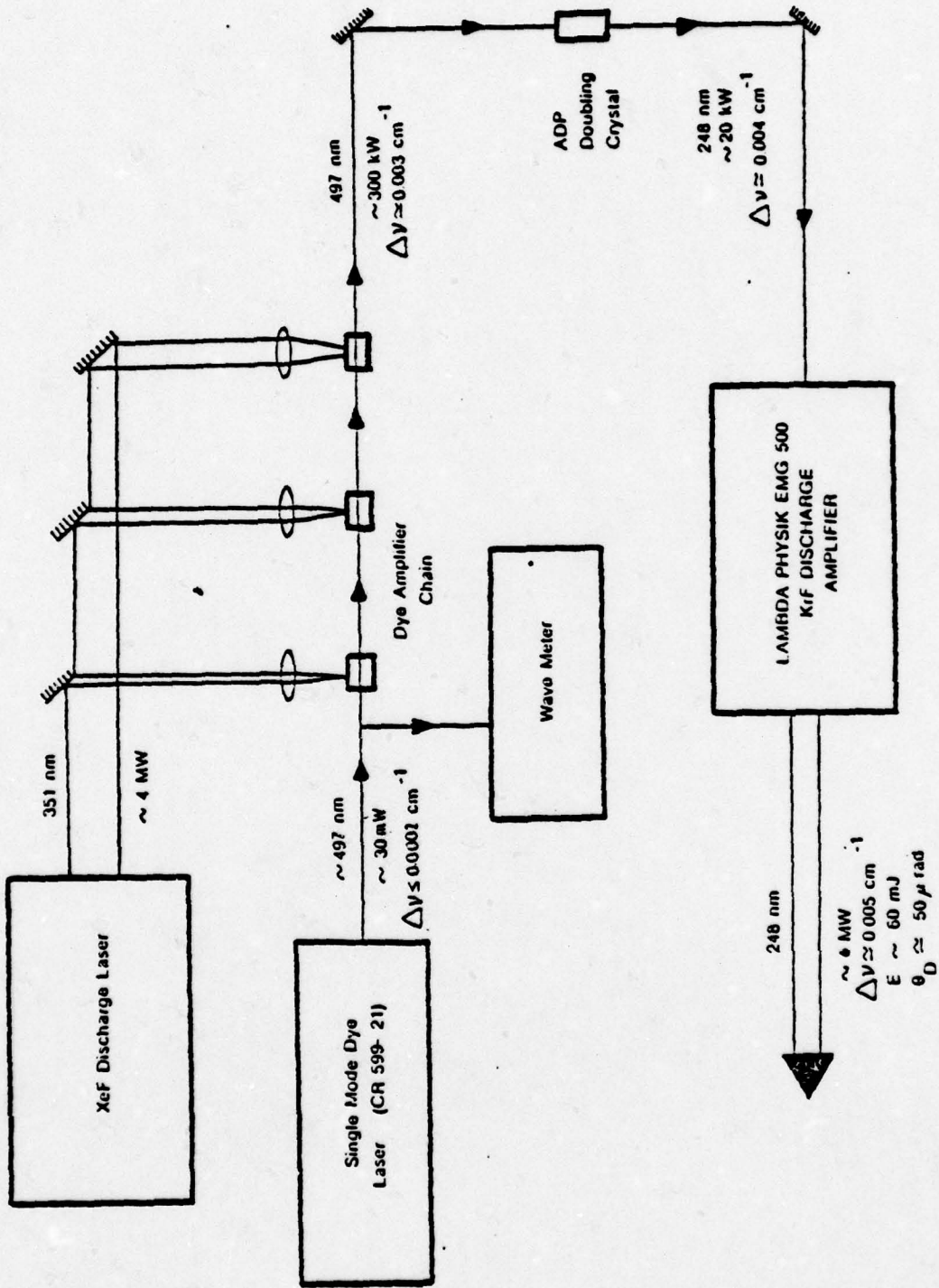


Figure 1

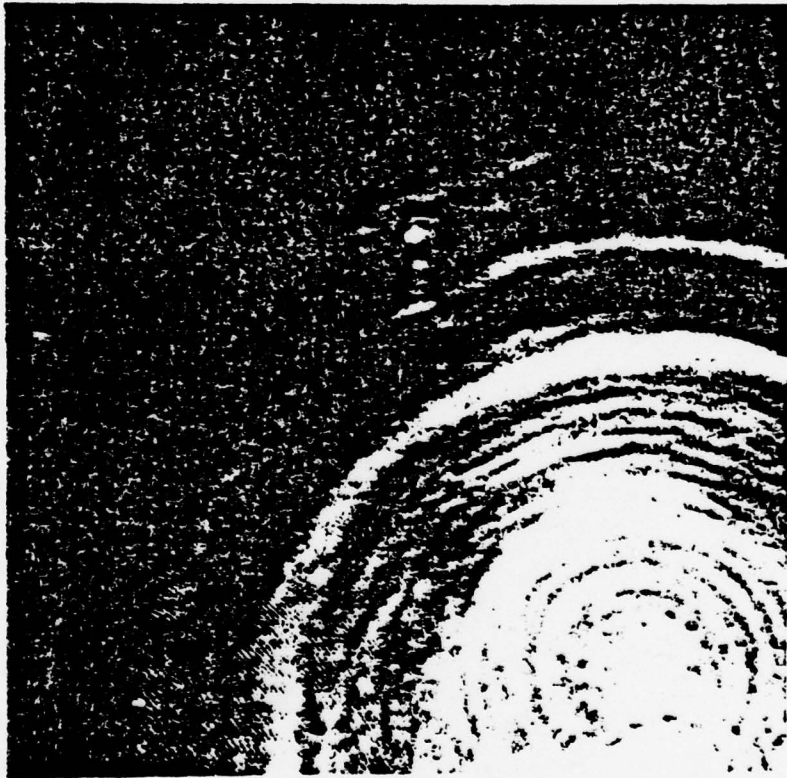


Figure 2

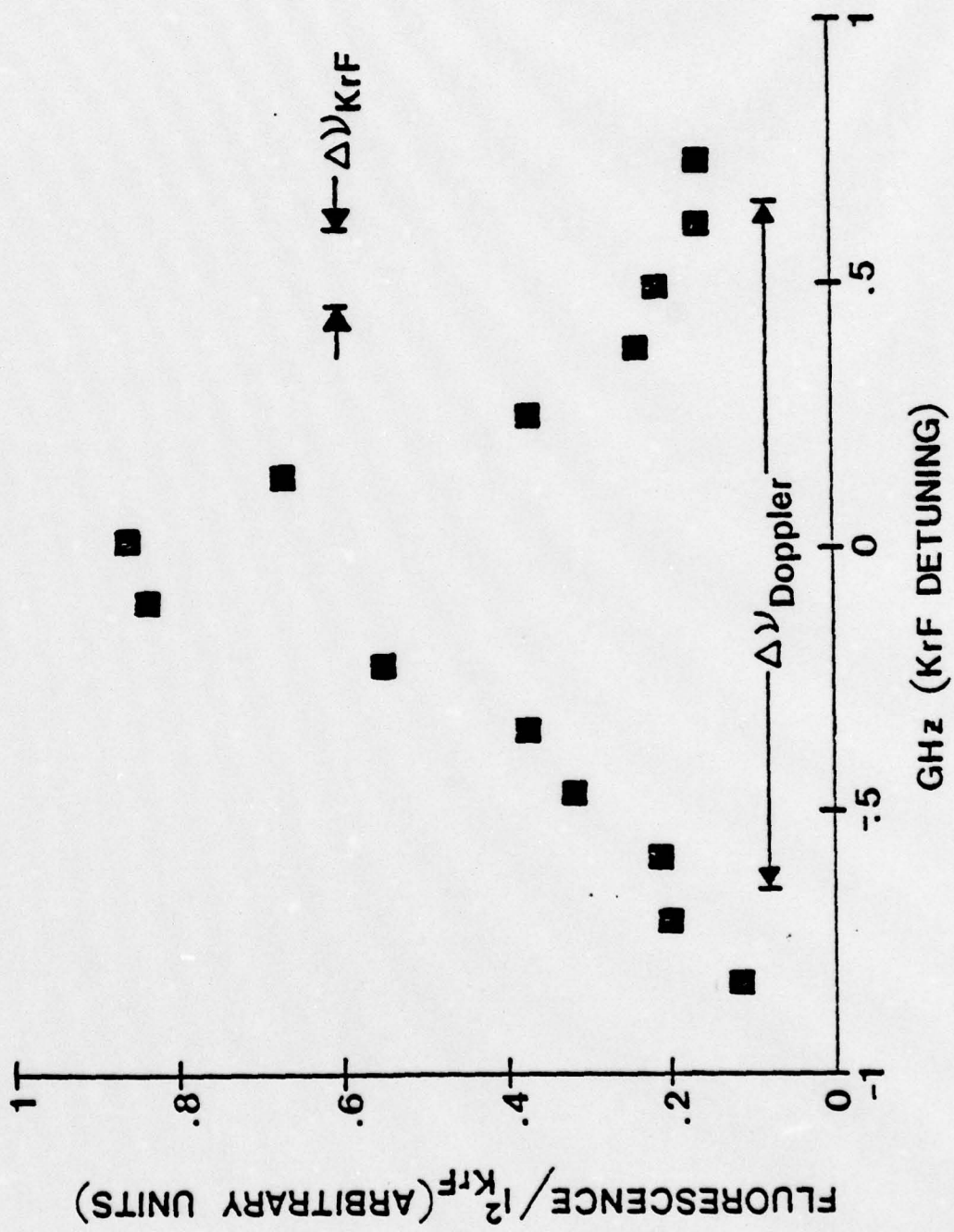


Figure 3

APPENDIX B

Multiphoton ultraviolet spectroscopy
of some 6p levels in krypton

Jeffrey Bokor[†],
Department of Electrical Engineering
Stanford University
Stanford, California 94305

Joshua (Yevsey) Zavelovich and Charles K. Rhodes
Department of Physics
University of Illinois at Chicago Circle
P. O. Box 4348, Chicago, Illinois 60680

(Received:

ABSTRACT

The observation of two-photon excitation of selected 6p levels in krypton atoms using tunable ArF* laser radiation at 193 nm is reported.

Using time resolved detection of visible fluorescence lines in the vicinity of 430 nm arising from 6p-5s transitions, radiative lifetimes for the $6p[4]_0$ and $6p[\frac{3}{2}]_2$ states of 123 ± 5 nsec and 115 ± 5 nsec, and collisional self-quenching rates of $(4.1 \pm 0.4) \times 10^{-10} \text{ cm}^3/\text{sec}$ and $(6.7 \pm 0.7) \times 10^{-10} \text{ cm}^3/\text{sec}$, respectively, have been determined. By carefully measuring the visible fluorescence intensity as a function of incident laser intensity, the photoionization cross section of the $6p[\frac{3}{2}]_2$ state has been established as $(3.2 \pm 2.0) \times 10^{-19} \text{ cm}^2$. The two-photon transition rates for both states have been theoretically calculated and good agreement is found with measurements of the relative excitation rates for the two transitions.

[†]Present address: Department of Physics, University of Illinois at Chicago Circle, P. O. Box 4348, Chicago, Illinois 60680.

By acceptance of this article, the publisher and/or recipient acknowledges the U. S. Government's right to retain a nonexclusive, royalty-free license in and to any copyright covering the article.

Note: This notation need not appear in the published article.

I. INTRODUCTION

Multiphoton spectroscopy is an extremely useful technique for studying the properties of excited states in atoms and molecules. Given an intense laser source, the technique allows one to obtain highly detailed information on states lying at excitation energies two, three, or more times the available laser photon energy. For example, with visible dye lasers, a wealth of information has been amassed on the properties of high-lying Rydberg states in atoms,¹ including level positions, fine structure and hyperfine structure, Zeeman and Stark effects, collisional mixing, and collisional quenching. Using carbon dioxide infrared lasers, high resolution measurements have yielded accurate level positions for excited vibrational states of symmetric-top molecules, as well as pressure broadening and pressure shift data and vibrational transition matrix elements.² The recent advent of intense, tunable, ultraviolet excimer lasers has opened up a new region of the spectrum to detailed spectroscopic investigation via multiphoton absorption processes. Such laser systems have already been used to study collisional and radiative properties of the E,F $1\Sigma_g^+$ state in molecular hydrogen,³ and isotopic effects in two-photon photolysis of CO molecules.⁴ A number of other multiphoton spectroscopic and photochemical studies have also been carried out^{5,6} utilizing untuned excimer lasers.

In this study, we have used a tunable ArF* laser, operating at 193 nm, to excite discrete fine structure components of the $4p^5 6p$ configuration in Kr by a two-photon absorption process. The population densities of the excited states were monitored via the $6p-5s$ fluorescence

signals at ~ 430 nm. Using time-resolved spectroscopy, we have directly measured radiative decay lifetimes. Our results are compared with theoretical calculations,^{7,8} as well as other experimental measurements.^{7,9} In addition, we have obtained data on collisional deactivation of the excited atoms by ground state krypton atoms. Our results are qualitatively comparable with those of Chang et al.,¹⁰ who studied collisional deactivation of 5p states in krypton in collisions with argon atoms.

As discussed in Refs. 3 and 5, often there is an important additional loss channel for electronically excited atomic and molecular systems excited by multiphoton ultraviolet absorption processes. This is due to excited state photoionization by the intense ambient radiation field. As has been demonstrated in molecular hydrogen,³ this process may be studied in detail to yield numerical values for excited state photoionization cross sections. In this manner, we have measured the cross section for photoionization of the 6p state in krypton at 193 nm. Hyman¹¹ has calculated photoionization cross sections for the 5p and 5s states in krypton and the 4p and 4s states in argon, while Dunning and Stebbings¹² have made measurements of the photoionization cross sections for metastable krypton ($5s \ ^3P_{0,2}$) and argon ($4s \ ^3P_{0,2}$) atoms. Our data for the 6p state in krypton may be qualitatively compared with these other results. A quantum defect model of atomic photoionization¹³ may be used to estimate directly the 6p photoionization cross section. We also note that Stebbings, Dunning, and Rundel¹⁴ used a two-photon ionization technique to study photoionization of He($np \ ^1,3P$) atoms which is, in many respects, quite similar to the one used here.

II. EXPERIMENTAL TECHNIQUE

The experimental arrangement used here is identical to that used in several similar studies.³⁻⁵ The output of a UV-preionized, discharge excited, rare-gas-halogen laser was focused by a 90 mm focal length calcium fluoride lens into a stainless steel cell containing the sample under study. Cell pressure measurements were made using a capacitance manometer. The cell was capable of withstanding absolute pressures of up to 4 atmospheres. Fluorescence was collected at right angles to the laser propagation direction by an f 1 magnesium fluoride lens and imaged onto the slit of a 0.3 meter spectrometer equipped with an optical multichannel analyzer (OMA). For visible fluorescence detection, the spectrometer was equipped with a 1200 groove/mm grating blazed at 500 nm. The OMA was interfaced to a PDP 11/34 computer which was used for the data reduction and analysis. Time resolved spectroscopic measurements were performed by replacing the OMA detector with a variable slit and a photomultiplier tube, converting the spectrometer to a standard monochromator configuration. The photomultiplier signal was processed by a transient digitizer which was also interfaced to the computer.

The ArF* laser was line-narrowed and tuned by means of two high-quality fused silica prisms inserted in the laser cavity.¹⁵ This laser produced pulses of up to 30 mJ in energy at the peak of the tuning curve, with a 13 ns pulse duration. The laser bandwidth was 0.1 nm and the effective tuning range was from 192.7 nm - 194.0 nm. The laser wavelength and linewidth was monitored during the experiments by a second 1 meter spectrometer/OMA combination. Wavelength calibration was conveniently provided by the O₂ Schumann-Runge absorptions.¹⁶

III. TWO-PHOTON EXCITATION ESTIMATES

Fig. 1 shows a partial energy level diagram for krypton, indicating the states which are involved in this experiment. Three sublevels of the $4p^5 6p$ configuration lie within the tuning range for two-photon excitation by the ArF* laser: namely $[4]_0$, $[\frac{3}{2}]_2$ and $[\frac{3}{2}]_1$. Here we use the $j\ell$ coupling scheme notation, in which the orbital angular momentum $\vec{\ell}$ of the excited electron is strongly coupled to the total angular momentum \vec{j} of the core, producing a resultant angular momentum \vec{k} . The spin \vec{s} of the excited electron is weakly coupled with \vec{k} to give the total angular momentum \vec{J} . Terms are designated by $n\ell [k]_J$ or $n\ell' [k]_J$, corresponding to the $^2P_{1/2}$ and $^2P_{3/2}$ core states, respectively. These states may decay radiatively to $5s$ and $5s'$ states, emitting visible radiation.

Using the perturbation theory technique described in Ref. 5, we may estimate the two-photon transition probabilities for each of these three transitions. We write the two-photon absorption parameter α for light at frequency ν with intensity I

$$\alpha = \frac{\sigma}{I} = \frac{(2\pi)^3}{\hbar c^2} \nu |M_{fg}|^2 g(\nu) \quad (1)$$

Appearing in (1) are the lineshape factor $g(\nu)$, which contains the line-width of the transition, and the two-quantum matrix element M_{fg} , which is written in the form

$$M_{fg} = 2 \sum_k \frac{\langle f | \hat{\epsilon} \cdot \vec{u} | k \rangle \langle k | \hat{\epsilon} \cdot \vec{u} | g \rangle}{E_{kg} - h\nu} \quad (2)$$

In this expression $\hat{\epsilon}$ denotes the polarization of the optical wave, $\vec{\mu}$ represents the electric dipole operator, and g , k , and f denote the ground, intermediate, and final states, respectively.

The laser output may be taken to be linearly polarized, due to the presence of several Brewster angle reflecting surfaces within the laser cavity. We now factor the dipole matrix elements appearing in (2), using the Wigner Eckart theorem,¹⁷ in order to derive angular momentum selection rules. First consider the matrix element

$$\langle k | \hat{\epsilon} \cdot \vec{\mu} | g \rangle = (-1)^{J_k - M_k} \langle \gamma_k J_k || \mu || \gamma_g J_g \rangle \begin{pmatrix} J_k & 1 & J_g \\ -M_k & 0 & M_g \end{pmatrix} \quad (3)$$

Here, the ground state is 1S_0 , hence $J_g = M_g = 0$. From the properties of the 3-j symbols,¹⁷ we immediately derive the selection rules $M_k = 0$, $J_k = 1$. With a similar factorization of the matrix element $\langle f | \hat{\epsilon} \cdot \vec{\mu} | k \rangle$, we obtain the selection rules on the final state quantum numbers $M_f = 0$, $J_f = 0, 2$. The transition to $J_f = 1$ is forbidden, since

$$\begin{pmatrix} 1 & 1 & 1 \\ 0 & 0 & 0 \end{pmatrix} = 0 \quad (4)$$

Within the electric dipole approximation, these selection rules hold rigorously, regardless of how the summation in (2) is performed. We, therefore, expect to observe no direct excitation of the $6p[\frac{3}{2}]_1$ state by the linearly polarized laser radiation. With a circularly polarized, or unpolarized laser, of course, this state may also be excited.

In order to estimate transition strengths for the $6p[4]_0$ and $6p[\frac{3}{2}]_2$ states, we use the "single-path approximation", in which only one dominant intermediate state is considered, and the sum in expression (2) collapses to a single term. The appropriate state is $5s[\frac{3}{2}]_1$, which is the lowest excited state in Kr with the appropriate parity and total angular momentum. The dipole matrix element for the $5s[\frac{3}{2}]_1 - 4p^6(^1S_0)$ resonance transition may be derived from the oscillator strength, $f=0.219$, measured¹⁸ by Irwin *et al.* The matrix elements for the $6p[4]_0 - 5s[\frac{3}{2}]_1$ and $6p[\frac{3}{2}]_2 - 5s[\frac{3}{2}]_1$ transitions are obtained by using our measured values for the $6p[4]_0$ and $6p[\frac{3}{2}]_2$ radiative lifetimes (see section IV) and previously measured radiative branching ratios.¹⁹ The lineshape factor $g(\nu)$ may be written as^{5,20}

$$g(\nu) = \frac{0.939}{(2\Delta^2 + \Delta\nu_D^2)^{\frac{1}{2}}} \quad (5)$$

at linecenter, if the laser spectral intensity may be assumed to be gaussian, and Δ and $\Delta\nu_D$ are the laser linewidth and transition Doppler width (FWHM) respectively. Using our measured laser linewidth of 25 cm^{-1} , and the intermediate state detuning value of $29,000 \text{ cm}^{-1}$, we obtain the two-photon coupling parameters shown in Table I.

IV. EXPERIMENTAL RESULTS

In spite of the rather large bandwidth of our laser excitation source (25 cm^{-1}) it was possible to obtain completely selective excitation of the $6p[4]_0$ and $6p[\frac{3}{2}]_2$ states. As predicted in section III, no excita-

ion of the $6p[\frac{3}{2}]_1$ state was detected. Laser excitation spectra for the $6p[\frac{3}{2}]_0$ and $6p[\frac{3}{2}]_2$ states are shown in Fig. 2 for a Kr pressure of 26 torr. These plots represent time integrated, fluorescence emission signals at 437.6 nm and 427.4 nm, respectively. The secondary peaks appearing in both spectra arise due to collisional intramultiplet energy transfer. The peak in Fig. 2(b) appears red shifted because it is off in the wing of the laser tuning range.

The time dependence of these emissions was investigated in order to extract radiative lifetimes and collisional quenching data. The laser frequency was adjusted to line center for the transition under study, and the monochromator was tuned to the appropriate visible emission wavelength. The decay rate for the visible fluorescence was then measured as a function of Kr pressure for pressures in the range 0-5 torr. The data obtained are shown in Fig. 3. For each data point in Fig. 3, the decay signals were averaged over 50 laser shots, and the decay rates obtained from a linear least-squares fit to the log of the averaged fluorescence signal. Good fits were obtained using a single exponential decay curve. The pseudo first-order fluorescence decay rate is given by

$$-\frac{1}{t} \ln[N(t)/N(0)] = (\tau_{\text{rad}}^{-1} + k_q [\text{Kr}]) \quad (6)$$

Here, $N(t)$ is the number of excited atoms, τ_{rad} is the radiative lifetime of laser excited level, and k_q is the collisional self-quenching rate. The solid lines in Fig. 2 are linear least-squares fits of the data to the right hand side of Eq. 6. The intercept gives the radiative decay constant τ_{rad}^{-1} , and the slope determines k_q .

The measured radiative lifetimes are listed in Table II, along with other experimental and theoretical results for comparison. For the $6p[\frac{3}{2}]_2$ level, our results are in good agreement with the measurements of Fonseca and Campos,⁷ and the dipole velocity calculation of Gruzdev and Loginov.⁸ For the $6p[\frac{1}{2}]_0$ level, however, we find rather poor agreement with Fonseca and Campos, but again reasonable agreement with the dipole velocity calculation of Gruzdev and Loginov. We find poor agreement in both cases with the measurements⁹ of Delgado, et al. Both previous experimental results utilized electron impact excitation and delayed coincidence detection. In those experiments, it was necessary to include at least two exponential terms in the data fits, in order to account for cascading effects. Due to the selective nature of our optical excitation method, such procedures are unnecessary, and a more direct measurement is obtained. Beyond this, the disagreement between the present results and previous experiments is not explained.

The measured self-quenching rates, obtained from the data in Fig. 3 are: for $6p[\frac{1}{2}]_0$, $k_q = (4.1 \pm 0.4) \times 10^{-10}$ cm³/sec, and for $6p[\frac{3}{2}]_2$, $k_q = (6.7 \pm 0.7) \times 10^{-10}$ cm³/sec. These states may quench by both intramultiplet and intermultiplet relaxation. Due to the presence of the nearby 4d' states (see Fig. 1), these two processes are expected to be competitive.

To our knowledge, these are the first measurements of these particular collisional parameters in krypton. Our results are in qualitative agreement with the results of Chang and Setser²¹ for self-quenching of 3p states in neon, and the results of Chang et al.¹⁰ for quenching of 5p states in krypton by ground state argon atoms. In particular, rate constants for argon quenching of Kr(5p) levels¹⁰ varied over the range of $(0.05 - 3) \times 10^{-10}$

cm³/sec.

In addition to radiative decay and collisional quenching, there is an additional loss mechanism for the two-photon excited atoms, namely photoionization by the excitation laser. As shown in Ref. 3, this process may be exploited to yield numerical values for excited state photoionization cross sections. The method involves making a careful measurement of the dependence of the two-photon excited fluorescence signal, S , on the excitation laser intensity, I . In the absence of photoionization, S is expected to vary as I^2 . The photoionization loss modifies this behavior in a manner which we now describe.

We start from a simple rate equation analysis and ignore ground state depletion. We write

$$\frac{dN^*}{dt} = \frac{\alpha I^2}{\hbar\omega} N_0 - N^* \left(\tau_{\text{rad}}^{-1} + k_q N_0 + \frac{\sigma_{\text{pi}} I}{\hbar\omega} \right) \quad (7)$$

Assuming a square pulse of length T_p , the solution to Eq. (7) is

$$N^*(t) = \frac{\alpha I^2 N_0}{\hbar\omega B} (1 - e^{-Bt}), \quad 0 \leq t \leq T_p \quad (8)$$

where the parameter B is defined as $B \equiv \tau_{\text{rad}}^{-1} + k_q N_0 + \sigma_{\text{pi}} I / \hbar\omega$, and N_0 is the ground state atom density. In many cases, the steady state approximation $BT_p \gg 1$ holds, and we obtain

$$N^* = \frac{\alpha I^2}{\hbar\omega} N_0 \left(\tau_{\text{rad}}^{-1} + k_q N_0 + \frac{\sigma_{\text{pi}} I}{\hbar\omega} \right)^{-1} \quad (9)$$

Since the fluorescent signal S is directly proportional to N^* , we see that the expected quadratic behavior of the fluorescent signal with I

will saturate and go over to a linear behavior when

$$I > \frac{h\nu}{\sigma_{pi}} (\tau_{rad}^{-1} + k_q N_0) \quad (10)$$

We rewrite Eq. (9) in the form

$$\frac{I}{N^*} = mI^{-1} + \beta \quad (11)$$

and notice that

$$\sigma_{pi} = \left(\frac{\beta}{m}\right) h\nu (\tau_{rad}^{-1} + k_q N_0)^{-1} \quad (12)$$

The parameters β and m are derived from the experimentally measured dependence of the visible fluorescence signal S on the laser intensity I , and τ_{rad} and k_q have been experimentally determined as well, as described above. We, therefore, obtain an experimental value for the cross section for phototization of the two-photon excited level, at the wavelength of the excitation laser. Note that neither the absolute number of excited atoms produced, nor a value for the two-photon coupling parameter α are needed for this measurement. These parameters cancel out in the ratio β/m .

This procedure was carried out for $6p(\frac{3}{2})_2$ level in krypton at 5 torr, and the results are shown in Fig. 4. The experimental points are plotted in the form of Eq. 11, and the solid line in the figure is a linear least-squares fit to the data. The result obtained by substi-

tuting the appropriate values into Eq. 12 is $\sigma_{pi} = (3.2 \pm 2.0) \times 10^{-19}$ cm². The major source of uncertainty in this experiment arises from the conversion of the measured laser output energy to the actual intensity at the laser focus. Since the laser output contains a large number of transverse modes, geometrical optics was used to estimate the dimensions of the focal spot. Most of our stated experimental uncertainty arises from uncertainty in this calculation. Additional uncertainties arise from the departure of the laser pulse shape from the square form assumed in the analysis of Eqs. 8 - 12, and statistical fluctuation in the data itself.

Photoionization of excited states in the rare gases has recently begun to receive attention in connection with the dynamics of rare-gas-halogen and rare-gas dimer laser systems. Hyman's calculations¹¹ for the first s and p excited states in krypton and argon indicate that losses due to the p level photoionization channel in these laser systems is significant. The experimental results of Dunning and Stebbings¹² support this theoretical result.

We know of no detailed calculations or other experimental results for photoionization of the 6p state in krypton. We may, however, compare our results with a simple quantum-defect approximation.¹³ This approximation method has been applied²² to a variety of cases of excited state photoionization for which experimental data already exist, including the rare gases.^{12,14} Excellent agreement is found, considering the simplicity of the model.

We write the photoionization cross section for a given atomic level as²²

$$\sigma = \frac{8 \times 10^{-18} \text{ cm}^2}{Z \left(\frac{IP}{Ry} \right)^4 \left(\frac{h\nu}{IP} \right)^3} \quad (13)$$

In this expression, Z represents the net charge on the ion, IP denotes the ionization potential for the atomic level in question, $h\nu$ is the incident photon energy, and Ry is the Rydberg constant. Using this formula we obtain the cross section for photoionization of the $6p$ level in krypton at $\lambda = 193.5 \text{ nm}$ as $\sigma_{pi} = 1.8 \times 10^{-19} \text{ cm}^2$, which is in good agreement with the experimentally determined value.

With the important loss mechanisms characterized, it is now possible to test the theoretical two-photon absorption rates calculated in section III against the observed signal strengths. Although our fluorescence detection sensitivity was not calibrated absolutely, we may compare the relative excitation strengths. At 9.5 torr pressure, the ratio of 437.6 nm fluorescence intensity to 427.4 nm fluorescence intensity when the $6p[4]_0$ and $6p[3]_2$ levels were excited at line center, respectively, was determined as 0.45. Using the two-photon coupling parameters derived in section III, the measured laser energies of 3.5 mJ and 8.5 mJ, and properly accounting for radiative/nonradiative branching and photoionization using our measured parameters (we assume equal photoionization cross sections for $6p[3]_2$ and $6p[4]_0$), we arrive at the predicted ratio of 0.42, in good agreement with the experimental value.

V. CONCLUSIONS

Several multiphoton absorption processes have been observed in krypton atoms using ArF* laser excitation at 193 nm. Since the ArF* laser was tunable, a detailed spectroscopic investigation of the $6p[4]_0$ and $6p[\frac{3}{2}]_2$ states in krypton could be performed. These measurements furnished radiative lifetimes and collisional quenching rates for both states as well as the photoionization cross section of the $6p[\frac{3}{2}]_2$ state at 193 nm. The relative two-photon excitation rates for the two states have also been measured.

The results on radiative lifetimes are compared with other experimental and theoretical results. For the $6p[\frac{3}{2}]_2$ state, we find agreement with one of two alternative experimental values, while for the $6p[4]_0$ state, we are in clear disagreement with both of the other experimental values. The photoionization cross section determined for the $6p[\frac{3}{2}]_2$ level, when compared with a simple model of atomic photoionization, was found to exhibit good agreement. Finally, the data on the relative two-photon excitation rates conforms well with rates calculated using a single path approximation.

It is clear, from expressions (1) and (5), that an enormous increase in excitation strength is to be gained by further narrowing the laser bandwidth. KrF* laser bandwidths better than 0.1 cm^{-1} have already been achieved²³ using injection locking techniques. ArF* laser linewidths on this order have also been achieved.²⁴ With such a laser, both the two-photon transition, and the photoionization process would saturate at a laser intensity of 10^{10} W/cm^2 with a laser fluence of 3-5 J/cm^2 . Such

conditions would result in essentially full ionization of a sample of krypton atoms and plasma densities of the order of 10^{16} cm^{-3} may be readily achieved in this manner.

ACKNOWLEDGEMENTS

The authors wish to thank D. L. Huestis, R. M. Hill, and H. Egger for useful discussions involving various aspects of these experiments. We also thank D. W. Setser for communicating his results to us prior to publication. J. Bokor acknowledges the support of the Fannie and John K. Hertz Foundation. This work was supported by the Department of Energy under Agreement No. ED-78-S08-1603, the National Science Foundation under grant PHY77-01849, and the Office of Naval Research.

REFERENCES

1. For a recent review, see S. A. Edelstein and T. F. Gallagher, *Adv. At. Mol. Phys.* 14, 365 (1978). See also N. Bloembergen and M. D. Levenson, in High Resolution Laser Spectroscopy, K. Shimoda Ed. (Springer, Berlin, 1976) p. 315.
2. J. Bokor, W. K. Bischel, and C. K. Rhodes, *J. Appl. Phys.* 50, 4541 (1979); W. K. Bischel, P. J. Kelly, and C. K. Rhodes, *Phys. Rev. A* 13, 1817 (1976); A13, 1829 (1976).
3. Daniel J. Kligler, Jeffrey Bokor, and Charles K. Rhodes, "Collisional and radiative properties of the H_2 E,F $1^1\Sigma_g^+$ state," (to be published).
4. J. Bokor, J. Zavelovich, and C. K. Rhodes, "Isotope effect in multi-photon ultraviolet photolysis of CO," *J. Chem. Phys.* (to be published, January 1980).
5. William K. Bischel, Jeffrey Bokor, Daniel J. Kligler, and Charles K. Rhodes, *IEEE J. Quantum Electron.* QE-15, 380 (1979).
6. D. J. Kligler, H. Pummer, W. K. Bischel, and C. K. Rhodes, *J. Chem. Phys.* 69, 4652 (1978); W. M. Jackson, Joshua B. Halpern, and Chung-San Lin, *Chem. Phys. Lett.* 55, 254 (1978); A. P. Baronavski, and J. R. MacDonald, *Chem. Phys. Lett.* 56, 369 (1978); J. R. MacDonald, A. P. Baronavski, and V. M. Donnelly, *Chem. Phys.* 33, 161 (1978); V. M. Donnelly, and Louise Pasternack, *Chem. Phys.* 39, 427 (1979).
7. M. V. Fonseca and J. Campos, *Phys. Rev.* A17, 1080 (1978).
8. P. F. Gruzdev and A. V. Loginov, *Opt. Spectrosk.* 38, 1056 (1975).
9. A. Delgado, J. Campos, and C. Sanchez del Rio, *Z. Phys.* 257, 9 (1972).
10. B. Chang, H. Horiguchi, and D. Setser, *J. Chem. Phys.*, (to be published).

11. H. A. Hyman, *Appl. Phys. Lett.* 31, 14 (1977).
12. F. B. Dunning and R. F. Stebbings, *Phys. Rev. A* 9, 2378 (1974).
13. J. A. Gaunt, *Phil. Trans. Roy. Soc. A* 229, 163 (1930); H. A. Bethe and E. Salpeter, *Quantum Mechanics of One and Two Electron Atoms*, (Academic Press, New York, 1957), p. 308.
14. R. F. Stebbings, F. B. Dunning, and R. D. Rundel, *Proc. 4th Int. Conf. on Atomic Physics*, G. zu Putlitz, E. W. Weber, and A. Winnaker, Eds. (Plenum Press, New York, 1975), p. 713.
15. T. R. Loree, K. B. Butterfield, and D. L. Barker, *Appl. Phys. Lett.* 32, 171 (1978).
16. M. Ackerman and F. Biaume, *J. Mol. Spectrosc.* 35, 73 (1970).
17. A. R. Edmonds, *Angular Momentum in Quantum Mechanics*, (Princeton University Press, Princeton, 1960).
18. D. J. G. Irwin, J. A. Kernahan, E. H. Pinnington, and A. E. Livingston, *J. Opt. Soc. Am.* 66, 1396 (1976).
19. W. F. Meggers, T. L. de Bruin, and C. J. Humphreys, *J. Res. Nat. Bur. Stand.* 7, 643 (1931).
20. B. R. Marx, J. Simons, and L. Allen, *J. Phys. B* 11, L273 (1978).
21. R. S. F. Chang and D. W. Setser, *J. Chem. Phys.* (to be published).
22. D. C. Lorents, D. J. Eckstrom, and D. L. Huestis, *SRI International Report MP 73-2* (Menlo Park, California, September, 1973).
23. J. R. Murray, J. Goldhar, and A. Szöke, *Appl. Phys. Lett.* 32, 551 (1978).
24. R. S. Hargrove and J. A. Paisner, "Tunable, efficient VUV generation using ArF-pumped, stimulated Raman scattering in H₂," *Proceeding of the Topical Meeting on Excimer Lasers*, (Optical Society of America, Charleston, 1979).

TABLE I

Estimates of two-photon excitation parameters for 6p states in Kr

state ($n\ell [k]_j$)	wavelength (nm)	μ_1 (debye)	μ_2 (debye)	α (cm^4/W)
$6p[4]_0$	192.75	1.39	0.806	1.31×10^{-31}
$6p[\frac{3}{2}]_2$	193.49	1.39	0.763	1.17×10^{-31}

TABLE II

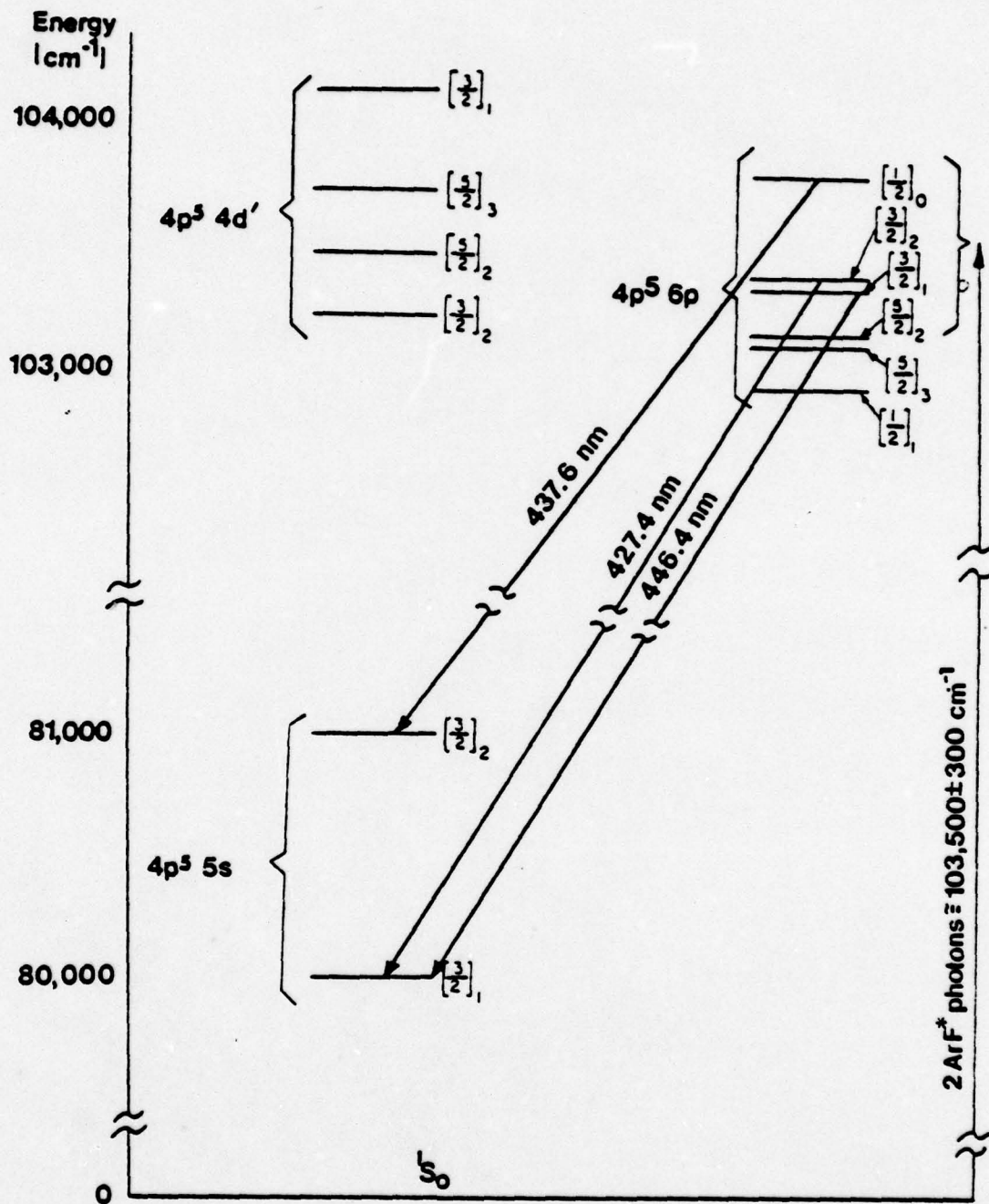
Radiative lifetimes (in nanoseconds) for some $4p^5 6p$ levels in Kr I

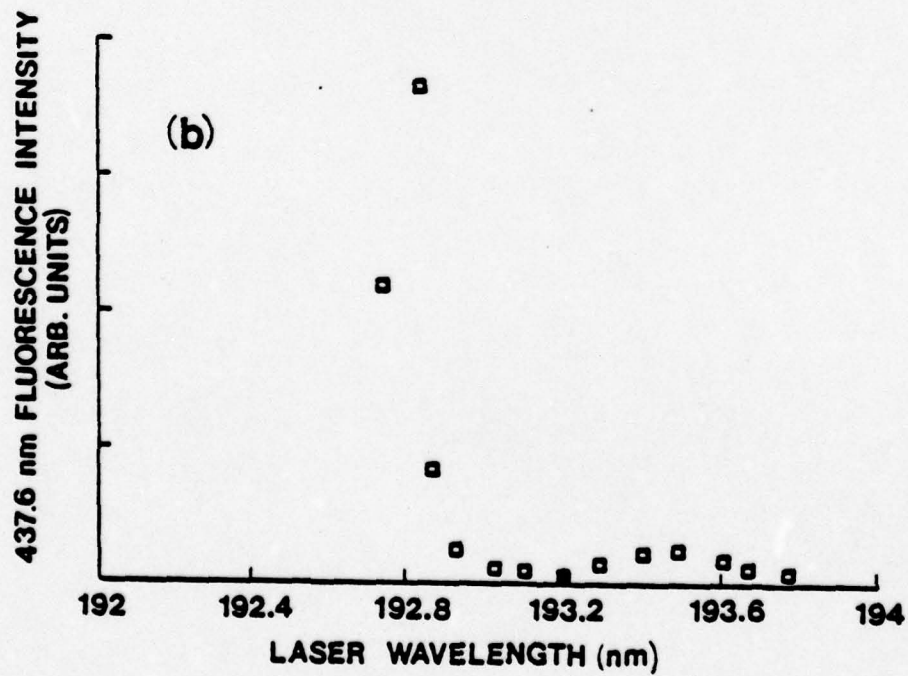
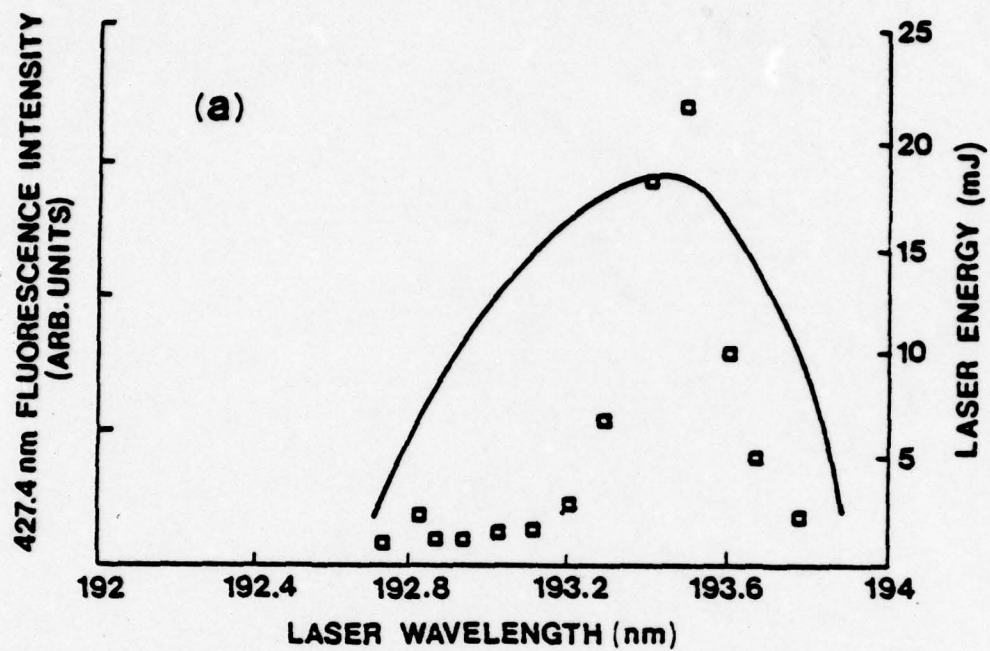
Level	λ (nm)	Experimental Lifetimes			Theoretical Lifetimes		
		This work	Ref. 7	Ref. 8	Ref. 7	Ref. 8 (a)	
					μ_L	μ_V	
$6p[4]_0$	437.6	123 ± 5	72 ± 3	74.3 ± 1	67.3	92.5	131
$6p[\frac{3}{2}]_2$	427.4	115 ± 5	118 ± 3	198 ± 4	80.4	79.8	117

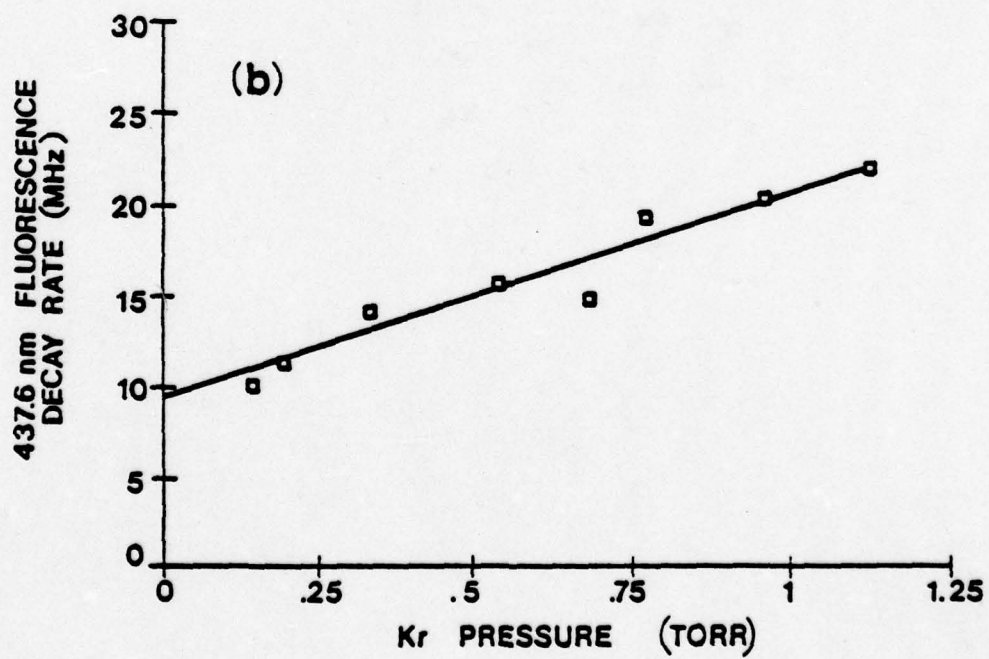
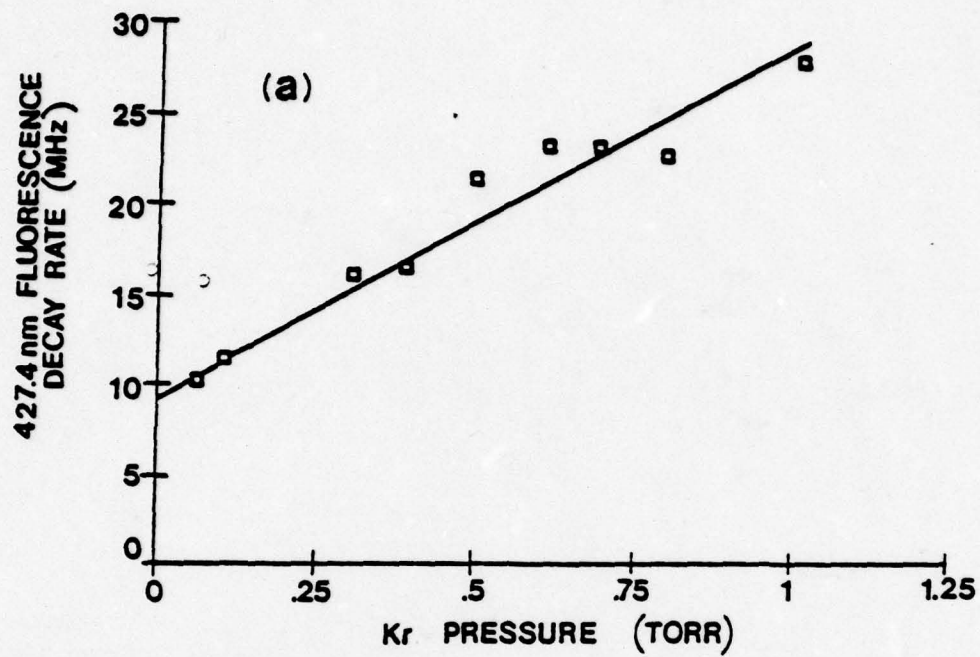
(a) μ_L - results obtained using dipole length integrals. μ_V - results obtained using dipole velocity integrals.

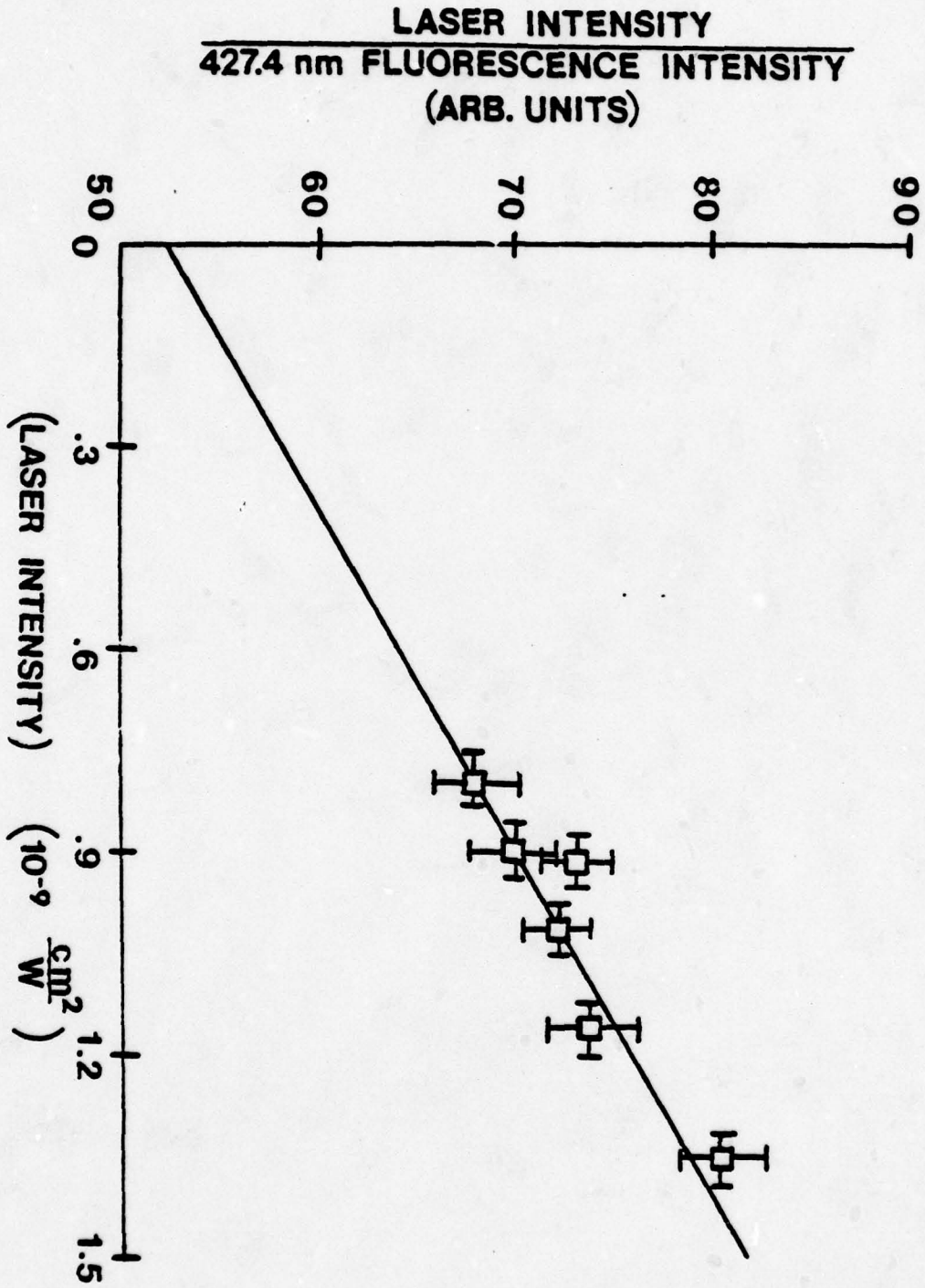
FIGURES

1. Partial energy level diagram for krypton showing states excited by two-photon excitation and some radiative decay transitions of the excited states.
2. Two-photon laser excitation spectra for krypton. (a) 427.4 nm fluorescence from $6p[\frac{3}{2}]_2$. (b) 437.6 nm fluorescence from $6p[\frac{1}{2}]_0$. The solid line in (a) is the laser output energy versus wavelength. Pressure in both cases is 26 torr.
3. Fluorescence decay rates for two-photon excited krypton. The squares are the experimental points. The solid lines are linear least squares fits to the data. (a) 427.4 nm fluorescence from $6p[\frac{3}{2}]_2$ state. (b) 437.6 nm fluorescence from $6p[\frac{1}{2}]_0$ state.
4. Dependence of 427.4 nm fluorescence intensity on laser intensity plotted in the form of Eq. 11. The solid line is a linear least squares fit to the data points.









APPENDIX C

COLLISIONAL AND RADIATIVE PROPERTIES OF THE H_2 E,F $1\Sigma_g^+$ STATE

Daniel J. Kligler[†] and Jeffrey Bokor[‡]
 Department of Electrical Engineering
 Stanford University, Stanford, California 94305

and

Charles K. Rhodes
 Department of Physics
 University of Illinois at Chicago Circle
 Chicago, Illinois 60680

ABSTRACT

Collisional and photoabsorption properties of electronically excited molecular hydrogen are studied by means of selective excitation of the H_2 (E,F $1\Sigma_g^+$) double minimum state. The $v=2$ level of the inner well of the E,F state is populated by two-photon absorption of ArF* laser radiation at 193 nm. Intracavity prisms are used to narrow the laser linewidth and tune the laser to excite single rotational levels selectively. Both H_2 and HD have been excited in this manner, but the D_2 absorption lines are outside the laser tuning range. The population densities of the E,F rovibrational levels are measured by monitoring the near infrared E,F $1\Sigma_g^+ \rightarrow B$ $1\Sigma_u^+$ fluorescent emission. The E,F state radiative lifetime, electronic and rotational collisional relaxation rates, and photoionization cross section at 193 nm are measured. The large electronic quenching cross section ($\sim 100 \text{ \AA}^2$) observed is compared to a Born approximation calculation of inelastic scattering in the H_2 (E,F $1\Sigma_g^+$) system and is found to be due to collisional population of the C $1\Pi_u$ state. Observations of vacuum ultraviolet C $1\Pi_u \rightarrow$

x $^1\Sigma_g^+$ emission support this conclusion. The rotational relaxation cross sections are $\leq 0.2 \text{ \AA}$ for H_2 , but are much larger in HD ($\sim 10 \text{ \AA}^2$).

⁺Present address: Racah Institute of Physics, The Hebrew University,
Jerusalem, Israel

⁺Present address: Department of Physics, University of Illinois at Chicago
Circle, P. O. Box 4348, Chicago, Illinois 60680

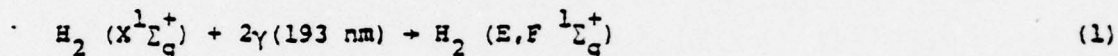
Prepared for the Department of Energy under Agreement No. ED-78-S-08-1603.

By acceptance of this article, the publisher and/or recipient acknowledges the U. S. Government's right to retain a nonexclusive, royalty-free license in and to any copyright covering the article.

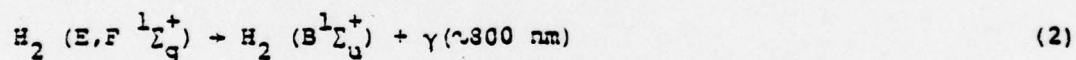
Note: This notation need not appear in the published article.

I INTRODUCTION

In an earlier letter¹, the first selective population of a gerade excited state of H₂, the E,F $1\Sigma_g^+$ state was reported. In that work it was demonstrated that multiphoton absorption of ArF* laser radiation at 193 nm could be used to create substantial populations in states whose excitation energies were far in the vacuum ultraviolet (VUV) - corresponding to single-photon wavelengths below 100 nm. Two-quantum absorption in the reaction



was used to excite the E,F state and its near infrared (ir) fluorescent emission



was monitored to make the first measurements of collisional and radiative properties of that state.

Kinetic studies of the hydrogen molecule are of particular interest and importance because of hydrogen's central position in the theory of molecular physics and quantum chemistry. Molecular hydrogen has been studied extensively from a theoretical point of view, but few experimental data on the collisional properties of the excited states exist because of the difficulty of selective excitation. Therefore, we have here extended and refined the studies of the E,F state discussed in Ref. 1, as well as made further comparisons of our results with theoretical predictions.

This report will present both experimental and new theoretical results concerning the relaxation and photoabsorption properties of the E,F $1\Sigma_g^+$ state. Section II will first discuss the manifold of states excited in these experiments. Section III will outline the experimental apparatus and procedures. Measurements of radiative and collisional electronic relaxation rates of the E,F $1\Sigma_g^+$ state will be reviewed in Section IV, and the mechanism of electronic quenching will be discussed and compared to a Born approximation calculation of the electronic quenching cross section derived here. Section V describes experimental determination of the cross section for three-photon ionization of H_2 , which again is compared with theory. Finally, results obtained using rotationally resolved excitation and fluorescence detection to measure rotational relaxation rates in H_2 and HD are presented in Section VI.

II EXCITATION MANIFOLD

As shown in Fig. 1, E,F ${}^1\Sigma_g^+$ is the first excited gerade singlet state of the hydrogen molecule². This state was originally thought to be two separate states³, until Davidson pointed out its double-minimum character⁴. Kolos and Wolniewicz⁵, Wolniewicz and Dressler⁶, and Alemar-Rivera and Ford⁷ have performed accurate calculations of the E,F potential curves and vibronic states.

The double minimum of the E,F state arises from the avoided crossing of the E $1s\sigma 2s\sigma$ and the F $(2p\sigma)^2$ curves⁵. Thus, in terms of molecular orbitals, the E,F electronic wave function is almost exclusively $1s\sigma 2s\sigma$ in the inner well, while in the outer well it is mostly $(2p\sigma)^2$. At larger internuclear separation, the state has ionic character in the separated-atom representation (correlates to $H^+ + H^-$). However, due to an avoided crossing at large separation, the E,F state dissociates to $H(1s) + H(2s)$.

Two other states are important in these studies, B ${}^1\Sigma_u^+$ and C ${}^1\Pi_u$. The B ${}^1\Sigma_u^+$ state serves both as the dominant intermediate state in two-photon absorption to E,F ${}^1\Sigma_g^+$ and as the final state for near ir emission originating from E,F ${}^1\Sigma_g^+$. At small internuclear separation, B ${}^1\Sigma_u^+$ has $1s\sigma 2p\sigma$ character⁸ while at larger separations the state is mainly ionic and nearly degenerate with E,F. It dissociates to $H(1s) + H(2p)$. The C ${}^1\Pi_u$ state⁹ is almost purely the $1s\sigma 2p\pi$ Rydberg level. In analogy to the degeneracy of the 2s and 2p atomic levels, C ${}^1\Pi_u$ ($2p\pi$) and the E ${}^1\Sigma_g^+$ ($2s\sigma$) inner well of the E,F state are nearly degenerate. The B ${}^1\Sigma_u^+$ and C ${}^1\Pi_u$ states may relax radiatively to the X ${}^1\Sigma_g^+$ ground state in the well-known VUV Lyman and Werner bands, respectively. However, E,F \rightarrow X radiation is

strictly forbidden by the $g \leftrightarrow u$ selection rule (except in the isotopically mixed species, such as HD)¹⁰; thus, the E,F state may radiate only in the near ir to $B \ ^1\Sigma_u^+$, and is consequently quasimetastable.

As we shall discuss later, the ArF laser used in these experiments had an untuned linewidth of $\sim 170 \text{ cm}^{-1}$ centered at 193.4 nm; and by means of an intracavity prism system could be tuned from 192.6 to 194.2 nm. It is thus expected that transitions in the energy range $\sim 103,000$ to $103,800 \text{ cm}^{-1}$ may be excited by two-photon absorption. For the $X \ ^1\Sigma_g^+ \rightarrow E,F \ ^1\Sigma_g^+$ transition in hydrogen, with the $B \ ^1\Sigma_u^+$ dominant intermediate state, and using linearly polarized light, Q branch rotational transitions are generally strongest, though O and S branch transitions are also allowed¹¹. Table I lists the energy ranges for the O, Q and S branch transitions from the lowest three rotational levels (which are populated at 300 °K) of the ground vibrational state of H_2 to the E,F ($v=2$) level. From the energies listed, we expect strong two-photon excitation of several E,F ($v=2$) rotational levels in H_2 , weaker excitation in HD, where the transitions are to the red of the laser line center, and no excitation in D_2 , whose levels are outside the laser's tuning range. Note that all other states in the vicinity of $\sim 12.8 \text{ eV}$ are forbidden for two-quantum excitation from the ground $X \ ^1\Sigma_g^+$ state by either parity, spin, or both; and Franck-Condon factors for absorption to the outer minimum are unfavorable. These points are clearly evident in Fig. 1.

III EXPERIMENT

The experimental apparatus used in this work has largely been described elsewhere^{12,13}. The focused beam of a transverse-discharge-pumped argon fluoride laser (Lambda Physik EMG-500) was used to excite hydrogen samples in the experimental cell. The sample fluorescence following irradiation was collected at right angles to the laser beam. When time-resolved detection was desired, the fluorescent emission was focused onto the photocathode of a RCA C31034A photomultiplier tube¹²; and the output of the tube was recorded by a transient digitizer (Tektronix R7912), which was interfaced to a PDP 11/34 computer. In this case, wavelength discrimination was provided by 10 nm-bandpass interference filters. Better wavelength resolution ($\sim 2 \text{ \AA}$) in detection was achieved, at the expense of temporal information, by using an optical multi-channel analyzer (CMA) to observe the fluorescence spectrum¹³. This apparatus, which was also interfaced to the computer, generated a plot of time-integrated emission intensity versus wavelength, but with lower overall detection efficiency than the photomultiplier system.

The untuned ArF laser emitted 100 mJ pulses of ~ 10 nsec (FWHM) duration in a band about 7 \AA wide. Because of the high gain of the laser medium, the beam was oblong (about 2×0.7 cm) and had divergence ~ 5 mrad. In order to excite single rotational levels of hydrogen selectively, a laser line-narrowing and tuning system of the type first described by Loree, *et al.*,¹⁴ consisting of two intracavity fused silica prisms, was constructed. A slit of adjustable width was placed at the opposite end of the laser cavity from the prisms in order to create a well defined optical axis. With these

modifications, the laser linewidth was reduced to $\sim 1 \text{ \AA}$ (25 cm^{-1}), with a tuning range $\sim 16 \text{ \AA}$, roughly the range of the ArF spontaneous emission. Laser energy near line center (193.4 nm) was between 30 and 50% of the untuned energy, but dropped off to a few percent far in the wings. The laser wavelength was measured by a second OMA, which was calibrated with 0.5 \AA accuracy by means of the dips in the laser emission spectrum due to O_2 absorption lines in the (4,0) vibrational band of the Schumann-Runge system ($\text{B } ^3\Sigma_u^- + \text{X } ^3\Sigma_g^-$)^{14,15,16}.

Using this apparatus, samples of H_2 , HD, and D_2 were irradiated at pressures ranging from 10 mtorr to several atm. As predicted by the spectroscopic data in Table 1, upon irradiation by the untuned laser, strong near ir emissions were observed in H_2 , weaker emissions in HD, and none in D_2 . When the laser was tuned into closer resonance with the HD E,F $^1\Sigma_g^+ + \text{X } ^1\Sigma_g^+$ (2,0) absorption band, ir emissions nearly as strong as those in H_2 were observed. At low laser intensity ($\leq 10^8 \text{ W/cm}^2$), the intensity of the fluorescent signals was determined to vary as the square of the incident laser intensity, the characteristic signature of a two-photon absorption.

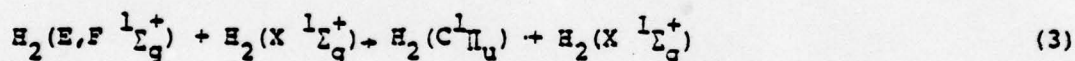
The near infrared emission observed in this manner is attributed to radiative decay from the initially excited $v = 2$ level of the E,F $^1\Sigma_g^+$ state (inner minimum) at $\sim 12.8 \text{ eV}$ to the B $^1\Sigma_u^+$ ($v=0$ and $v=1$) vibrational levels in reaction (2). The approximate wavelengths of the (2,0) and (2,1) emission bands are listed in Table 1. The ratio of observed emission intensity in the H_2 (2,1) band to that in the (2,0) band was found to be 1.4 ± 0.2 , which agrees well with theoretical calculations of the Einstein A coefficients¹⁷ giving $A_{2,1}/A_{2,0} = 1.51$. A rotationally resolved E,F \rightarrow B (2,0) spectrum, observed following excitation of H_2 by the untuned laser is shown in Fig. 2. Emission originating from $J' = 0, 1$, and 2 is observed, but $J' = 3$ is not excited. More than 90% of the emission is

in the P(2) and R(0) lines, indicating that $J' = 1$ is predominantly populated by the untuned laser. The reasons for this behavior, as well as results of excitation using a line-narrowed source, will be discussed in Sec. VI of this paper.

Finally, we should make mention of the vibrational bands that we did not observe in these experiments. Any emissions emanating from $v=0$ or $v=1$ of the inner well of $E,F \ ^1\Sigma_g^+$, which might arise due to vibrational relaxation of $v = 2$, as well as emissions from vibrational levels in the outer well, would be outside the spectral sensitivity of our photomultiplier and were not detected. However, Fink and co-workers¹⁸ have measured vibrational relaxation rates for the B state in HD, and they are approximately two orders of magnitude smaller than the total quenching rate for H_2 ($E,F \ ^1\Sigma_g^+$; $v=2$) measured in Ref. 1. Assuming that vibrational relaxation is not markedly different in the E,F state in H_2 we expect that it does not play an important role in the collisional deactivation of H_2 ($E,F \ ^1\Sigma_g^+$; $v=2$). Similarly, our system was insensitive to emissions terminating on $v'' > 2$. This is not of consequence, since the probabilities for these $(2,v'')$ transitions, calculated from the Franck-Condon factors of Spindler¹⁹, are negligible by comparison with the $(2,1)$ and $(2,0)$ transitions.

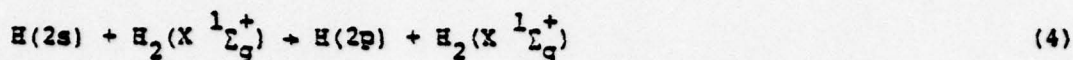
IV MECHANISMS OF ELECTRONIC RELAXATION

In earlier work¹ the decay rate of the H₂ E,F → B fluorescence was measured as a function of pressure, and the radiative and collisional electronic relaxation rates of the E,F state were determined from these data. The E,F state radiative lifetime was found to be 100 ± 20 nsec, in excellent agreement with the calculated value^{17,19} of 90 nsec. The total deactivation rate due to collisions with ground state H₂ molecules was found to be (2.1 ± 0.4) × 10⁻⁹ cm³/sec; with helium as the collision partner, the rate was (0.8 ± 0.4) × 10⁻⁹ cm³/sec. On the basis of the large (nonreactive) helium quenching rate, it was hypothesized that the dominant electronic relaxation channel was



followed by the rapid radiative decay (∼ 1 nsec) of the C ¹Π_u state. In this section we shall calculate the cross section for reaction (3) for comparison with the measured H₂ quenching rate.

The E,F ¹Σ_g⁺ (inner minimum) → C ¹Π_u transition in H₂ is remarkable in its resemblance to the hydrogen atomic 2s → 2p fine structure transition. The potential curves shown in Fig. 1 illustrate that these two molecular states are nearly degenerate in the E,F inner minimum. Thus, the E,F → C transition requires only a small perturbation in the nuclear motion. Calculations by Kolos and Wolniewicz^{5,9} indicate that at the internuclear separations of interest here (∼ 1 Å), the E(2sσ) and C(2pπ) molecular orbitals maintain a strong resemblance to their atomic counterparts. Consequently, scattering in reaction (3) should resemble the atom-molecule interaction



This atomic quenching has been studied both experimentally^{20,21}, and theoretically^{22,23}.

Since the 2s and 2p states of hydrogen are connected by a strong dipole moment ($\mu = 3ea_0$), while ground-state H_2 has a permanent quadrupole moment, a dipole-quadrupole potential is used for the transition Hamiltonian for reactions (3) and (4). Because of the long range of this interaction (R^{-4}) and the near-degeneracy of initial and final channels, the problem may be treated by the first Born approximation. We shall now outline a Born approximation calculation of the scattering matrix for the dipole-quadrupole interaction of H_2^* and H_2 and derive from this the inelastic scattering cross section for process (3). A more complete derivation can be found in Ref. 24.

We begin by defining the T matrix for scattering from state α to state α' as

$$T_{\alpha'\alpha l'm'0} = S_{\alpha'\alpha l'm'0} - \delta_{\alpha'\alpha} \delta_{l'l'} \delta_{m'm'} \quad (5)$$

where S is the standard scattering matrix relating the amplitude of scattered waves in channels (α', l', m') to that of the incident wave in channel $(\alpha, l, 0)$. Here $l(l')$ and $m(m')$ give the initial (final) orbital angular momentum of the projectile relative to the target; but we set $m=0$ by taking the initial velocity parallel to the z axis. Taking interaction potential V , we write

$$V_{\alpha'\alpha} = \langle \psi_{\alpha'} | V | \psi_{\alpha} \rangle \quad (6)$$

where ψ_{α} ($\psi_{\alpha'}$) is the initial (final) state of the system, including electronic, vibrational, and rotational components. Now we write the first Born approximation expression for the T matrix²⁵:

$$T_{\alpha'\alpha l'2m'0} = - \frac{4 m i (k k')^{\frac{1}{2}}}{\hbar^2} \int j_{l'}(k'R') Y_{l'm'}^*(\Theta', \phi') V_{\alpha'\alpha}(\vec{R}) \cdot j_l(kR) Y_{l0}(\Theta', \phi') R'^2 dR' d\Omega' \quad (7)$$

In this expression k (k') is the initial (final) projectile wave vector, and the j_l are the spherical Bessel functions.

The classical dipole-quadrupole expression²⁶ for the interaction of the excited electron's $2s\sigma \rightarrow 2p\pi$ transition dipole moment with the H_2 ground state quadrupole moment is

$$V_{dq} = \frac{4\pi Q r}{R^4} \sum_{\mu} C(1\ 2\ 3; \mu\ -\mu) Y_{1,\mu}(\Theta_e, \phi_e) Y_{2,-\mu}(\Theta_2, \phi_2) \quad (8)$$

Here Q is the ground state quadrupole moment, R is the intermolecular separation, r is the coordinate of the excited electron, C is a Clebsch-Gordon coefficient, and (Θ_e, ϕ_e) and (Θ_2, ϕ_2) give the angular orientations of the excited electron position and the ground state molecule's internuclear axis, respectively, referred to the (time-varying) intermolecular axis. V_{dq} proportional to R^{-4} , is the longest-range possible potential in our system; dipole-induced dipole and Van der Waals potentials both vary as R^{-6} .

We now write the wave function for the two-molecule system (neglecting the

electronic and vibrational states of the ground-state E_2):

$$\psi = |\psi_e\rangle |\psi_v\rangle |j_1 M_1\rangle |j_2 M_2\rangle |l m\rangle \quad (9)$$

We shall continue to indicate initial state by unprimed and final state by primed symbols. $|\psi_e\rangle = |2s\sigma\rangle$; $|\psi_e'\rangle = |2p\pi\rangle$; and $|\psi_v\rangle, |\psi_v'\rangle$ are the vibrational states. j_i and M_i indicate the molecules' internal rotational states, where subscript 1(2) indicates the excited (ground state) molecule.

Inserting expressions (8) and (9) into Eq. (7) and transforming the angular coordinates from the time-varying collision frame to space-fixed and molecule-fixed axes yields an expression for the T matrix:

$$\begin{aligned} T_{\alpha'\alpha l' l m' 0} = & -\frac{4mi}{\hbar^2} \frac{(4\pi)^{\frac{1}{2}}}{\sqrt{7}} Q_{\mu} \langle \psi_v', |\psi_v\rangle \langle l' | R^{-4} | l \rangle \\ & \cdot \sum_{m_1, m_1'} \sum_{m_2, m_2'} (-1)^{m_1' + m_2'} C(1 \ 2 \ 3; m_1' \ m_2') \langle 1M | 1m | 00 \rangle \\ & \cdot \delta_{M, \pm 1} \langle j_1' \ M_1' | D_{m, m_1}^{(1)} | j_1 M_1 \rangle \langle j_2' \ M_2' | 2 \ m_2' | j_2 \ M_2 \rangle \\ & \cdot \langle l' m' | 3 \ m_1' + m_2' | l 0 \rangle \end{aligned} \quad (10)$$

Here $\mu = 3ea_0$ is the $2s \rightarrow 2p$ dipole moment, and $\langle \psi_v' | \psi_v \rangle$ is the Franck-Condon factor $q_{v', v}$. $D_{m, m_1}^{(1)}$ is a rotation-matrix element²⁷. The radial integral is

$$\langle l' | R^{-s} | l \rangle \equiv (kk')^{\frac{1}{2}} \int_0^\infty j_{l'}(k'R) R^{-s} j_l(kR) R^2 dR, \quad (11)$$

which contains the resonance dependence of the scattering. The $\delta_{M, \pm 1}$ in

Eq. (10) arises from the fact that the $M = 0$ term would connect $|2s\sigma\rangle$ to $|2p\sigma\rangle$, which is the $B^1\Sigma_u^+$ state, not included in this calculation. We note that scattering to $B^1\Sigma_u^+$ is allowed, but unimportant compared to reaction (3) due primarily to the substantially smaller Franck-Condon factors¹⁹ for $E \rightarrow B$ transitions of small energy defect.

If we define the impact parameter as $b = (2l+1)/2k$, then we may obtain the scattering probability for a given b by summing $|T_{\alpha'\alpha l' l m' 0}|^2$ over final angular momentum states and averaging over initial rotational projections (M_1 and M_2)²⁵. The result obtained is a simplified sum over l' , independent of initial rotational states j_1 and j_2 :

$$P(b) = \left(\frac{m_1 Q q_{v'v}}{\hbar^2} \right)^2 \frac{32}{3} \sum_{l'} C(l 3 l'; 00)^2 \langle l' | R^{-4} | l \rangle^2. \quad (12)$$

This expression is identical to the probability for atomic $2s \rightarrow 2p$ scattering²⁵ except for the Franck-Condon factor, $q_{v'v}$, and an additional factor of $2/3$ here. This latter factor arises from our consideration of transitions only to the two $2p_\pi$ states, while in the atomic case transitions to all three $2p$ levels ($M=+1$ and 0) are included.

The cross section for the inelastic scattering process is now found by integrating

$$\sigma(k) = \int_0^\infty 2\pi P(b) b db. \quad (13)$$

However, $P(b) > 1$ for small b , because the Born approximation breaks down at close range. Hence, as suggested by Cross and Gordon²⁵ and by Slocumb, et al.²³, we set $P(b) = 1$ for $b < b_h$, where b_h is given by $P(b_h) = 1$ from Eq. (12). Now

$$\sigma = \pi b_h^2 + 2\pi \int_{b_h}^{\infty} P(b) b db. \quad (14)$$

A simple computer program was written to calculate scattering probability from Eq. (12) and cross section from Eq. (14) as functions of initial projectile momentum and detuning of initial and final states. The radial integral of Eq. (12) was solved explicitly in terms of the hypergeometric function^{25,28}. The energy detuning was obtained from spectroscopic data on the energies of the rotational levels in the E,F $1\Sigma_g^+$ ($v=2$) and C $1\Pi_u$ ($v=2$) manifolds. These data, shown graphically in Fig. 3, indicate that the J=1 levels, from which > 90% of the observed emission originates (see Fig. 2 and ensuing discussion), are separated in energy by only 22 cm^{-1} . The other data that must go into calculation are the H_2 ground state quadrupole moment²⁹, $Q = 0.484 \text{ a.u.}$, the Franck Condon factor³⁰, $q_{2,2} = 0.794$, and the projectile velocity. Averaging the product of velocity and cross section over a Boltzmann distribution of kinetic energies gives a rate constant for process (3) of $2.3 \times 10^{-9} \text{ cm}^3/\text{sec}$ at 300°K . This result agrees remarkably well with the experimental determination of $(2.1 \pm 0.4) \times 10^{-9} \text{ cm}^3/\text{sec}$, and supports our hypothesis that reaction (3) is the primary mechanism in collisional deactivation of H_2 (E,F $1\Sigma_g^+$; $v=2$).

These theoretical conclusions are lent further support by experimental observation of C $1\Pi_u \rightarrow X 1\Sigma_g^+$ vuv Werner band emissions following two-photon excitation of the E,F state. Fig. 4 is a spectrum of this emission near 125 nm, showing the (2,6) and (2,7) vibrational bands of the C \rightarrow X fluorescence. (The (2,5) band, which should be present, is beyond the transmission cutoff of our optical system). These observations of emission in the Werner Bands

confirm that large populations are created in the $v=2$ level of the C ${}^1\Pi_u$ state following E,F ${}^1\Sigma_g^+$ ($v=2$) two-photon excitation. The absence of emission from other C-state vibrational levels confirms our model of electronic quenching, as well as the contention that vibrational relaxation is much slower than the electronic.

Because of the near-degeneracy of the E and C states, at pressures above ~ 20 torr these levels will reach thermal equilibrium with ~ 1 nsec of excitation. (The principle of detailed balance requires that the C \rightarrow E quenching rate be nearly equal to the E \rightarrow C rate.) Under these circumstances, when other losses are neglected, the probability that a H_2 molecule in the E,F ${}^1\Sigma_g^+$ state will radiate in its E,F \rightarrow B IR bands is simply τ_C/τ_E , where τ_E and τ_C are the radiative lifetimes of the E and C states, respectively. From the theoretical calculations of Allison and Dalgarno for the C ${}^1\Pi_u \rightarrow$ X ${}^1\Sigma_g^+$ transition probabilities³¹, we obtain $\tau_C(v=2) = 0.88$ nsec. The effective radiative lifetime of a molecule excited to the E,F state at high pressure is given by a rate equation analysis:

$$\tau_{\text{eff}} = \frac{2\tau_E\tau_C}{\tau_E + \tau_C} \quad (15)$$

In our case, for $\tau_E \gg \tau_C$, $\tau_{\text{eff}} \approx 2\tau_C$. This analysis will be important in our later estimates of rotational relaxation and photoionization rates.

V PHOTOIONIZATION OF THE E,F STATE

While the electronic relaxation processes we have examined are quite rapid, at higher laser intensities the fastest loss process - and hence the limiting factor in achievable excitation density - is photoionization of the excited molecules. This is a pervasive problem in two-photon studies using rare gas halide lasers, because three ArF* photons (= 19.2 eV) are sufficient to ionize almost all atoms and molecules. While the characteristic signature of a two-photon process is a signal which grows as the square of laser intensity, when photoionization is prevalent, the signal "saturates" and grows only linearly with intensity; meanwhile the laser energy is increasingly channeled into ion production.

The nature of this behavior may be seen in a rate equation analysis of the two-photon excited state density N^* :

$$\frac{dN^*}{dt} = \frac{\alpha I^2}{h\nu} [H_2] - \frac{N^*}{\tau_{eff}} - \frac{\sigma_{pi} I}{h\nu} N^* \quad (16)$$

Here $\alpha = \sigma/I$ (cm^4/W) is the two-photon absorption coefficient¹², I is the laser intensity (W/cm^2), ω is the laser frequency, and σ_{pi} is the photoionization cross section for the excited state. At high pressure and high laser intensity, radiative and ionization losses are fast enough so that we can assume a steady state solution to Eq. (16):

$$N^* = \frac{\alpha I^2 [H_2]}{h\nu/\tau_{eff} + \sigma_{pi} I} \quad (17)$$

As noted earlier, $\tau_{\text{eff}} = 2\tau_c = 1.8$ nsec at high pressure. This solution clearly shows the saturation of N^* at large I . (As a further note, while photoionization is a broadband process, two-photon absorption terminates on a discrete state. Hence, decreasing the laser linewidth, much broader in our case than the transition Doppler width, will increase α but not σ_{pi} and, thus, will increase the excitation efficiency and excited state density.^{13,32})

If we can measure the saturation of the two-photon signal with laser intensity, we can extract from these data the photoionization cross section for the excited state. We begin by using the fact that the ir fluorescent signal is simply $S = N^*/2\tau_E$ to rearrange eq. (17):

$$\begin{aligned} \frac{I}{S} &= \frac{\hbar\omega}{2\tau_c \alpha [H_2]} \frac{1}{I} + \frac{\sigma_{\text{pi}}}{\alpha [H_2]} \\ &= mI^{-1} + B. \end{aligned} \quad (18)$$

The significance of this equation is that if we now plot the quotient I/S from our data as a function of I^{-1} , we can extract the photoionization cross section, σ_{pi} , from the ratio of intercept to slope, B/m , in our plot:

$$\sigma_{\text{pi}} = \frac{\hbar\omega}{2\tau_c} \frac{B}{m} \quad (19)$$

Fig. 5 shows a measurement of ir fluorescent signal as a function of laser energy, plotted in accordance with Eq. (18). The plot is fairly linear, and the non-zero intercept indicates that photoionization losses lead to the expected saturation of the signal at high laser intensity. On the basis of these data, we estimate that $3 \times 10^{-19} \text{ cm}^2 \leq \sigma_{\text{pi}} \leq 4 \times 10^{-18} \text{ cm}^2$. This

large uncertainty arises primarily from the uncertainty in converting the measured laser energy to the actual laser intensity at the focus. This estimate is, however, in agreement with the theoretical calculations of Cohn³³. For photoionization from H_2 (E,F $1\Sigma_g^+$; $v=2$) to H_2^+ (X $2\Sigma_g^+$; $v=2$) at 6.4 eV (3.3 eV above threshold), Cohn calculates $\sigma_{pi} = 2.6 \times 10^{-18} \text{ cm}^2$. It must be noted, however, that this experiment does not actually measure the E,F state photoionization cross section, but rather the cross section for photoionization of the collisionally mixed E,F and C^2 states.

VI ROTATIONALLY SELECTIVE MEASUREMENTS

While we have observed very rapid electronic de-excitation processes in the H_2 E,F state, rotational relaxation is considerably slower. If the data of Fig. 2 are compared to a theoretical formula for the intensities of rotational lines in a vibrational band in thermal equilibrium¹¹, it is found that even at the high pressure (20 psig) at which this spectrum was taken, the rotational levels are not equilibrated¹³. On the contrary, Table 2, which lists the ground state equilibrium rotational populations and two-photon X \rightarrow E,F transition energies for $J = 0 - 3$ (populated at 300°K), demonstrates that the relative intensities of the E,F \rightarrow B rotational lines are due to a nearly total absence of rotation-changing collisions in the excited state. Thus, since only the Q(0) and Q(1) excitation transitions fall squarely within the two-photon laser band, only $J = 0$ and $J = 1$ levels are seen to emit substantially in the spectrum of Fig. 2.

In order to measure the rate of this very slow rotational relaxation, we installed the prism system and tuned the laser to excite selectively each of the first four rotational levels of H_2 (E,F $^1\Sigma_g^+$; $v=2$) in turn. We then attempted to observe emission from J-levels other than the one excited. The results of these observations are shown in Fig. 6. In no case was any rotational relaxation evident above the $\sim 10\%$ noise level in the measurements.

We can use this signal/noise ratio to set an upper bound on $2 \rightarrow 0$ and $3 \rightarrow 1$ rotational relaxation rates. (We do not expect any odd \leftrightarrow even relaxation because of the strict ortho/para separation in homonuclear diatomics)¹¹. Assuming that the laser is tuned to excite the J+2 level and that the Jth level is populated only by rotational relaxation from J+2, which is much

slower than electronic relaxation, the ratio of populations in the two levels is given by a steady-state analysis:

$$\frac{n_J}{n_{J+2}} = \frac{k_R^{J+2,J} [H_2]}{R_L} \quad (20)$$

In this equation, $R_L = \sigma_{pi} I / h\nu + 1 / (2\tau_c) = 3 \text{ nsec}^{-1}$ is the electronic loss rate, and $k_R^{J+2,J}$ is the two-body rate coefficient for rotational transitions from level $J+2$ to level J . The ratio of rotational level populations is also related to the fluorescent emission intensities S of the P lines originating in the J and $J+2$ rotational levels by¹¹

$$\frac{S[P(J+1)]}{S[P(J+3)]} = \left(\frac{\nu_J}{\nu_{J+2}} \right)^4 \left(\frac{J+1}{J+3} \right) \left(\frac{2J+5}{2J+1} \right) \frac{n_J}{n_{J+2}} \quad (21)$$

where ν_J and ν_{J+2} are the respective transition frequencies³⁴. Finally, we observe in Fig. 6 that $S[P(2)]/S[P(4)]$ and $S[P(1)]/S[P(3)] \leq 0.1$, leading us to conclude on the basis of equations (20) and (21) that $k_R^{2,0} \leq 3 \times 10^{-12} \text{ cm}^3/\text{sec}$ and $k_R^{3,1} \leq 6 \times 10^{-12} \text{ cm}^3/\text{sec}$. These rate constants are more than two orders of magnitude smaller than the observed electronic quenching rates for the E,F state.

Rotational relaxation will be greatly enhanced in the isotopically mixed species of hydrogen as shown by Heukels and Van de Ree³⁵. Firstly, the shift of the center of mass away from the center of charge has the net effect of slightly increasing the cross section for a given rotational transition. More importantly, however, additional channels open up in the mixed species that are forbidden in the homonuclear species. Specifically, $\Delta J = 1$ transitions are

allowed in the heteronuclear case, while J must retain its parity in the homonuclear molecule, due to nuclear spin symmetry considerations. $\Delta J=1$ transition cross sections are calculated³⁵ to be roughly one order of magnitude larger than the $\Delta J=2$ cross sections for He - HT collisions in the ground electronic state, and the $\Delta J=2$ transition cross section for He - D₂ collisions is calculated³⁵ to be roughly forty percent smaller than for He - HT collisions.

Figure 7 shows the lower rotational levels of the HD E,F $^1\Sigma_g^+$ ($v=2$, inner well) and C $^1\Pi_u$ ($v=2$) states, with + and - signs to indicate the parities of the levels¹². The rapid electronic collisions (studied in Sec. IV of this paper) that equilibrate the E,F and C levels of opposite symmetries are shown by bold arrows. The parity-changing rotational collisions, forbidden in H₂ and D₂, are indicated by the fine arrows. We shall now describe a measurement of the collisional rate of this latter process in HD.

In this experiment, the laser was tuned to the Q(0) and Q(1) two-photon excitation lines in HD, at 103,221 and 103,173 cm⁻¹ respectively¹⁰. Because the lines are closely spaced and located in the wing of the laser gain band, it was not possible to excite one line to the total exclusion of the other. Thus, the ratio of intensities in the P(1) and P(2) E,F $^1\Sigma_g^+ \rightarrow \text{B } ^1\Sigma_u^+$ (2,0) emission lines was measured as a function of HD pressure as the laser was tuned to excite predominantly Q(0) or Q(1) in turn. The results of these measurements are presented in Fig. 8, which, in contrast to Fig. 6, shows a clear tendency toward equilibrium at high pressure.

In order to extract rate constants $k_R^{0,1}$ and $k_R^{1,0}$ from these data, we examine a rate equation model that includes both $1 \rightarrow 0$ and $0 \rightarrow 1$ rotational transitions:

$$\frac{dn_0}{dt} = R_p^{(0)} [HD] - R_L^{(0)} n_0 - k_R^{0,1} [HD] n_0 + k_R^{1,0} [HD] n_1 \quad (22)$$

$$\frac{dn_1}{dt} = R_p^{(1)} [HD] - R_L^{(1)} n_1 - k_R^{1,0} [HD] n_1 + k_R^{0,1} [HD] n_0 \quad (23)$$

Here $R_p^{(0)}$ and $R_p^{(1)}$ are the two-quantum production rates of the $J=0$ and $J=1$ rotational levels, which will vary as the laser is tuned through the levels' excitation frequencies, and the $R_L^{(J)}$ are the corresponding electronic loss rates. We assume that the excited system is in quasi-steady state and that $R_L^{(1)} = R_L^{(0)} = 3 \text{ nsec}^{-1}$, as above, and solve for the ratio n_0/n_1 :

$$\frac{n_0}{n_1} = \frac{k_R^{1,0} [HD] + (R_p^{(0)}/R_p^{(1)}) R_L}{k_R^{0,1} [HD] + (R_p^{(1)}/R_p^{(0)}) R_L} \quad (24)$$

where $R_p = R_p^{(0)} + R_p^{(1)}$. From a formula similar to Eq. (21), we have $S[P(1)]/S[P(2)] = 1.5 n_0/n_1$. A three parameter fit ($k_R^{1,0}$, $k_R^{0,1}/k_R^{1,0}$, and $R_p^{(0)}/R_p^{(1)}$ of Eq. (24) to the data of Fig. 8 gives $k_R^{1,0} = (3 \pm 1) \times 10^{-10} \text{ cm}^3/\text{sec}$ and $k_R^{0,1}/k_R^{1,0} = 2.1 \pm 0.5$. The fit is shown by the solid lines in the figure.

These rate constants do not refer simply to rotational transitions within the E,F manifold, but rather must be thought of as composite rates for all the transitions in Fig. 7 that are indicated by the fine arrows. However, the ratio $k_R^{0,1}/k_R^{1,0}$ is rigorously fixed theoretically by the principle of detailed balance³⁶ at 2.46, in good agreement with the experimental result.

For comparison with other experimental results, we transform the rate

constants we have measured to average cross sections (by dividing by the mean thermal velocities at 300°K) and list these results in Table 3. Our results in H_2^+ are quite similar to the ground state rotational relaxation cross sections found by Jonkman, et al³⁷. The reasons that these cross sections are so small are that (1) these $\Delta J = 2$ transitions can proceed only through a quadrupole moment (in contrast to the strong electric-dipole electronic transition that we studied) and (2) the energy defects between initial and final states are comparable to or greater than thermal energies at the temperatures studied.

On the other hand, the cross section we measured in HD for $\Delta J = 1$ transitions is on the order of gas dynamic. Akins, et al.³⁸, also measured large collisional cross sections for rotational transitions in HD, although their results for the B $^1\Sigma_u^+$ state were still smaller than ours for the E,F state. The faster relaxation rate that we measured may be attributable to the contribution of coupling of the E,F levels through the C state manifold; no comparable coupling exists in the B or X states.

VII CONCLUSIONS

In the experiments described here and in Ref. 1, we have, for the first time, selectively excited a gerade state of the hydrogen molecule, the quasi-metastable E,F $1\Sigma_g^+$ state in H_2 and HD. By line-narrowing and tuning the ArF laser excitation source, we have excited single rotational levels in H_2 , and also achieved some rotational selectivity in HD. We have measured a number of the properties of the E,F state, including radiative lifetime, rates for collisional electronic quenching and rotational relaxation, two photon absorption cross section, and photoionization cross section. The radiative lifetime, electronic quenching rate for $H_2^* + H_2$ collisions, two-photon excitation cross section, and excited state photoionization cross section agree well with theoretical predictions. The rotational relaxation rates are roughly in line with other experimental results. These experiments demonstrate the utility of ultraviolet two quantum absorption in investigating many different aspects of this most fundamental excited molecular system.

We have also studied in detail the mechanism of rapid electronic deactivation of H_2 (E,F $1\Sigma_g^+$) to the C $1\Pi_u$ state. Our Born approximation calculation of the cross section for this reaction gives very close agreement with the experimental determination of the quenching rate. Observations of VUV Werner band emission further supports our model of the collisional processes involved here.

This experimental technique may be extended to further spectroscopic and collisional studies in excited H_2 . Starting with two-photon-excited E,F $1\Sigma_g^+$ molecules, a tunable dye laser can probe higher ungerade states; while from

$C^1\Pi_u$ molecules created by collisional quenching of H_2 ($E, F^1\Sigma_g^+$) higher gerade states may be reached as well. A two-photon-pumped laser operating on the H_2 Werner bands near 120 nm between $C^1\Pi_u$ ($v=2$) and high vibrational levels of $X^1\Sigma_g^+$ is also feasible¹³. Finally, it may be possible to study such exotic processes as para-ortho conversion and production of HD^* in four-center reactions of H_2^* and D_2 by this technique.

ACKNOWLEDGMENTS

We are grateful to D. L. Huestis for many useful discussions during the course of this work and to R. T. Hawkins for expert computer programming. The expert technical assistance of K. Skala and G. Murphy was invaluable in the construction of the tunable ArF* laser. Daniel J. Kligler also wishes to thank the Molecular Physics Laboratory of SRI International for allowing him to use its PDP 11/40 computer for the calculations described in this paper and to acknowledge the helpful advice of W. H. Miller and A. P. Hickman in the scattering calculations. Jeffrey Bokor gratefully acknowledges the support of the Fannie and John K. Hertz Foundation.

This work supported by the National Science Foundation under Grant PHY-77-01849 and NSF78-27610, the Office of Naval Research under Grant and the U. S. Department of Energy under Agreement No. ED-78-S-08-1603.

REFERENCES

1. Daniel J. Kligler and Charles K. Rhodes, *Phys. Rev. Lett.* 40, 309(1978).
2. T. E. Sharp, *At. Data* 2, 119(1971).
3. G. H. Dieke, *J. Mol. Spectrosc.* 2, 494(1958).
4. E. R. Davidson, *J. Chem. Phys.* 33, 1577(1960); *ibid.* 35, 1189(1961);
R. J. Boye, *J. Mol. Spectrosc.* 26, 36(1968).
5. W. Kolos and L. Wolniewicz, *J. Chem. Phys.* 50, 3228(1969).
6. L. Wolniewicz and K. Dressler, *J. Mol. Spectrosc.* 67, 416(1977).
7. Jose D. Alemar-Rivera and A. Lewis Ford, *J. Mol. Spectrosc.* 67, 336(1977).
8. W. Kolos and L. Wolniewicz, *J. Chem. Phys.* 48, 3672(1968).
9. W. Kolos and L. Wolniewicz, *J. Chem. Phys.* 43, 2429(1965).
10. I. Dabrowski and G. Herzberg, *Can. J. Phys.* 54, 525(1976).
11. Gerhard Herzberg, *Spectra of Diatomic Molecules* (New York, Van Nostrand Reinhold, 1950).
12. D. Kligler, D. Pritchard, W. K. Bischel, and C. K. Rhodes, *J. Appl. Phys.* 49, 2219(1978).
13. W. K. Bischel, J. Bokor, D. J. Kligler, and C. K. Rhodes, *IEEE J. Quant. Electron.* QE-15, 380(1979).
14. T. R. Loree, K. B. Butterfield, and D. L. Barker, *Appl. Phys. Lett.* 32, 171(1978).
15. R. Burnham and N. Djeu, *Appl. Phys. Lett.* 29, 707(1976).
16. M. Ackerman and F. Biaueme, *J. Mol. Spectrosc.* 35, 73(1970).
17. L. Wolniewicz, *J. Chem. Phys.* 51, 5002(1969).
18. Ewald H. Fink, Daniel L. Akins, and C. Bradley Moore, *J. Chem. Phys.* 59, 900(1972).
19. R. J. Spindler, *J. Quant. Spectrosc. Radiat. Transf.* 9, 1041(1969).

20. W. L. Fite, R. T. Brackmann, D. G. Hummer, and R. F. Stebbings, Phys. Rev. 116, 363(1959); 124 2051(1961).
21. S. R. Ryan, S. J. Czuchlewski and M. V. McCusker, Phys. Rev. A16, 1892(1977).
22. Joel I. Gersten, J. Chem. Phys. 51, 637(1969).
23. C. A. Slocomb, W. H. Miller, and H. F. Schaeffer III, J. Chem. Phys. 55, 926(1971).
24. Daniel J. Kligler, Thesis (unpublished, Stanford University, Stanford CA, 1979).
25. R. J. Cross, Jr., and R. G. Gordon, J. Chem. Phys. 45, 3571(1966).
26. J. O. Hirschfelder and W. J. Meath, Adv. Chem. Phys. 12, 3(1967).
27. A. R. Edmonds, Angular Momentum in Quantum Mechanics (Princeton University Press, 1957).
28. Milton Abramowicz and Irene A. Stegun, eds., Handbook of Mathematical Functions (National Bureau of Standards, Washington, D. C., 1964), p. 556.
29. W. Kolos and L. Wolniewicz, M. Chem. Phys. 41, 3674(1964).
30. C. S. Lin, J. Chem. Phys. 60, 4660(1974).
31. A. C. Allison and A. Dalgarno, At. Data 1, 289(1970).
32. B. R. Marx, J. Simons, and L. Allen, J. Phys. B 11, 1273(1978).
33. Arthur Cohn, J. Chem. Phys. 57, 2456(1972).
34. The Hydrogen Molecule Wavelength Tables of Gerhard Heinrich Dieke, edited by H. M. Crosswhite (John Wiley & Sons, New York, 1972).
35. W. F. Heukels and J. Van de Ree, J. Chem. Phys. 57, 1393(1972).
36. M. Mitchner and C. H. Kruger, Partially Ionized Gases (John Wiley & Sons, New York, 1973).
37. R. M. Jonkman, G. J. Prangma, and J. J. M. Beenakker, Sixth Rarefied Gas Dynamics (1969, New York, Academic Press), p. 1413.
38. Daniel L. Akins, Ewald H. Fink, and C. Bradley Moore, J. Chem. Phys. 52, 1604(1970).

TABLE 1

 H_2 Transition Frequencies

		H_2 ^{a)}	HD ^{b)}	D_2 ^{c)}
Two-photon transition	Q branch	103282-103552	102926-103221	102555-102741
energy range in	S branch	103674-103869	103239-103370	102817-102855
cm^{-1} for $X \ ^1\Sigma_g^+$ ($v=0$) \rightarrow	O branch	102893-103198	102729-102954	102410-102561
E,F $\ ^1\Sigma_g^+$ ($v=2$), $J' = 0-3$				

Wavelengths of

E,F \rightarrow B emission

bands in nm

(2,1)	830	850	890
(2,0)	750	780	830

a) Ref. 34.

b) Ref. 10.

c) G. H. Dieke and S. P. Cunningham, J. Mol. Spectrosc. 18, 288 (1965).

TABLE 2

Rotational level populations (relative to $J=0$) and frequencies (in cm^{-1}) of $\text{H}_2 \text{ X } ^1\Sigma_g^+$ ($v=0$) \rightarrow E,F $^1\Sigma_g^+$ ($v=2$, inner well) two-photon transitions.

\underline{J}	$\underline{n(J)/n(0)}$	BRANCH		
		<u>0</u>	<u>Q</u>	<u>S</u>
0	1		103,552	103,682
1	4.9		103,479	103,869
2	0.83	103,197	103,328	103,797
3	0.52	102,892	103,282	103,673

TABLE 3

 H_2 and HD rotational relaxation cross sections

	STATES	$\sigma_R (\text{\AA}^2)$
This work	$H_2(E,F; v=2, J'=3, J''=1)$	$\leq .12$
	$(J'=2, J''=0)$	$\leq .24$
Jonkman, <u>et al</u> ^(a)	$H_2(X; v=0, J'=2, J''=0)$	0.10 (para H_2 , 170°K)
		0.26 (ortho H_2 , 77°K)
This work	HD(E,F; $v=2, J'=1, J''=0$)	14
Akins, <u>et al</u> ^(b)	HD(B; $v=3, J'=2, J''=1$)	3.0

(a) Ref. 37.

(b) Ref. 38.

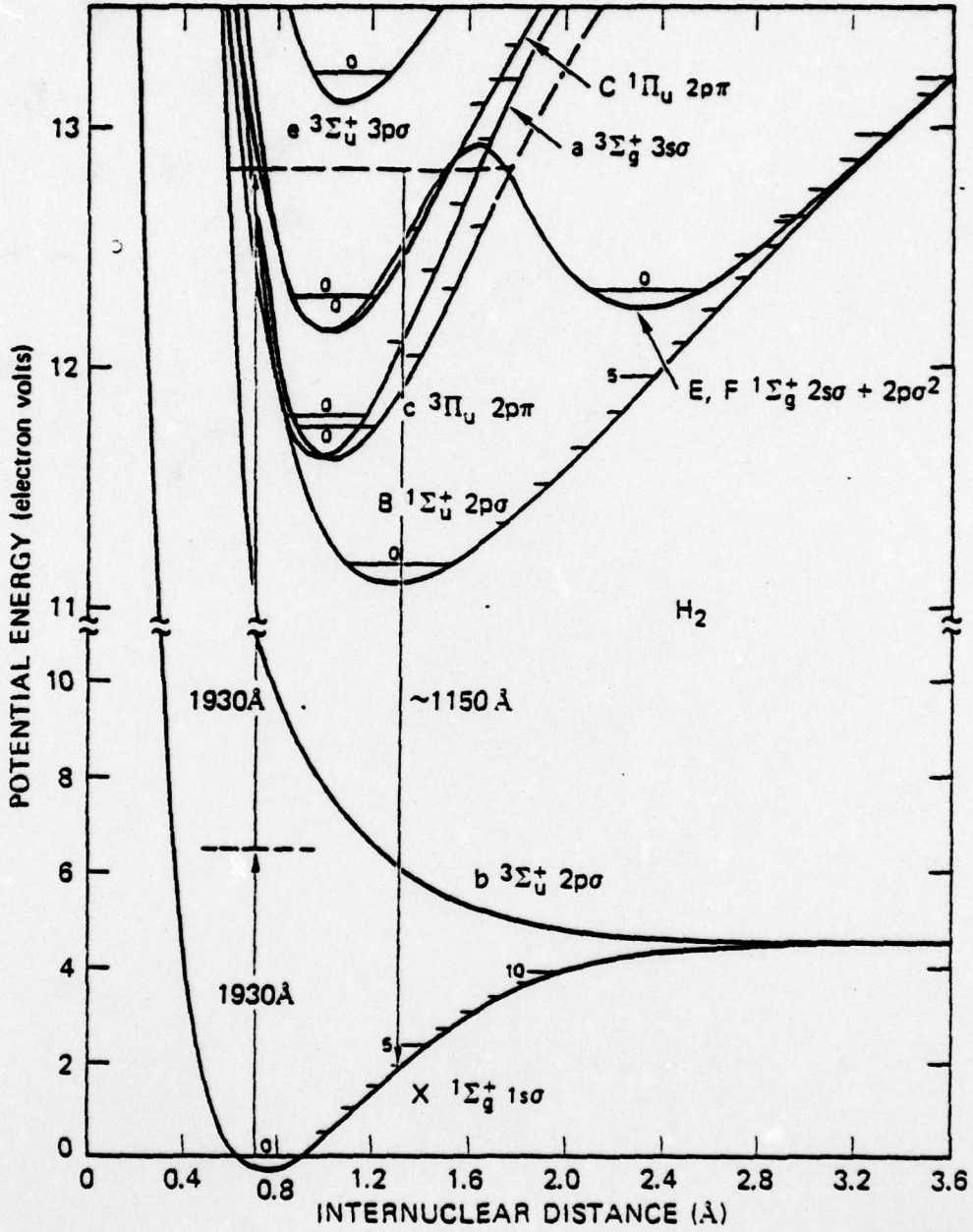
FIGURES

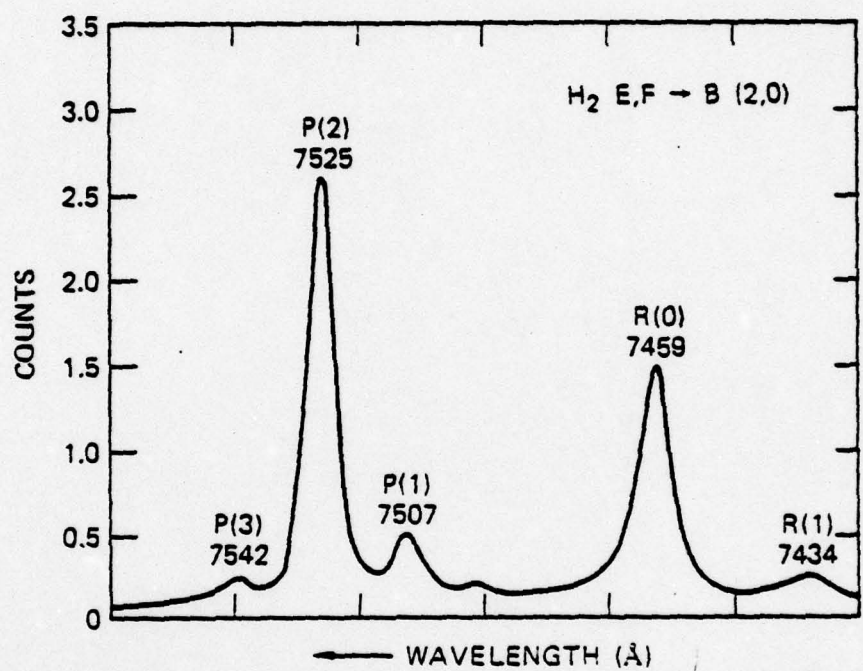
1. Energy level diagram of H_2 showing the X, B, C, and E,F states of interest in this experiment, as well as other states in this energy range, based on potential curves in T. E. Sharp, Atomic Data 2, 119 (1971). Note the change in vertical scale above 10 eV.
2. H_2 E,F \rightarrow B²(2,0) fluorescence spectrum detected by the OMA following ArF laser broadband excitation. Five rotational lines are observed. Resolution is 4 Å; H_2 pressure 2 atm.
3. Energies of rotational levels in H_2 E,F $^1\Sigma_g^+$ (inner minimum, v=2) and C $^1\Pi_u$ (v=2). Ref. 34.
4. H_2 C $^1\Pi_u$ \rightarrow X $^1\Sigma_g^+$ VUV Werner Bands fluorescence spectrum detected by OMA following ArF laser excitation of the E,F state. The (2,6) and (2,7) vibrational bands are observed, but the (2,5) band is beyond the wavelength cutoff of the detection system. The rotational structure is not resolved.
5. Ratio of laser energy (193 nm) to fluorescent signal (E,F \rightarrow B, 930 nm), plotted as a function of the reciprocal of laser energy. Ratio of intercept to slope of straight line fit to data is 0.05 mJ^{-1} .
6. H_2 E,F \rightarrow B (2,0) fluorescence spectra detected by OMA following rotationally selective excitation by a line-narrowed ArF laser. H_2

pressure is 20 psig. Excitation line: (a) Q(0), (b) Q(1), (c) Q(2), (d) Q(3). Appearance of R(1) emission in (d) arises from direct excitation of the Q(2) absorption line, due to the presence of some laser oscillation at this frequency when laser is tuned to Q(3), not from rotational relaxation.

7. Energies of lower rotational levels in HD ($E, F \ ^1\Sigma_g^+$; inner well, $v=2$) and $C \ ^1\Pi_u$; $v=2$. Bold arrows indicate rapid electronic quenching collisions, while fine arrows show slower rotational quenching paths. Lambda-doubling in the C state see Paul S. Julienne, J. Mol. Spectrosc. 48, 503(1973) is exaggerated for clarity.

8. Ratio of fluorescent intensity, S, of P(1) line to that of P(2) in the HD $E, F \rightarrow B (2,0)$ band following rotationally selective excitation by ArF laser. For upper curve (boxes) laser was tuned to excite primarily $J=0$, while for lower curve (triangles) laser was tuned to $J=1$.





SA-4685-70

H₂

 $E^1\Sigma_g^+ \ v=2$
 $C^1\Pi_u \ v=2$

J=3 103987 cm⁻¹

103892 cm⁻¹ J=3

103729 J=2

J=2 103682

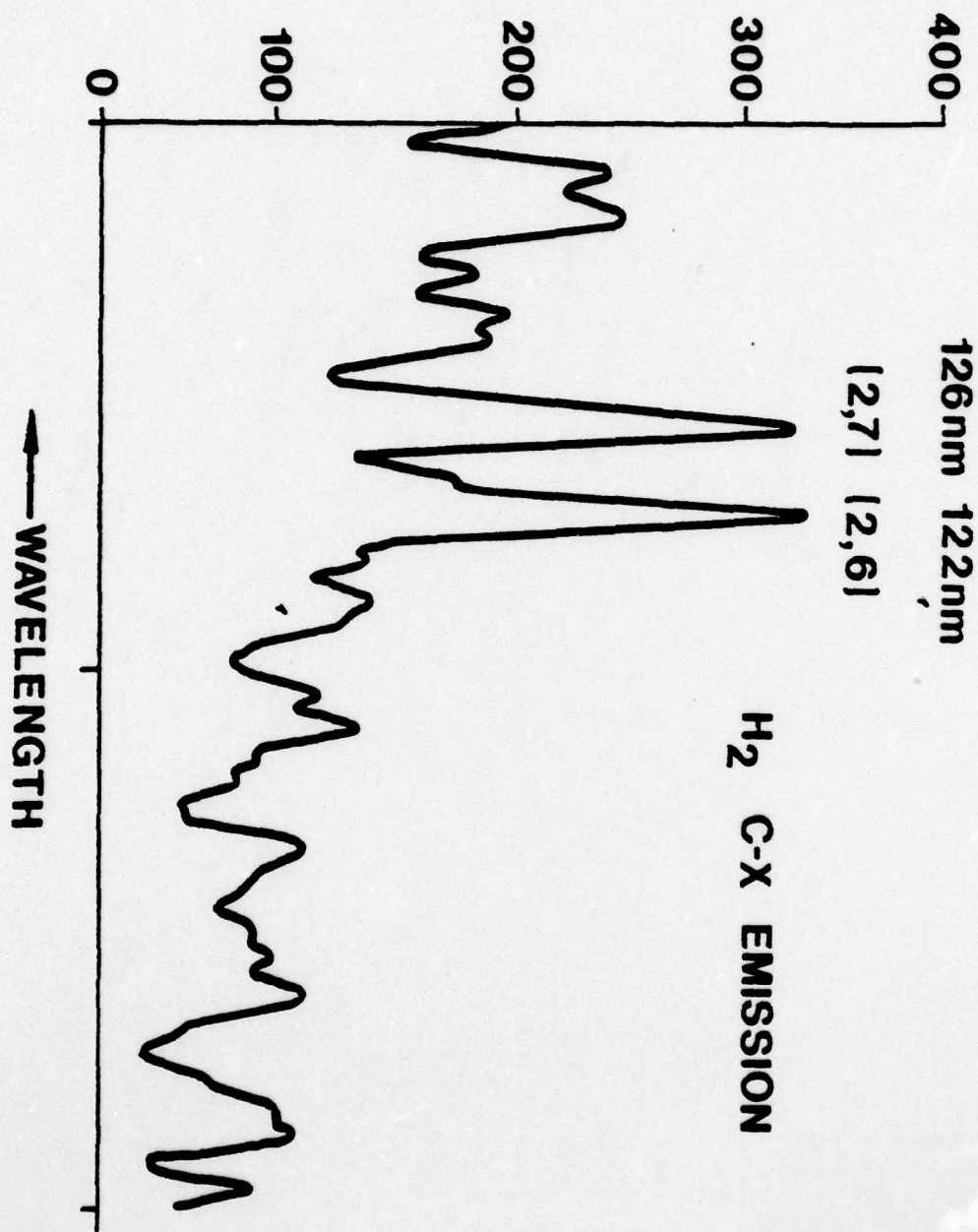
103620 J=1

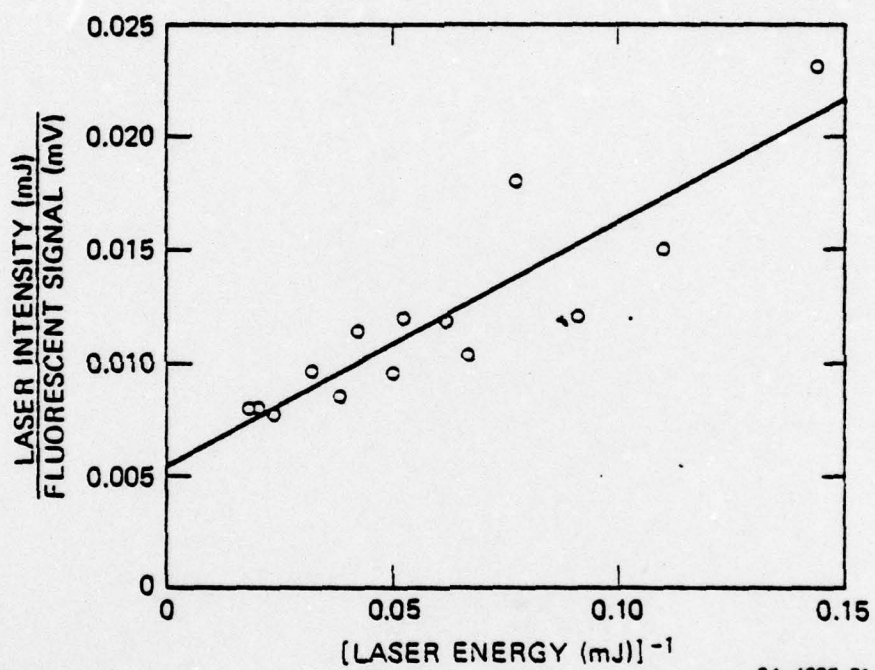
J=1 103598

↓
22 cm⁻¹
↑

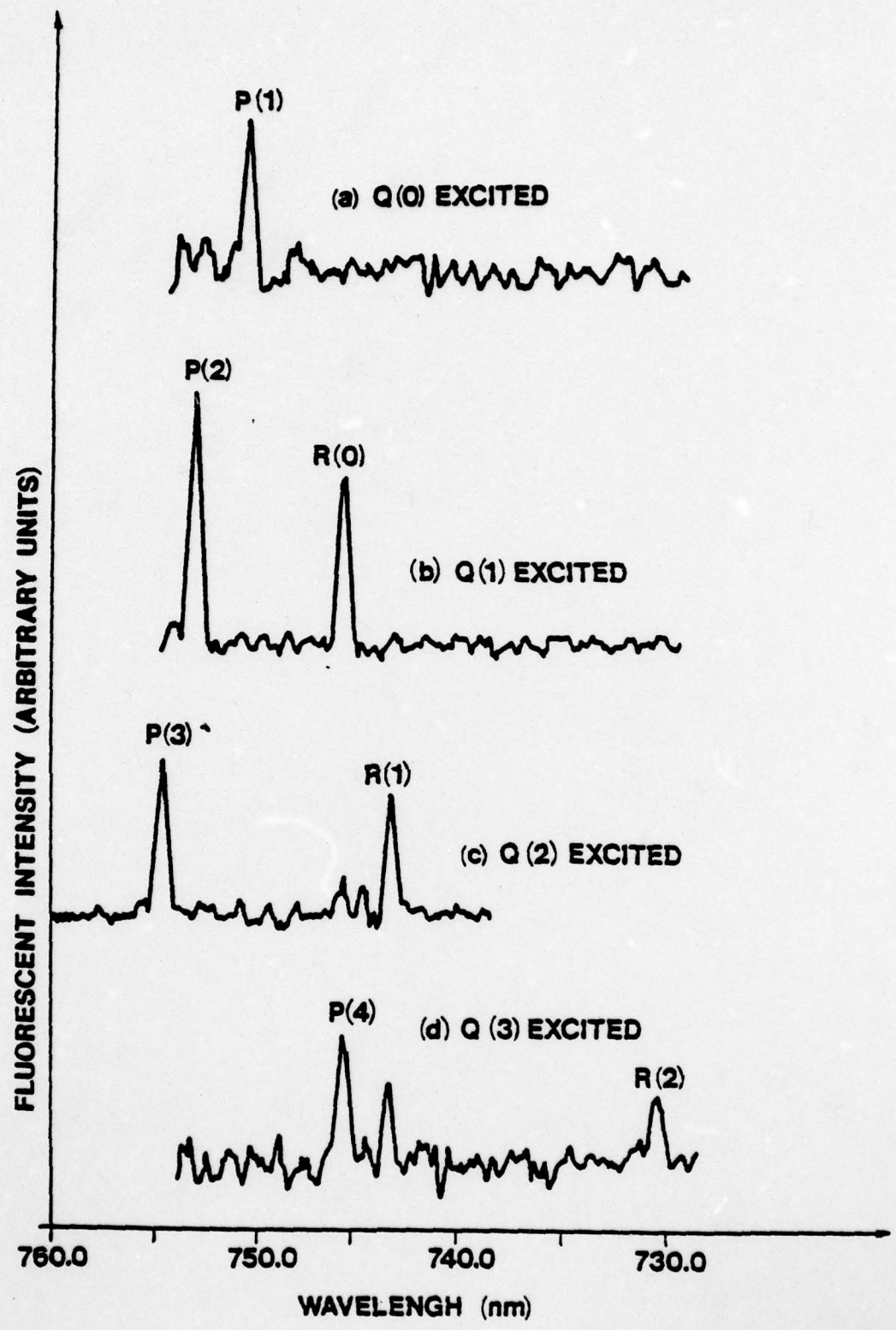
J=0 103552

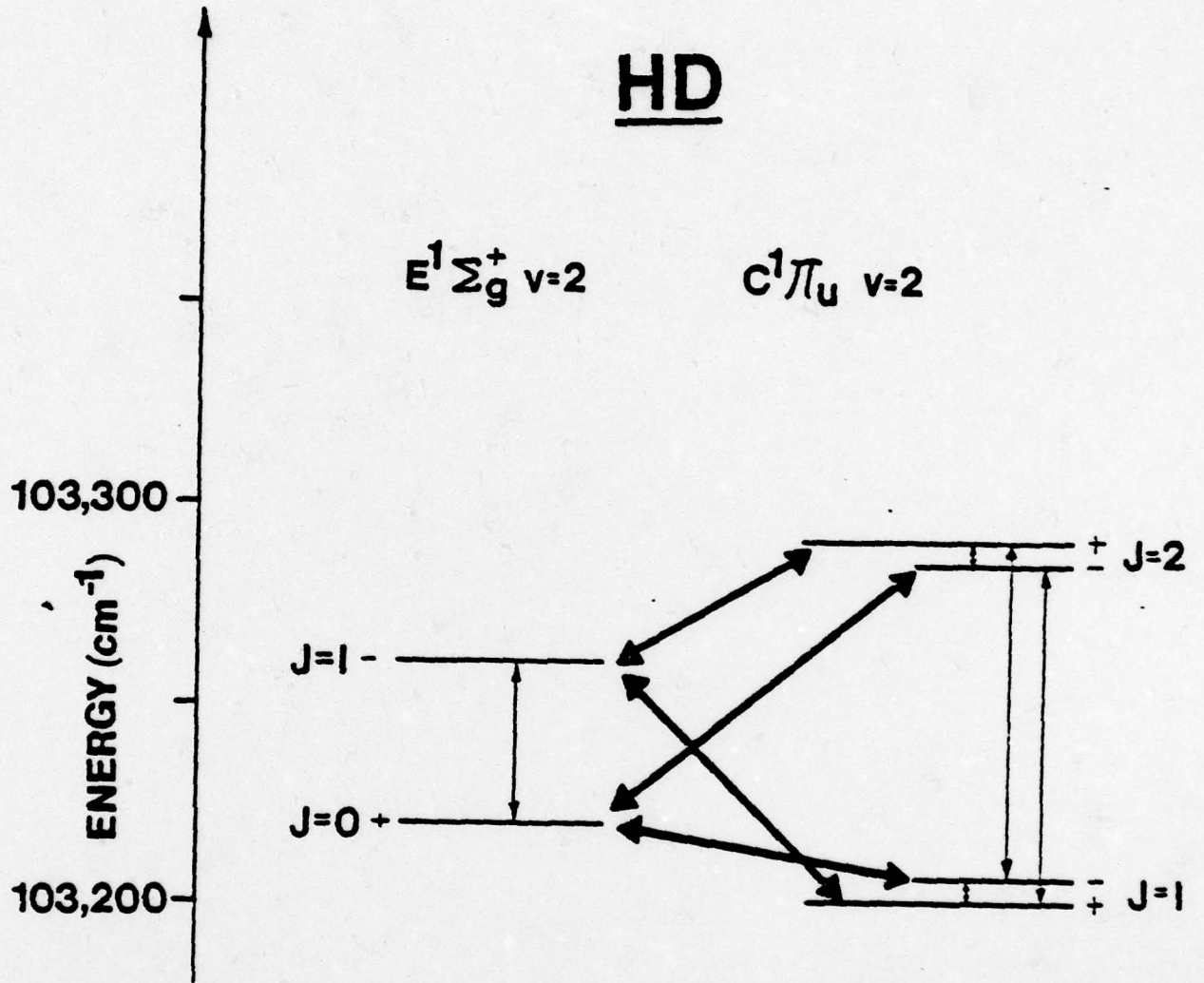
FLUORESCENT INTENSITY (ARBITRARY UNITS)

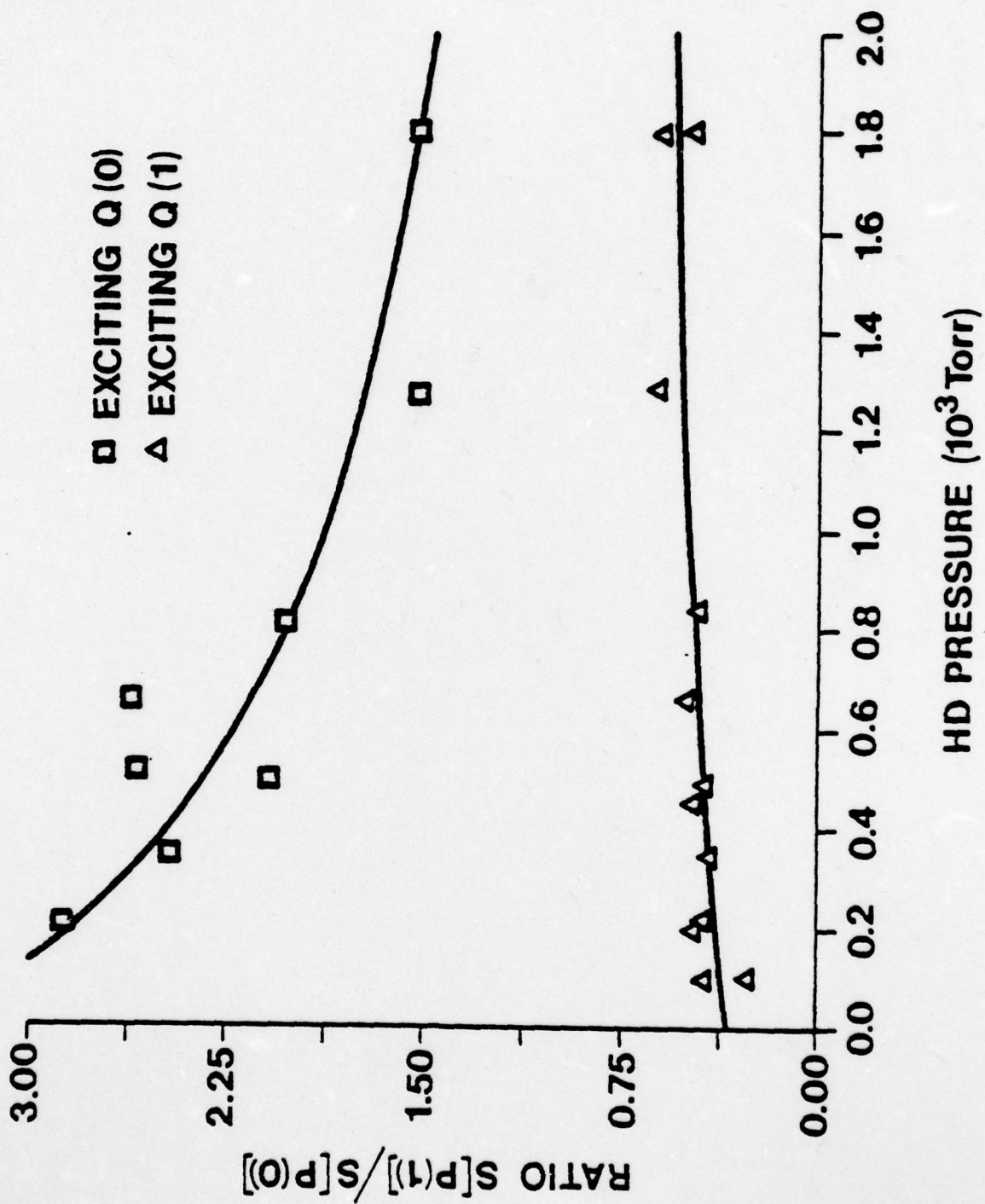




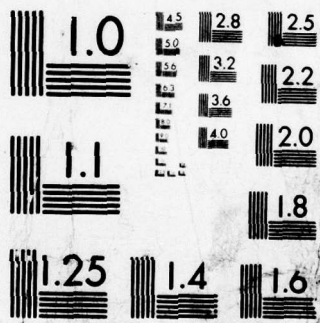
SA-4685-71







APPENDIX D



MICROCOPY RESOLUTION TEST CHART
NATIONAL BUREAU OF STANDARDS-1963-A

Isotope effect in multiphoton ultraviolet photolysis of CO

J. Bokor[†],

Department of Electrical Engineering

Stanford University

Stanford, California 94305

J. Zavelovich and C. K. Rhodes

Department of Physics

University of Illinois at Chicago Circle

P. O. Box 4348, Chicago, Illinois 60680

ABSTRACT

Two-photon dissociation of carbon monoxide near 193 nm with a tunable ArF* laser to yield excited $C(2^1D)$ atoms is reported. The atoms are detected by subsequent absorption of a third laser photon to $C(3^1P^o)$ followed by emission of 248 nm fluorescence to $C(2^1S)$. The process is found to be isotopically sensitive; the $C(2^1D)$ yield from $^{13}C^{16}O$ and $^{12}C^{18}O$ is a factor of 6 greater than from $^{12}C^{16}O$. The isotope effect is attributable to an enhancement in the two-photon matrix element due to the shift in the near resonant a $^3\Pi$, $v=2$ intermediate state. C_2 Swan band emission is also observed, arising from association of the free carbon atoms, and exhibits a

corresponding isotope effect. Finally, collisional processes are observed involving excited carbon atoms and electrons, using two-photon ionization of a small quantity of added xenon atoms as a new technique for producing a controlled density of free electrons.

[†] Present address: Department of Physics, University of Illinois at Chicago Circle, P. O. Box 4348, Chicago, Illinois 60680.

By acceptance of this article, the publisher and/or recipient acknowledges the U.S. Government's right to retain a nonexclusive, royalty-free license in and to any copyright covering the article.

Note: This notation need not appear in the published article.

I INTRODUCTION

In recent years, a great deal of research has been conducted on multiphoton photochemistry using infrared lasers. These studies have exploited the strong coupling between an intense infrared laser field and the vibrational/rotational motions of a target molecule. In particular, selective isotopic separation has been achieved in a variety of systems using this technique. The separation of boron¹ from BCl_3 , nitrogen² from NH_3 , sulfur³ from SF_6 and osmium⁴ from OsO_4 all derive their selectivity from isotopic shifts in the vibrational/rotational motions. It has been well established⁵, particularly in the work on SF_6 , that multiquantum processes involving infrared excitation of molecular vibrations can have strong isotopic signatures.

A rich variety of isotopic processes, however, is also expected to be characteristic of molecular electronic spectra even though the purely electronic isotope shifts are normally quite small. The isotopic character of the electronic bands can arise from two sets of basic phenomena. The first is associated with the isotopically shifted vibrational and rotational frequencies; these usually greatly exceed the electronic contribution. The second group arises from perturbations, particularly those which mix electronic states at crossings of molecular potential energy surfaces. These crossings give rise to patterns of predissociation^{6,7} which can exhibit extremely sensitive isotopic behavior. The vibrational analogue of these perturbations has already been analyzed⁸.

In this work, we report the observation of isotopic effects in the multiphoton ultraviolet dissociation of the CO molecule. CO is an attractive candidate for this study for a number of reasons. With three isotopic

choices available for both carbon and oxygen, there are nine possible isotopic molecular variants providing a rich assortment for the examination of isotopically dependent properties. Furthermore, since the C-O bond in carbon monoxide is the strongest chemical bond found in nature ($D^{\circ} = 11.091$ eV)⁹, this system maximally tests our ability to manipulate molecular and chemical processes with existing laser technology. Finally, we note that carbon and oxygen isotopes are fundamental elements of considerable significance in a multitude of chemical and biological systems.

Rare gas halogen lasers have been successfully used to excite several atomic and molecular systems¹⁰ by multi-quantum processes. For example, two-photon excitation of H_2 has been used to study¹¹ a number of spectroscopic properties of the electronically excited molecules. Several recent studies¹² have used multiphoton ultraviolet dissociation processes to study the kinetic properties and internal energy distributions of electronically excited photo-fragments. The relevant theoretical considerations are reviewed in Ref. 10, with special attention paid to the crucial issues of linewidth effects and excited state photoionization. An estimate for two-photon excitation of CO by an ArF* laser at 193 nm is given in Ref. 10 for excitation of the $F^1\Sigma^+$ state. For a free-running ArF* laser, with a linewidth of ~ 100 cm^{-1} , the two-photon coupling parameter, $\alpha = \sigma/I$, is given as 5×10^{-33} cm^4/W . However, ab initio calculations^{13,14} indicate that in the region of 12.8 eV (the energy of two ArF* laser quanta), there are, in fact, several Rydberg states of appropriate symmetry for two-photon excitation from the $X^1\Sigma^+$ ground state. Note that this energy is approximately 0.44 eV above that of the excited $C(^1D) + O(^3P)$ asymptote⁹. (See Fig. 1.)

II EXPERIMENTAL RESULTS

The apparatus used in these experiments has been largely described elsewhere^{10,15}. Only a brief description will be given here.

The output of a UV-preionized discharge ArF* laser (Lambda-Physik EMG-500) was line-narrowed and rendered tunable by the incorporation of two intracavity fused silica prisms¹⁶. This laser was capable of producing approximately 30 mJ in a 10 nsec pulse at the maximum of the tuning curve (~ 193.4 nm) in a bandwidth of $\sim 0.05 - 0.1$ nm, and was tunable over a range of ~ 1.6 nm about the peak. Samples of $^{12}\text{C}^{16}\text{O}$ (99.99% purity), $^{13}\text{C}^{16}\text{O}$ (90 atom% ^{13}C) and $^{12}\text{C}^{18}\text{O}$ (99 atom% ^{18}O) at pressures ranging from 50 mtorr to ~ 300 torr were irradiated with the focused output from this laser at intensities in the range of $10^7 - 10^9$ W/cm². The isotopically normal CO samples were flowed continuously through a dry ice/methanol slush cold trap and then through the experimental cell. The rare isotope samples were contained in pyrex sample bulbs, which were directly immersed in the slush. Since it was impractical to flow these rare samples through the cell continuously, each static cell fill was subjected to a limited number (≤ 200) of laser shots before being replaced. These precautions were necessary to preclude spurious effects due to impurities, or the buildup of photolytic products. Laser induced fluorescence was collected at right angles to the laser beam, and focused onto the slit of a polychromator (McPherson 218) equipped with an optical multichannel analyzer (OMA). The spectra obtained were further processed by means of a PDP 11/34 computer to which the OMA was interfaced. In order to obtain temporally resolved information, the polychromator could be converted to a monochromator by removing the OMA

and installing a slit and a photomultiplier (PMT). The PMT signal was processed by a transient digitizer (Tektronix R7912), which was also interfaced to the computer.

An unusual coincidence occurs in the case of carbon atoms in experiments utilizing 193 nm radiation. This aspect, which involves the fully allowed $C(2^1D) \rightarrow C(3^1P^o)$ transition at 193.1 nm, is illustrated in Fig. 1. Owing to the accidental correspondence of this transition frequency with the ArF* laser frequency, it is apparent that any $C(2^1D)$ atoms that may be produced by two-quantum excitation of CO by ArF* laser radiation will be rapidly excited to the $C(3^1P^o)$ state. Two convenient diagnostics are available; the $C(3^1P^o) \rightarrow C(2^1P)$ transition at 248 nm which provides a means to detect $C(3^1P^o)$ and the $C(3^3P^o) \rightarrow C(2^3P)$ transition at 166 nm which furnishes an equivalent means to detect the excited $C(3^3P^o)$ state, which lies close to the $C(3^1P^o)$ level. As noted above, two ArF* laser quanta have sufficient energy to produce $C(2^1D)$ in the dissociation of ground state CO.

Intense carbon atom emissions at 248 nm and 166 nm were indeed observed in CO irradiated with intense 193 nm radiation. A laser excitation spectrum of the 248 nm emission is shown in Fig. 2. The variation of laser output energy with tuning is also shown in Fig. 2. A similar spectrum is obtained for the 166 nm emission. The peak of this spectrum occurs at 193.1 nm, which corresponds exactly to the $C(2^1D) \rightarrow C(3^1P^o)$ transition.

The dependence of the 248 nm emission intensity on CO pressure is shown in Fig. 3. The plot is linear from 50 mtorr to about 10 torr, which we take as evidence that the production of $C(2^1D)$ proceeds via a collisionless process. Additional support for this interpretation was obtained by examining the temporal behavior of the 248 nm emission. Within the time resolution

of the PMT (10 nsec), the signal directly followed the laser pulse.

Normally, the signature of an n-photon absorption is a fluorescent signal which varies as I^n , where I is the excitation laser intensity. Since the production of $C(3^1P^o)$ proceeds via a collisionless process, a minimum of three quanta from the ArF* laser must be absorbed per molecule in order to reach this level, which lies a full 18.75 eV above the ground state in CO (see Fig. 1). However, the data of Fig. 2 indicate that $C(2^1D)$ is first produced as an intermediate, followed by the resonant absorption of a third quantum on the fully allowed $C(2^1D) \rightarrow C(3^1P^o)$ transition. This final absorption is strongly saturated and power broadened at the laser intensities used in these experiments (10^7 - 10^9 W/cm²). Hence, if $C(2^1D)$ is produced by a two-quantum photolytic absorption, the $C(3^1P^o) \rightarrow C(2^1S)$ fluorescence at 248 nm would be expected to vary only as the square of the incident laser intensity. To check this the 248 nm signal was measured as a function of laser intensity, for laser intensity in the range of 10^7 - 10^9 W/cm². The quadratic behavior observed confirms this model.

In order to assess the isotopic selectivity of the dissociation process, the experiments were performed separately with $^{12}C^{16}O$, $^{13}C^{16}O$ and $^{12}C^{18}O$. Results obtained with $^{13}C^{16}O$ are shown together with the $^{12}C^{16}O$ results in Fig. 2 and Fig. 3. The laser excitation spectra of 248 nm C atom emission for the two isotopes both peak at 193.1 nm. However, as can be seen in both Figs. 2 and 3, the yield of $C(2^1D)$ is substantially greater for the heavier isotope. The ratio of the low pressure (≤ 10 torr) slopes of the pressure dependence data shown in Fig. 3 gives the isotopic ratio of the quantum yields for production of $C(2^1D)$.

This ratio is determined as 6.2 ± 0.5 . Results obtained with $^{12}\text{C}^{18}\text{O}$ were essentially identical. The laser excitation spectrum exactly matched that of $^{13}\text{C}^{16}\text{O}$, and the quantum yield isotopic ratio relative to $^{12}\text{C}^{16}\text{O}$ was 6 ± 1 . Note that the reduced masses of $^{12}\text{C}^{18}\text{O}$ and $^{13}\text{C}^{16}\text{O}$ are within 0.3% of each other, while that of $^{12}\text{C}^{16}\text{O}$ is 4.6% smaller. It is therefore reasonable that $^{12}\text{C}^{18}\text{O}$ and $^{13}\text{C}^{16}\text{O}$ show quite similar isotopic effects.

As mentioned above, the 166 nm emission from $\text{C}(3^3\text{P}^\circ)$ showed a laser excitation spectrum which matched that of the 248 nm emission from $\text{C}(3^1\text{P}^\circ)$. The pressure dependence of this emission was investigated and found to increase faster than linearly for pressures below 10 torr. From this we conclude that $\text{C}(3^3\text{P}^\circ)$ is created via collisional energy transfer from $\text{C}(3^1\text{P}^\circ)$. Such a process is expected to be quite fast, due to the small (endothermic) energy defect ($\sim 1600 \text{ cm}^{-1}$) between these two states. The rate constant for collisional deactivation of $\text{C}(2^1\text{D})$ to $\text{C}(2^3\text{P})$ ground state atoms by CO has been measured¹⁷ as $1.6 \pm 0.6 \times 10^{-11} \text{ cm}^3/\text{sec}$. The rate for $\text{C}(3^1\text{P}^\circ)$ to $\text{C}(3^3\text{P}^\circ)$ collisions may be expected to be even larger.

In addition to neutral body collisions, charged particle collisions will be effective in mixing $\text{C}(3^1\text{P}^\circ)$ with $\text{C}(3^3\text{P}^\circ)$. In pure CO, under these conditions, electrons can be produced either by three-photon ionization of CO, three-photon ionization of $\text{O}(^3\text{P})$, or one-photon ionization of $\text{C}(3^1\text{P}^\circ)$. The latter process is surely the most important by far, and a substantial fraction of the $\text{C}(3^1\text{P}^\circ)$ atoms created will be photoionized.

Singlet-triplet mixing¹⁸⁻²⁰ and superelastic scattering²¹ by free electrons have received a great deal of attention recently in connection

with a number of laser media. Such processes are rather difficult to experimentally quantify, primarily due to the difficulty of producing an appropriately controlled density of free electrons. However, under the conditions of the present experiment, two-photon photoionization of an appropriate additive appears to be an attractive method for experimentally studying these processes. For example, it has been demonstrated^{10,20} that Xe atoms may be readily photoionized by two-quantum absorption at 193 nm.

In a preliminary effort to exploit this process, we undertook to examine the effect of small quantities of added Xe on the C atom emissions at 248 nm and 166 nm. We first duplicated the experiments on pure xenon described in Ref. 10, using the tunable laser, to check for spectral structure in the two-photon ionization cross section arising from possible autoionizing resonances²². At a high pressure (1000 torr) of pure xenon, the Xe^+ ions produced recombine to form Xe_2^* excimers with essentially 100% efficiency¹⁰. We, therefore, monitored the Xe_2^* fluorescence continuum at ~ 172 nm as a function of excitation laser wavelength. No structure was observed. The fluorescent emission intensity simply varied in the expected nonlinear fashion with the laser intensity, as the laser was tuned over its full wavelength range.

We then investigated the behavior of the 166 nm and 248 nm emissions upon the addition of xenon. For a fixed concentration of CO (2 torr), the ratio of 166 nm to 248 nm emission increased monotonically with Xe concentration over the range from 0-10 torr. The rate of rise was found to increase with laser intensity. Species such as Xe^* or Xe_2^* , formed by recom-

ination of Xe^+ ions, cannot be responsible for this effect. The emissions follow the laser pulse in time (~ 10 nsec), and at the pressures involved here (≤ 10 torr), recombination will be quite slow¹⁸ (tens of microseconds) by comparison. Thus, the collisional process



has been observed. With further refinements, including an experimental determination of the xenon two-photon ionization cross section, it will soon become possible to carry out quantitative studies of such important charged particle processes.

In addition to C atom emission, fluorescence in the C_2 Swan bands was observed upon irradiation of CO at 193 nm. The C_2^* emission was prominent at pressures of about 10 torr and above. The observed spectrum showed the selective excitation of $v' = 6$, the characteristic signature of the "high-pressure" bands²³. A sample spectrum of this emission from $^{12}\text{C}^{16}\text{O}$ is presented in Fig. 4. Shown there is the $v' - v'' = 1$ progression at about 470 nm. The dominance of the double headed $v' = 6$ band is clearly evident. Emission from lower vibrations is observed as well. Also shown in Fig. 4 is the same emission band observed upon irradiation of $^{13}\text{C}^{16}\text{O}$. This spectrum is quite clearly shifted with respect to the $^{12}\text{C}_2^*$ spectrum and matches the known spectrum²³ of $^{13}\text{C}_2^*$. The laser excitation spectrum of the C_2^* emissions was measured in an effort to elucidate the wavelength dependence of the C atom yield. For this measurement, the emission band shown in Fig. 5 was integrated over its full width from ~ 476 nm to ~ 466 nm. The results are shown in Fig. 5 for both $^{12}\text{C}^{16}\text{O}$ and $^{13}\text{C}^{16}\text{O}$ with the laser output energy curve also shown. Although

no isotopic shift is resolved, these spectra are slightly shifted with respect to those in Fig. 2. As is also shown in Fig. 5, the C_2^* emission intensity shows an isotopic behavior which is qualitatively consistent with the results on the atomic carbon yield.

DISCUSSION

The carbon monoxide molecule has been extensively investigated both theoretically and experimentally. The data available prior to 1966 is reviewed in the exhaustive compilation of Krupenie⁹. New data were published in 1972 by Tilford and Simmons²⁴. Spectroscopic data on the states of $^{12}C^{16}O$ and its isotopic variants in the range of 10 eV and above, however, is not abundant. Ref. 9 includes data on several very high lying Rydberg series in $^{12}C^{16}O$. Data for the $A \Pi \rightarrow X^1\Sigma^+$, and $B^1\Sigma^+ \rightarrow A^1\Pi$ transitions in $^{13}C^{16}O$ are included in Refs. 9 and 24. Kepa et al.²⁵, report studies of the $E^1\Pi \rightarrow A^1\Pi$ system in $^{12}C^{16}O$, $^{13}C^{16}O$, and $^{12}C^{18}O$. Domin et al.²⁶ have observed the $A^1\Pi \rightarrow X^1\Sigma^+$ transition in $^{14}C^{16}O$. Tilford and Vanderslice²⁷ observed (in $^{12}C^{16}O$) the $B^1\Sigma^+ \rightarrow X^1\Sigma^+$, and $C^1\Sigma^+ \rightarrow X^1\Sigma^+$ transitions under high resolution and discovered the $j^3\Sigma^+ \rightarrow X^1\Sigma^+$ transition. Brunt²⁸ et al., observed a number of metastable and ultra-violet emitting levels in this region by electron impact excitation. Progress toward a theoretical understanding of the high lying states in CO has been made with the calculations of Lefebvre-Brion et al.¹³, whose simple configuration interaction wavefunctions were quite successful in predicting the positions of several Rydberg levels and resolving prevailing ambiguities regarding state assignments. More recently, O'Neill

and Schaefer¹⁴ have performed a comprehensive calculation of the potential functions for all 72 valence states which dissociate to a 3P , 1D , 1S or 5S carbon atom plus a 3P , 1D or 1S oxygen atom.

The available spectroscopic data clearly indicate that at an energy of 12.8 eV, there is an abundance of electronic states of both valence¹⁴ and Rydberg¹³ character. Although detailed information regarding vibrational frequencies, perturbations, and predissociation in these high-lying states is not available, we may make some general remarks concerning the physical processes underlying the experimental results presented in the previous section.

The coincidence of the 193 nm laser ArF* laser wavelength with the $C(2^1D) \rightarrow C(3^1P^o)$ atomic absorption is, of course, crucial to the detection of $C(2^1D)$ excited carbon atoms. This same absorption has been exploited in the past, in kinetic absorption studies, to yield accurate collisional quenching data on $C(2^1D)$ with a variety of collisional partners¹⁷. The penalty for this coincidence is that, with the given laser bandwidth of ~ 0.1 nm, the $C(2^1D) \rightarrow C(3^1P^o)$ resonance confuses and obscures any possible resonance in the two-photon photolytic process. Yet, we observe a strong isotopic selectivity at the peak of this excitation spectrum. In view of this, and the relatively broad laser bandwidth, it is extremely unlikely that the isotope effect derives from a shift in the overall two-photon transition frequency.

We believe that this isotope effect is to be explained in terms of the two-photon coupling parameter¹⁰,

$$\alpha = \sigma/I = \frac{(2\pi)^3}{hc^2} \nu |M_{fg}|^2 g(\nu) \quad (2)$$

$$M_{fg} = 2 \sum_k \frac{\langle f | \hat{\epsilon} \cdot \vec{\mu}_{op} | k \rangle \langle k | \hat{\epsilon} \cdot \vec{\mu}_{op} | g \rangle}{E_{kg} - h\nu} \quad (3)$$

In these expressions ν is the optical frequency, $\hat{\epsilon}$ denotes the polarization of the optical wave, $\vec{\mu}_{op}$ represents the electric dipole operator, and g , k , and f denote the ground, intermediate and final states, respectively.

Referring to Fig. 1, we see that one ArF* laser photon is very close in energy to the $a^3\Pi, v=2$ state, which is certainly the dominant intermediate state, assuming that our final state is spin triplet. This is a reasonable assumption since a 1D carbon atom plus a 3P oxygen atom correlate only to triplet molecular states^{14,29}. We know of no measurements of the isotopic shifts for the CO ($a^3\Pi - X^1\Sigma^+$) transition (Cameron bands); these may be simply estimated²⁸ by

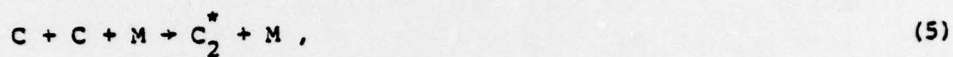
$$\Delta\nu = [\omega_e' (v'+\frac{1}{2}) - \omega_e'' (v''+\frac{1}{2})] (\rho - 1) - [\omega_e x_e' (v'+\frac{1}{2})^2 - \omega_e x_e'' (v''+\frac{1}{2})^2] (\rho^2 - 1) \quad (4)$$

where $\rho = \mu/\mu^i$, and μ and μ^i are the reduced masses for normal and isotopically substituted CO, respectively. For $^{13}C^{16}O$, a red shift of 68.9 cm^{-1} is predicted for the $a^3\Pi - X^1\Sigma^+$ (2,0) transition. The observed isotope effect is easily accounted for by this variation of the intermediate state detuning in the two-photon matrix element.

This leaves open the important question of the nature of the state at 12.8 eV in CO leading to the dissociation of the molecule. The two-photon absorption may terminate on a discrete vibronic level, which is predissociated, or to a true dissociation continuum. These two alternatives are depicted schematically in Fig. 6. The difference is normally detected easily with tunable excitation. Quite simply, for the former case, a resonance will be observed in the dissociation yield, while in the

latter, the yield varies more slowly and continuously. However, as noted above, the tuning curve for the atomic carbon yield is dominated by the atomic resonance at 193.1 nm.

An alternative diagnostic for the presence of carbon atoms is the C_2 Swan band emission. The C_2^* radical is formed from free carbon atom association in the presence of CO either directly by three-body collisions³⁰



or, by the mechanism³¹



Note that in either case, one C_2 molecule is formed from two free carbon atoms. We may, therefore, look to the C_2^* laser excitation spectrum in Fig. 5 for information regarding the character of the two-photon excited state in CO. The fact that the spectra of Fig. 2 and Fig. 5 are quite similar suggests, however, that there may be a connection between the excitation of the carbon atoms at 193.1 nm and enhanced efficiency for formation of C_2^* . On the other hand, a careful examination of these spectra reveals a small, but nonetheless, definite shift between the two, which is just at the resolution limit of our system. This fact tends to suggest that case (b) in Fig. 6 is correct. That is, the two-photon absorption leads to a discrete molecular level, which predissociates to yield carbon and oxygen

atoms. With improved resolution, it will be possible to map out the dissociation dynamics in detail.

We now examine the potential of this process for practical separation of carbon isotopes. We note that a somewhat similar scheme involving ultraviolet photopredissociation of H_2CO has been used³² to produce CO enriched in ^{12}C , and a method for enrichment of ^{13}C in CO photochemistry has been studied by Liuti et al.³³. In the latter work, an atomic iodine lamp, emitting at 206.2 nm was used to preferentially excite the (0,0) transition in the $^{13}\text{C}^{16}\text{O}$ Cameron band system. Subsequent chemical reactions of the excited molecules led to isotopically enriched C_3O_2 product. Due to limited lamp intensity, coupled with the low absorption coefficient, the absolute yield of enriched ^{13}C was small. In addition, some of the isotopic selectivity achieved in the first step was lost in the subsequent chemical reactions. The two-photon photolysis of CO studied here has the potential of overcoming both of these difficulties. The extremely bright emissions observed indicate a high yield of carbon atoms. Under the present conditions, essentially no loss of isotopic selectivity may be expected in the production of C_2^* , since, as discussed above, C_2^* is formed from two free carbon atoms. The C_2 radicals formed in this way will eventually precipitate out as particulate carbon which is readily collected. We found, in fact, that after static samples of CO were subjected to several hundred to one thousand laser shots, a substantial quantity of carbon was deposited on the cell walls.

SUMMARY AND CONCLUSIONS

The production of $C(2^1D)$ atoms by direct two-photon photolysis of CO at ~ 193 nm has been observed. The $C(2^1D)$ atoms absorb a third photon at 193.1 nm to $C(3^1P^o)$ and subsequently radiate to $C(2^1S)$ at 248 nm. The yield of $C(2^1D)$ from $^{13}C^{16}O$ and $^{12}C^{18}O$ is found to be a factor of 6 greater than that from $^{12}C^{16}O$. Emission in the C_2 "high pressure" bands is observed, arising from recombination of the free carbon atoms, and a similar isotope effect is observed in these emissions. No isotope shift is resolved in the laser excitation spectrum of either emission. The observed isotope effect is attributable to a difference in the two-photon coupling strengths for the different isotopic species, arising from a shift in the position of the dominant intermediate state resonance. The application of this process for the practical separation of carbon isotopes appears possible.

Preliminary results have been obtained using a new method for studying collisional processes involving free electrons. Small quantities of a suitable donor species, in this case xenon atoms, are photoionized by the intense excitation laser to produce the free electrons. Collisional energy transfer from $C(3^1P^o)$ to $C(3^3P^o)$ has been observed in this way.

The results obtained in these experiments clearly demonstrate the enormous potential of the tunable excimer laser for spectroscopic and photochemical investigations. Further improvement of this technology will clearly bring about the possibility of detailed investigations of molecular dynamics involving highly excited electronic states, including such important subjects as sub-Doppler spectroscopy, both heavy body and charged particle collisional processes, photochemical reaction kinetics, and isotope separation.

ACKNOWLEDGEMENTS

The authors wish to thank H. Egger, D. J. Kligler, R. M. Hill, D. L. Huestis, T. G. Slanger, and G. Black for useful discussions involving various aspects of these experiments. The expert technical assistance of K. Skala and G. Murphy is also acknowledged. This work was supported by the Department of Energy under Agreement No. ED-78-S08-1603, the National Science Foundation under grant PHY77-01849, and the Office of Naval Research under Contract . J. Bokor gratefully acknowledges the support of the Fannie and John K. Hertz Foundation.

REFERENCES

1. S. D. Rockwood and S. W. Rabideau, *IEEE J. Quantum Electron.* QE-10, 789 (1974).
2. R. V. Ambartzumian, V. S. Letokhov, G. N. Makarov, and A. A. Pureskii, *Zh. Eksp. Teor. Fiz. Pisma Red.* 17, 19 (1973).
3. J. L. Lyman, R. J. Jensen, J. Rink, C. P. Robinson, and S. D. Rockwood, *Appl. Phys. Lett.* 27, 87 (1975).
4. R. V. Ambartzumian, Yu. A. Gorokhov, V. S. Letokhov, and G. N. Makarov, *Sov. Phys. - JETP Lett.* 22, 43 (1975).
5. V. S. Letokhov, *Ann. Rev. Phys. Chem.* 28, 133 (1977).
6. M. S. Child in Molecular Spectroscopy, Vol. 2 (The Chemical Society, London, 1974) p. 466; J. K. Lewis and J. T. Hougen, *J. Chem. Phys.* 48, 5329 (1968).
7. R. S. Mulliken, *J. Chem. Phys.* 33, 247 (1960).
8. C. K. Rhodes and C. D. Cantrell in The Significance of Nonlinearity in the Natural Sciences, edited by Behran Kursunoglu, Arnold Perlmutter and Linda Scott (Plenum Publishing Co., New York, 1977) p. 293.
9. Paul H. Krupenie, The Band Spectrum of Carbon Monoxide, NSRDS-NBS 5 (U. S. Department of Commerce, USGPO, 1966).
10. William K. Bischel, Jeffrey Bokor, Daniel J. Kligler, and Charles K. Rhodes, *IEEE J. Quantum Electron.* QE-15, 380 (1979).
11. Daniel J. Kligler and Charles K. Rhodes, *Phys. Rev. Lett.* 40, 309 (1978).
12. D. J. Kligler, H. Pummer, W. K. Bischel, and C. K. Rhodes. *J. Chem.*

- Phys. 69, 4652 (1978); W. M. Jackson, Joshua B. Halpern, and Chung-San Lin, Chem. Phys. Lett. 55, 254 (1978); A. P. Baronavski, and J. R. MacDonald, Chem. Phys. Lett. 56, 369 (1978); J. R. MacDonald, A. P. Baronavski and V. M. Donnelly, Chem. Phys. 33, 161 (1978); V. M. Donnelly and Louise Pasternack, Chem. Phys. 39, 427 (1979).
13. H. Lefebvre-Brion, C. M. Moser, and R. K. Nesbet, J. Mol. Spectrosc. 13, 418² (1964).
14. Stephen V. O'Neill and Henry F. Schaefer III, J. Chem. Phys. 53, 3994 (1970).
15. Daniel J. Kligler, Jeffrey Bokor, and Charles K. Rhodes, "Collisional and Radiative Properties of the H₂ E,F ¹Σ_g⁺ State", (to be published).
16. T. R. Loree, K. B. Butterfield, and D. L. Barker, Appl. Phys. Lett. 32, 171 (1978).
17. D. Husain and L. J. Kirsch, Trans. Farad. Soc. 67, 2886 (1971); 67, 3166 (1971).
18. Charles W. Werner, Edward V. George, Paul W. Hoff and Charles K. Rhodes, IEEE J. Quant. Electron. QE-13, 769 (1977).
19. A. E. Green and C. A. Brau, IEEE J. Quant. Electron. QE-14, 951 (1978).
20. D. Kligler, H. H. Nakano, D. L. Huestis, W. K. Bischel, R. M. Hill, and C. K. Rhodes, Appl. Phys. Lett. 33, 39 (1978).
21. H. T. Powell, D. Prosnitz, and B. R. Schleicher, Appl. Phys. Lett. 34, 571 (1979); H. T. Powell and A. V. Hazi, Chem. Phys. Lett. 59, 71 (1978); T. J. McIlrath and T. B. Lucatorto, Phys. Rev. Lett. 38, 1390 (1977).

22. R. E. Hoffman, Y. Tanaka, and J. E. Larrabee, *J. Chem. Phys.* 39, 902 (1963); R. F. Stebbings, F. B. Dunning, and R. D. Rundel, *Proc. 4th Int. Conf. on Atomic Physics*, G. zu Putlitz, E. W. Weber, and A. Winnaker, Eds. (Plenum Press, New York, 1975) p. 713.
23. R. K. Dhumwad and N. A. Narasimham, *Can. J. Phys.* 46, 1254 (1968).
24. S. G. Tilford and J. D. Simmons, *J. Phys. Chem. Ref. Data* 1, 147 (1972).
25. R. Kepa, M. Rytel, and Z. Rzeszut, *Acta Phys. Pol.* A54, 353 (1978); R. Kepa and M. Rytel, *Acta Phys. Pol.* A39, 629 (1971).
26. J. Domin, V. Domin and M. Rytel, *Acta Phys. Acad. Sci. Hungar.*, 43, 197 (1977).
27. S. G. Tilford and Joseph T. Vanderslice, *J. Mol. Spectrosc.* 26, 419 (1968).
28. John N. H. Brunt, George C. King, and Frank H. Read, *J. Phys. B: Atom Molec. Phys.* 11, 173 (1978).
29. G. Herzberg, *Spectra of Diatomic Molecules*, (D. Van Nostrand Co., New York, 1950).
30. A. R. Fairbairn, *Proc. Roy. Soc. A* 312, 207 (1969).
31. C. Kunz, P. Harteck and S. Dondes, *J. Chem. Phys.* 46, 4158 (1967); D. W. Naepli and H. B. Palmer, *J. Mol. Spectrosc.* 26, 152 (1962).
32. J. H. Clark, Y. Haas, P. L. Houston, and C. B. Moore, *Chem. Phys. Lett.* 35, 82 (1975).
33. G. Liuti, S. Dondes, and P. Harteck, *J. Chem. Phys.* 44, 4052 (1966).

FIGURES

1. Partial energy level diagram of CO showing the three lowest separated-atom asymptotes, and the 193 nm two-photon excitation energy. The inset shows the atomic carbon energy levels and radiative transitions discussed in the text. Each level in the inset is labeled with its energy (in cm^{-1}) above the $\text{C}(2^3\text{P})$ ground state.
2. Laser excitation spectrum of 248 nm atomic carbon emission resulting from two-photon photolysis of CO at 193 nm. The squares are the data for 10 torr of $^{13}\text{C}^{16}\text{O}$. The triangles are the data for 10 torr of $^{12}\text{C}^{16}\text{O}$. The solid line is the laser output energy tuning curve.
3. Dependence of 248 nm atomic carbon emission on CO pressure. The triangles are the data for $^{13}\text{C}^{16}\text{O}$. The squares are the data for $^{12}\text{C}^{16}\text{O}$. The ratio of the slopes of the two straight lines is 6.2 ± 0.5 .
4. C_2 Swan band emission spectra arising from two-photon CO photolysis. The upper spectrum (a) was obtained with 10 torr of $^{12}\text{C}^{16}\text{O}$ and corresponds to $^{12}\text{C}_2^*$. The lower spectrum (b) was obtained with 10 torr of $^{13}\text{C}^{16}\text{O}$ and corresponds to $^{13}\text{C}_2^*$.
5. Laser excitation spectrum of 470 nm C_2 Swan band emission. Each data point represents the spectrally integrated emission over the entire band shown in Fig. 4. The squares are the data for 10 torr of $^{13}\text{C}^{16}\text{O}$. The triangles are the data for 10 torr of $^{12}\text{C}^{16}\text{O}$. The solid curve is the laser output energy tuning curve.
6. Schematic of alternative dissociation dynamics for two-photon excited CO. Case (a) represents excitation directly into a dissociative continuum correlated with $\text{C}(^1\text{D}) + \text{O}(^3\text{P})$. Case (b) represents excitation

to a discrete vibronic state of Rydberg character, which is pre-dissociated.

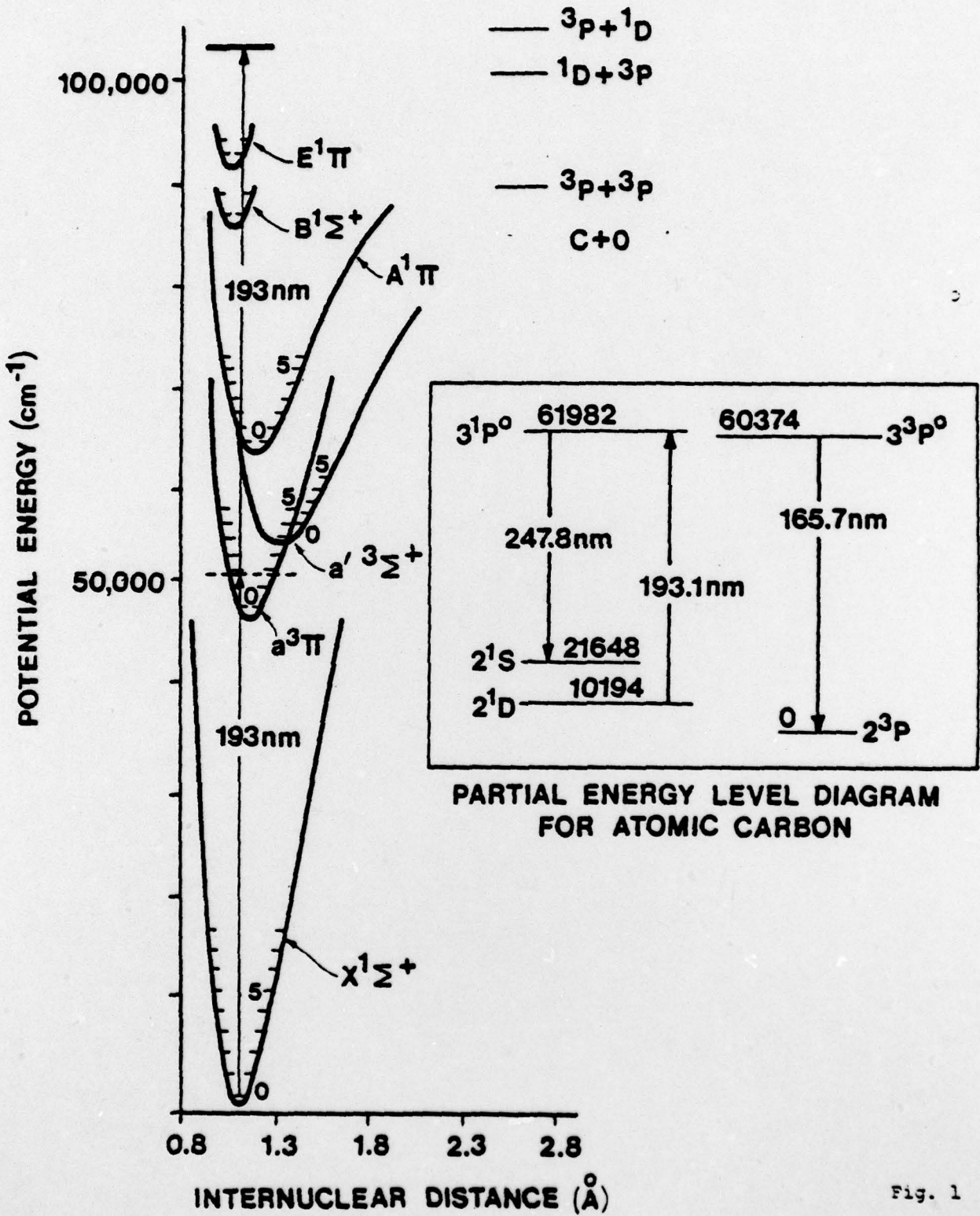


Fig. 1

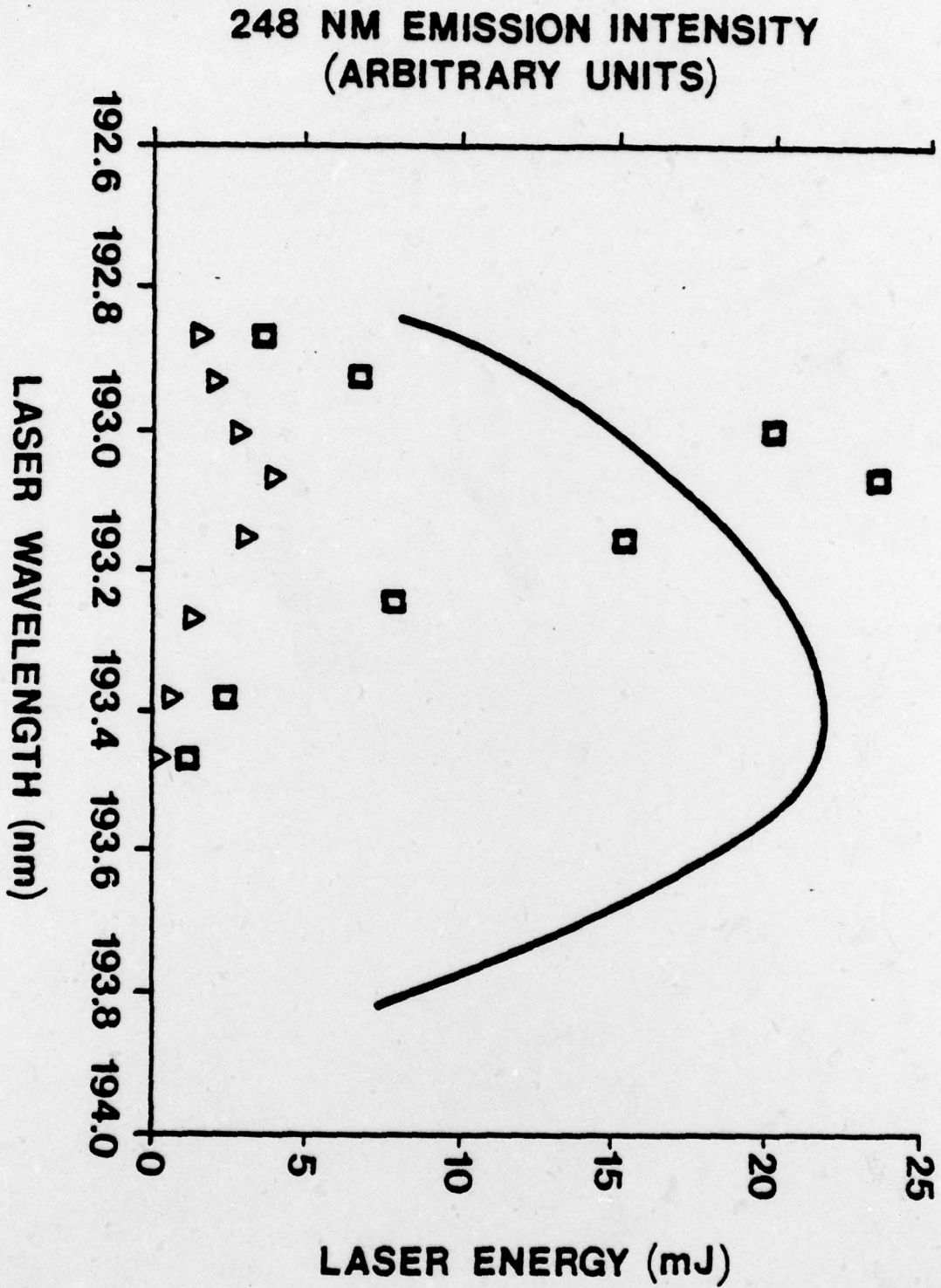


Fig. 2

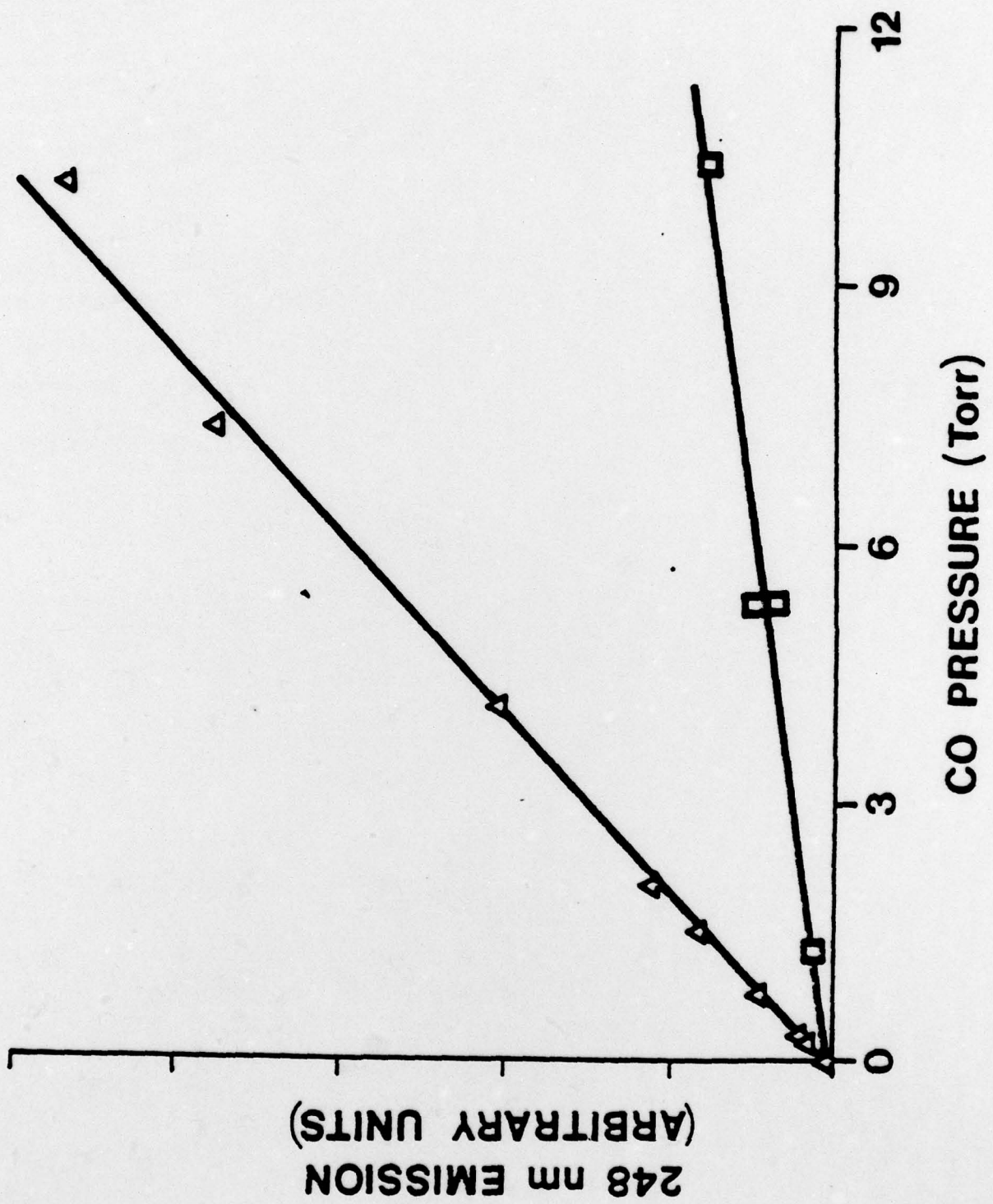


Fig. 3

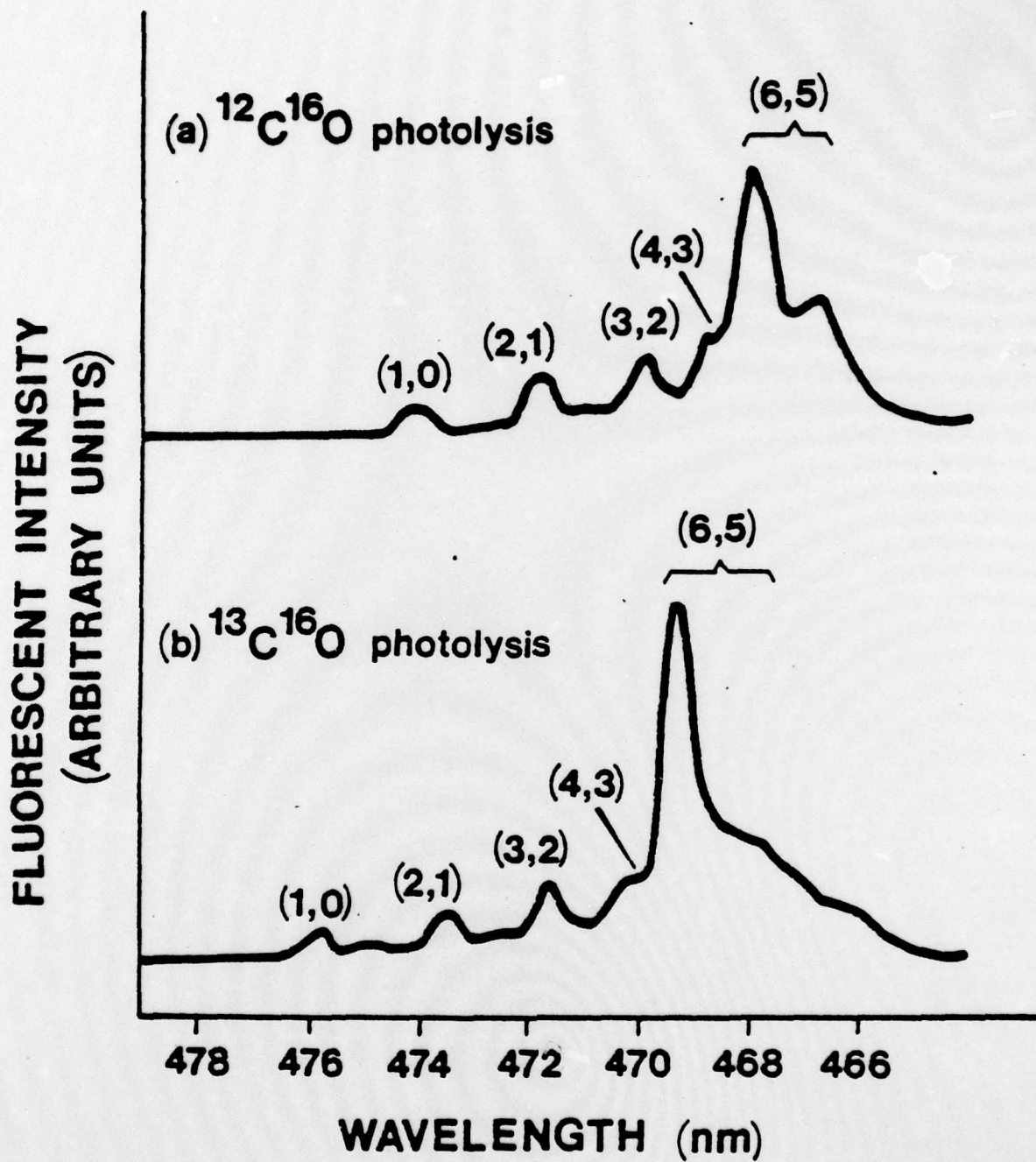


Fig. 4

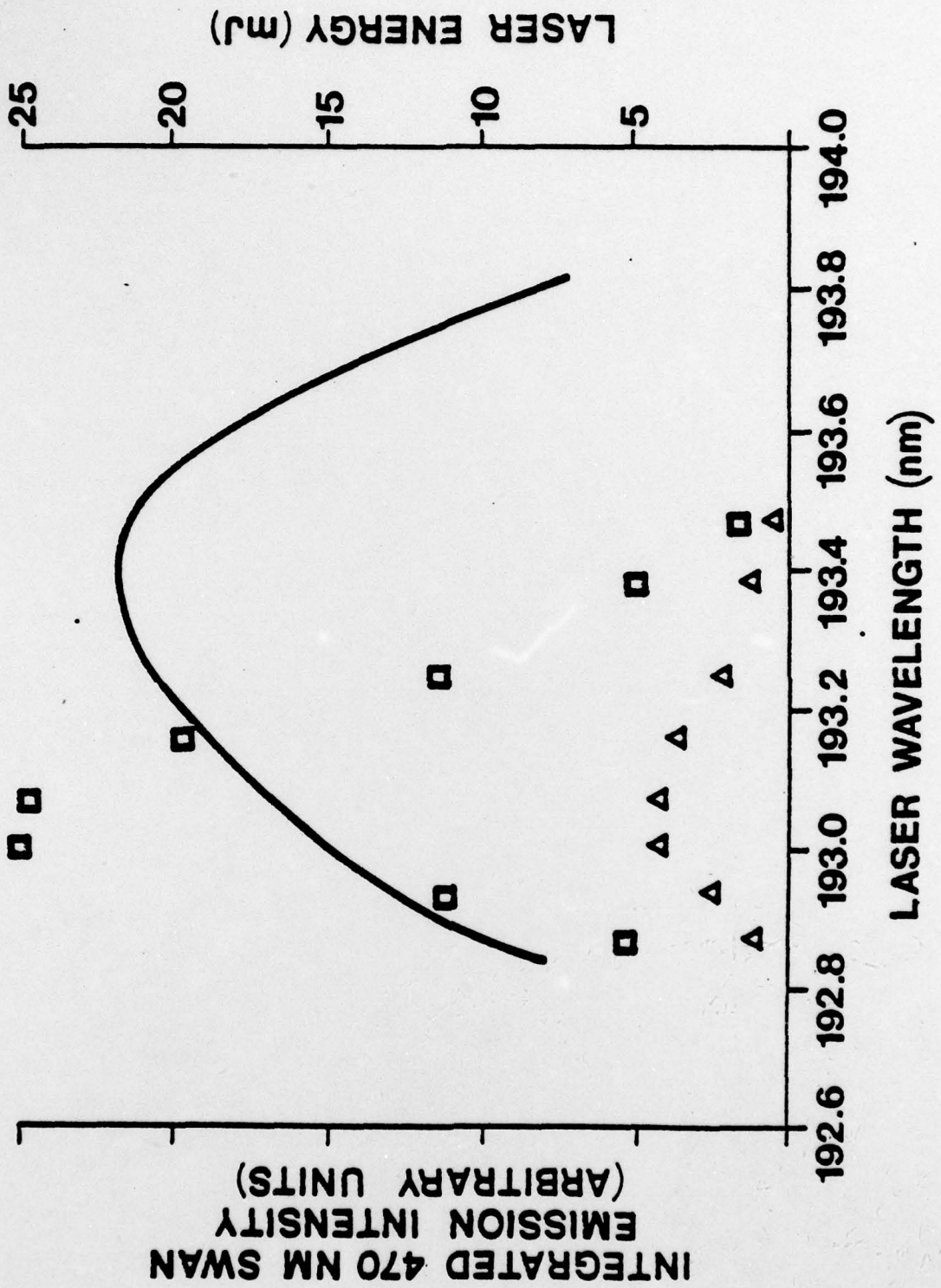


Fig. 5

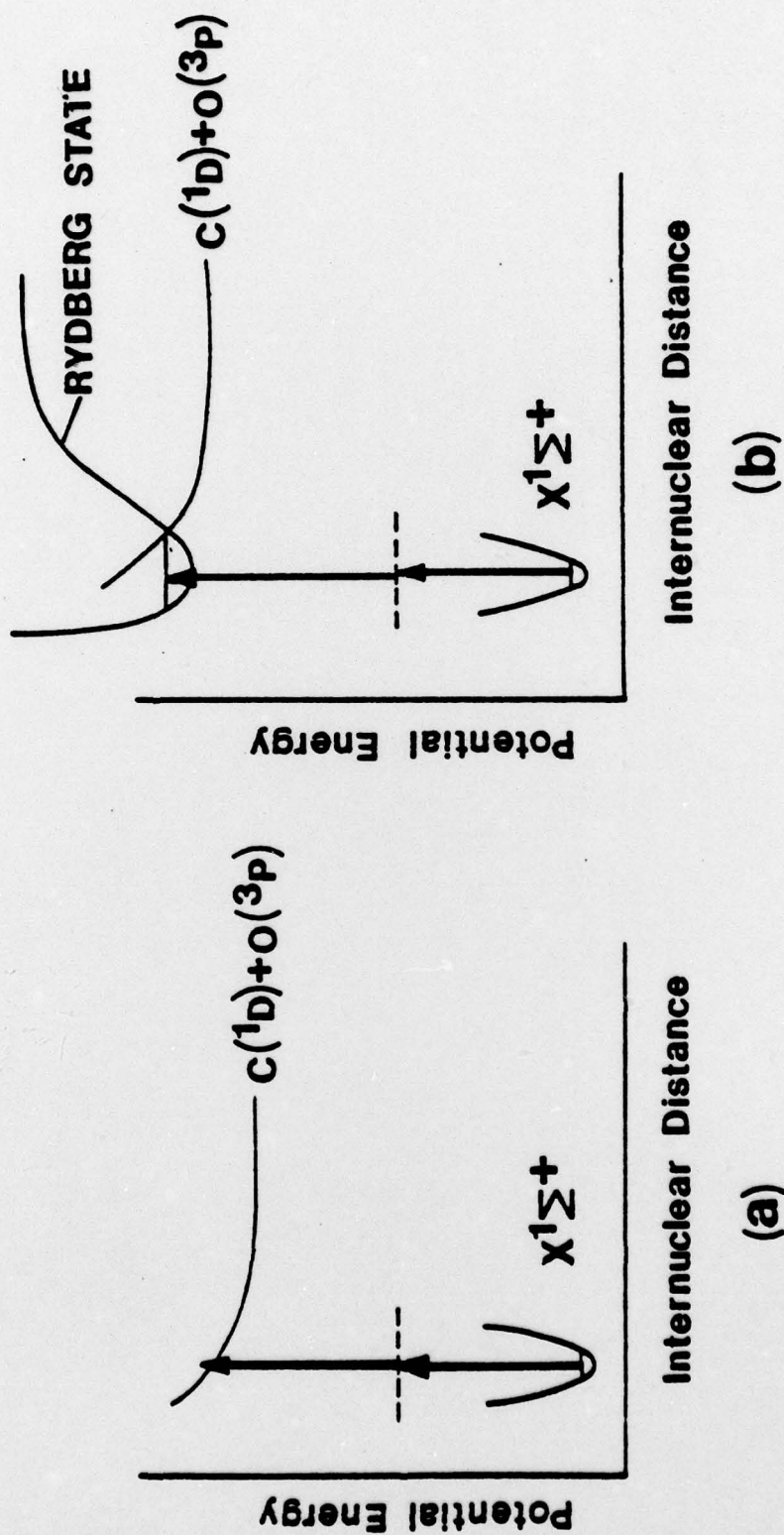


Fig. 6

APPENDIX E

ESTIMATE OF FOUR QUANTUM EXCITATION OF
RUBIDIUM CORE EXCITED STATES AT 248 NM

First ionization limit in Rb of core excited states: $19.854 \text{ eV} = 160$
 $132 \text{ cm}^{-1} = 4 h\nu_{\lambda=2498\text{\AA}}$. If we assume $n=30$, at 248 nm we estimate the
single photon ionization cross section $\sigma^{(1)}$ and the two photon ionization
cross section $\sigma^{(2)}$ as

$$\sigma^{(1)} \approx 10^{-20} \text{ cm}^2 \text{ and}$$

$$\sigma^{(2)} \leq 5 \times 10^{-52} \text{ cm}^4 \text{ sec} \cdot I \text{ (photons cm}^{-2} \text{ sec}^{-1}) \text{ .}$$

The production rate by four quantum excitation can be written as

$$\frac{dW^{(4)}}{dt} = \frac{4!}{(2\pi)^3} \cdot \frac{\alpha^4}{h^4 c^6} \cdot \frac{1}{\Delta\nu} |M_{fg}|^2 I^4 \quad (\text{E-1})$$

$$\sigma^{(4)} = \frac{dW^{(4)}/dt}{I/h\nu} \quad (\text{E-2})$$

$$M_{fg} = \sum_k \sum_j \sum_i \langle f | \underline{R} \cdot \underline{\epsilon} | k \rangle \frac{\langle k | \underline{R} \cdot \underline{\epsilon} | j \rangle}{\hbar(\omega_{kj} - 3\omega)} \cdot \frac{\langle j | \underline{R} \cdot \underline{\epsilon} | i \rangle}{\hbar(\omega_{ji} - 2\omega)} \cdot \frac{\langle i | \underline{R} \cdot \underline{\epsilon} | g \rangle}{\hbar(\omega_{ig} - \omega)} \quad (\text{E-3})$$

$$M_{fg} = \left(\frac{1}{2}\right)^4 \langle 4p^5 5snf | R | 4p^5 5snd \rangle \frac{\langle 4p^5 5snd | R | 4p^6 nd \rangle}{\Delta E_3} \cdot \frac{\langle 4p^6 nd | R | 4p^6 np \rangle}{\Delta E_2} \cdot \frac{\langle 4p^6 np | R | 4p^6 5s \rangle}{\Delta E_1} \quad (\text{E-4})$$

with

$$\Delta E_1 \approx 7000 \text{ cm}^{-1}$$

$$\Delta E_2 \approx 47000 \text{ cm}^{-1}$$

$$\Delta E_3 \approx 6000 \text{ cm}^{-1} \text{ .}$$

Therefore,

$$M_{fg} = \left(\frac{1}{2}\right)^4 \left(\frac{3}{2} n \sqrt{n^2 - 9} a_0\right) \left(\frac{10^{-9}}{6 \cdot 10^3}\right) \left(\frac{\frac{3}{2} n \sqrt{n^2 - 4} a_0}{4.7 \times 10^4}\right) \left(\frac{30 n^{-\frac{3}{2}} a_0}{7 \times 10^3}\right) \quad (E-5)$$

giving a value of

$$M_{fg} = 3.16 \times 10^{-46} n^{5/2} \text{ cm}^4.$$

$$\begin{aligned} \frac{dW^{(4)}}{dt} &= \frac{24}{(2\pi)^3} \cdot \frac{(1/137)^4}{(1.055 \times 10^{-34})^4 \times (3 \times 10^{10})^6} \cdot \frac{1}{\Delta\nu} (1.00 \times 10^{-91}) I n^5 = \\ &= 3.04 \times 10^{-28} \frac{I^4}{\Delta\nu} n^5 \end{aligned}$$

At saturation: $\frac{dW^{(4)}}{dt} \cdot \tau = 1$

$\tau = 10^{-8}$ sec, hence:

$$I_{\text{sat}} = 10^8 \left(\frac{\Delta\nu}{3.04 \times 10^{-28} n^5} \right)^{1/4}$$

With $\Delta\nu \approx 0.01$
 $n \approx 30$

$$I_{\text{sat}} \approx 3.4 \times 10^6 \text{ W/cm}^2$$

$$\sigma_{\text{sat}}^{(4)} = \frac{dW^{(4)}/dt}{I_{\text{sat}}/h\nu} = \frac{10^8}{(4.8 \pm 0.3) \times 10^6 / 7.96 \times 10^{-19}} = (1.66 \pm 0.11) 10^{-17} \text{ cm}^2$$

Thus,

$$\sigma_{\text{sat}}^{(4)} \sim 1.7 \times 10^{-17} \text{ cm}^2$$

for core excitation with $I \sim 4 \times 10^6 \text{ W/cm}^2$ at 248 nm.